ABSTRACT

BEARDSLEE, RENEE ANN. Biochemical Analysis of Human DNA Polymerase η Structure and Fidelity. (Under the direction of Dr. Scott D. McCulloch.)

Myriad agents initiate chemical reactions with reactive nucleobases that result in DNA damage. Such damage to DNA increases the likelihood of nucleotide mispairing during DNA replication and can lead to introduction of fixed mutations into the genome. These mutations are linked to adverse human health outcomes including aging, neurodegeneration and cancer.

Damaged bases introduce distortion to the helix, obstructing successful replication of the genome. To overcome this, a strategy has evolved that allows replication to proceed in the presence of DNA damage. Called translesion synthesis (TLS), this process engages specialized TLS DNA polymerases (pols) that are able to accommodate damaged bases within their binding pocket and use those bases as templates to facilitate nucleotide pairing during replication past the damaged site.

Polymerase η (pol η) is the most thoroughly studied TLS polymerase, largely due to the fact that lack of functional pol η results in a condition known as xeroderma pigmentosum variant (XPV). XPV is characterized by an increased sensitivity to UV and incidence of UV-induced skin cancer. The XPV phenotype develops because, during replication, pol η is responsible for the bypass of ubiquitous cyclobutane pyrimidine dimers (CPD) generated in response to UV exposure. XPV cells accumulate mutations at CPD sites, likely due to the action of a more error-prone TLS polymerase in the absence of pol η. In addition to CPD bypass, pol η has been implicated in TLS past 7,8-dihydro-8-oxoguanine (8-oxoG) generated by reactive oxygen species (ROS). The frequency of nucleotide misincorporation opposite

both lesions by pol η, however, is high relative to that of the high fidelity replicative polymerases.

While it is understood that pol η is responsible for the bypass of CPDs *in vivo*, details of this process are incomplete and the disparity between poor polymerase fidelity *in vitro* and its clear function in mutation suppression *in vivo* is unresolved. In response, this work provides insight into how the structure of the polymerase stabilizes damaged DNA templates, contributing to its remarkable damage bypass capability, as well as how abnormal conditions in which pol η may operate could affect polymerase activity and function. The intent is to provide greater understanding of DNA damage bypass, pol η fidelity and mechanisms of mutagenesis.

To accomplish this, we used purified polymerase η and DNA oligomers synthesized with both thymine-thymine CPDs and 8-oxoG lesions in *in vitro* assays to evaluate polymerase properties during replication of undamaged and damaged DNA. In our structural study, we investigated the role of the β-strand in the little finger subdomain by generating single amino acid substituted forms of the polymerase that disrupted its DNA binding surface, allowing us to assess the β-strand function. The results confirm the importance of the β-strand to polymerase function and show that fidelity is most often altered when undamaged DNA is copied. Additionally, it is shown that DNA–protein contacts distal to the active site can significantly affect the fidelity of synthesis.

Because pol η possesses a distinctive open active site unique to TLS polymerases, we also hypothesized that the polymerase may be especially sensitive to changes in dNTP concentrations. Thus, again using *in vitro* assays, we assessed the response of pol η activity and fidelity to changing dNTP pools and demonstrate that error rates of the polymerase vary

with dNTP concentrations. As modified dNTP levels are associated with cancer cells we propose that this dynamic fidelity in concert with dysregulated pol η levels could contribute to the mutator phenotype significant to cancer progression.

Biochemical Analysis of Human DNA Polymerase η Structure and Fidelity

by
Renee Ann Beardslee

A dissertation submitted to the Graduate Faculty of
North Carolina State University
in partial fulfillment of the
requirements for the degree of
Doctor of Philosophy

Toxicology

Raleigh, North Carolina

2015

APPROVED BY:

_____	_____
Scott D. McCulloch Committee Chair	Robert Smart Vice-Chair
_____	_____
Jun Tsuji	Jason Haugh

BIOGRAPHY

Renee A. Beardslee was born and raised in southeastern Michigan. She graduated from University of Michigan with a Bachelor of Science in Chemistry and relocated to Raleigh, NC to pursue a Ph.D. in Toxicology at North Carolina State University. Following completion of her degree she intends to pursue post-doctoral training at the US EPA in Research Triangle Park, NC.

TABLE OF CONTENTS

LIST OF TABLES

LIST OF FIGURES

LIST OF SYMBOLS AND ABBREVIATIONS

β – beta

δ – delta

ε – epsilon

η – eta

ι – iota

κ – kappa

ζ – zeta

5mC – 5-methylcytosine

(6-4)PP – pyrimidine-pyrimidone (6-4) photoproduct

8-oxoG – 7,8-dihydro-8-oxoguanine

BUdR – bromodeoxyuridine

f_{inc} – frequency of incorporation

CPD – *cis–syn* cyclobutane pyrimidine dimer

K_m – Michaelis constant

OPRA – oligonucleotide probe retrieval assay

PIP – PCNA interacting peptide

pol – polymerase

RIR – Rev1 interacting region

ROS – reactive oxygen species

RFC – replication factor C

RPA – replication protein A

TLS – translesion synthesis

TTD/TT dimer – *cis–syn* cyclobutane thymine–thymine dimer

UBZ – ubiquitin-binding zinc domain

UDG – uracil-DNA glycosylase

WT – wild type

XP – xeroderma pigmentosum

XPV – xeroderma pigmentosum variant

CHAPTER 1: GENERAL INTRODUCTION

Successively imparting the genetic information stored in DNA between generations is essential to the conservation of life. Found within the nucleotide sequence of an organism's genome is the blueprint from which every biological molecule is assembled as well as the elements necessary to direct the cell's activity. The implications for failing to preserve and accurately perpetuate this information can span from the inconsequential to loss of life.

Structure and Chemistry of DNA

Fundamental to the proficiency with which DNA is able to maintain and transfer its genetic information is its unique and remarkable structure. First described in 1953, the DNA molecule comprises 2 polymer chains of phosphate groups covalently bonded via ester bonds to β-D-deoxyribose molecules at the 3′ and 5′ carbon atoms (Watson and Crick, 1953). Either a pyrimidine (cytosine, thymine) or purine (adenine, guanine) base is joined to the 1′ carbon by an *N*-β-glycosidic bond. The two sugar-phosphate backbones are oriented antiparallel to each other and together, in the most commonly recognized B-form, adopt a double helical shape in three-dimensional space (Figure 1.1) (Watson and Crick, 1953; Bansal, 2003; Nelson and Cox, 2005; Pray, 2008). Crucial to the three-dimensional structure as well as the stability of DNA are interactions between the bases and include both base stacking and hydrogen bonding (Figure 1.2) (Sattin et al., 2004; Nelson and Cox, 2005).

Pyrimidines are aromatic heterocyclic structures with nitrogen heteroatoms located at positions one and three. Cytosine has a carbonyl located at position two and an amino group at position four, while thymine possesses carbonyls at positions two and four along with a

methyl group located at position five (Figure 1.3). The purine bases, adenine and guanine, consist of an imidazole ring and pyrimidine ring joined together at the fourth and fifth, and fifth and sixth positions, respectively, with substitutions located on the pyrimidine ring. Only a single amino group substituent at position six is found in adenine, while guanine has two substituents: an amino group at position two and a carbonyl at position six (Figure 1.3). Chemical modifications to the bases can occur on either the main ring structure or the substituent functional groups (Eğe, 1994; Nelson and Cox, 2005).

DNA Damage

While the DNA molecule is remarkably stable, it has been clearly established that the pyrimidine and purine bases are chemically reactive and subject to modification as the result of exposure to both endogenous and exogenous agents (Friedberg et al., 2004) which can result in DNA damage and the possible subsequent introduction of fixed mutations within the genome. Endogenous sources of DNA alterations can be broadly classified into two categories: those for which the alterations occur without the action of any additional reactants other than the nucleobases themselves, and those for which additional reactants participate in chemical reactions with the bases (Friedberg et al., 2006; Hodgson and Smart, 2013). The former comprises only two types: nucleotide mispairing during replication and the incorporation of nucleotides into DNA that have been modified prior to the initiation of DNA replication. The later category is much more extensive, however, and includes a large number of reactions between DNA and oxygen, water and other naturally occurring inorganic and biological molecules within the cell.

Nucleotide mispairing. Critical to the maintenance of genetic information and cell function is the preservation of Watson-Crick base pairing. Even in the absence of damage to the bases, the major replicative DNA polymerases, δ and ε incorporate incorrectly paired nucleotides that are overlooked by their intrinsic proofreading activities approximately once for every 100,000 and 220,000 nucleotides incorporated, respectively (Schmitt et al., 2009; Korona et al., 2011). Persistence of such mispairs will result in a permanent change to the genetic sequence following the next round of replication. Fortunately, the presence of a highly conserved canonical mismatch repair that operates in concert with replication can increase replication fidelity up to 1000 fold (Iyer et al., 2006) to produce a complete system that yields approximately one mismatch per genome copied. The significance of the protective action of MMR has been highlighted by findings that cells and mouse models deficient in MMR proteins exhibit a mutator phenotype and are subject to premature development of lymphoma (Baker et al., 1995; de Wind et al., 1995; Edelmann et al., 1996; 1997). Furthermore, heterozygous mutations in humans cause Lynch syndrome (often referred to as hereditary non-polyposis colorectal cancer) in humans that is characterized by the development of hematological malignancies and brain tumors in children as well as early-onset colorectal cancer (Lynch and la Chapelle, 2003; Peltomäki, 2003; Wimmer and Etzler, 2008).

Base deamination. Three of the four canonical DNA bases, cytosine, adenine and guanine are subject to deamination Figure 1.4 (Lindahl, 1979; Friedberg et al., 2006). In addition, the methylated form of cytosine, 5-methylcytosine (5mC), is also susceptible to deamination (Figure 1.4) (Shen et al., 1994). The deamination of cytosine to generate uracil

and the deamination of 5mC to generate thymine, however, occur at rates much faster than those for deamination of the purines (Lindahl, 1979) and are arguably of greater consequence to conservation of a nucleotide sequence. In particular, deamination of cytosine can be amplified by a variety of conditions including the presence of *cis-syn* cyclobutane pyrimidine dimers (CPD) at cytosine residues generated in response to exposure to UV light (Tessman and Kennedy, 1991; Lemaire and Ruzsicska, 1993) and, along with the deamination of 5mC, is the proposed mechanism to explain the preferential generation of C → T mutations observed in experimental studies, (Miller, 1985; Brash, 1988; Hsia et al., 1989; Armstrong and Kunz, 1990), epidemiological studies (Dumaz et al., 1993; Ziegler et al., 1994; Wikonkal and Brash, 1999) and the recent analysis of a whole-genome mutation spectrum generated from COLO-829 cells derived from a malignant melanoma metastasis (Pleasance et al., 2010). To mediate the mutagenicity of deaminated cytosine bases, several families of uracil-DNA glycosylases (UDG) exist across all kingdoms that are capable of recognizing and excising uracil from DNA in a variety of contexts (Friedberg et al., 2006). While early studies in *E. coli* revealed a 30x increase in G·C → A·T transitions in *ung* mutants (Duncan and Weiss, 1982), later studies in mice appeared contradictory; *Ung*$^{-/-}$ mice lacked any overt cancer-prone phenotype. Further investigation suggested, however, that SMUG-1 enzyme acts as a replacement UDG in the absence of UNG in mice (Nilsen et al., 2001; 2003). This duplication of enzyme function is not singular. Redundancy in many repair pathways has been described and underlines the importance of DNA repair itself as well as the potential risk to the genome should DNA damage remain unrepaired.

Oxidative stress. The generation of reactive oxygen species (ROS) during normal cellular events including cellular respiration and the immune response is inevitable and the result of essential biological processes without which organism survival would not be possible. In theory, two states exist: one in which homeostasis prevails and ROS is maintained at normal physiological levels by antioxidative pathways and a second in which normal cell function has become dysregulated, resulting in disproportionate concentrations of ROS that could lead to an increase in cellular damage. Important here is that even when a cell is functioning in a normal and expected manner, ROS are generated and therefore biological molecules, including DNA, are at risk for target and damage by those species. Almost 4% of molecular oxygen is incompletely reduced during ATP production and estimates suggest that the superoxide anion radical ($O_2^{\cdot -}$) that follows is normally present at a picomolar concentration and hydroxyl radical ($OH^{\cdot}$) is present at a nanomolar concentration (Hodgson and Smart, 2013). ROS, however, is not solely the product of endogenous processes; it can also be generated as the result of exposure to exogenous agents including air pollution, smoking, UV and ionizing radiation. Due to the ubiquitous nature of ROS as well as the scope of damage it can cause, it has been the subject of great interest.

Of particular risk to DNA is the hydroxyl radical. Generated by either the Haber-Weiss reaction (1) (Haber and Weiss, 1934; McCord and Day, 1978) or the Fenton reaction (2) (Fenton, 1894; Halliwell and Gutteridge, 1992),

$$O_2^{\cdot -} + H_2O_2 \rightarrow O_2 + OH^- + OH^{\cdot} \quad (1)$$

$$Fe^{2+} + H_2O_2 \rightarrow Fe^{3+} + OH^{\cdot} + OH^- \quad (2)$$

it is extremely reactive with a diffusion-limited reaction rate. Thus, it is short lived and generally reacts at the location at which it was generated. The two primary reactions that are precipitated by the radical with DNA are abstraction of hydrogen atoms from the sugar moieties and addition across base double bonds (Cooke et al., 2003; Hodgson and Smart, 2013). $OH^{\cdot}$ can react with all DNA bases and after base radicals are produced, succeeding reactions can generate a multitude of products that vary with local environmental conditions (reviewed in Cooke et al., 2003).

7,8-dihydro-8-oxoguanine. 7,8-dihydro-8-oxoguanine (8-oxoG) (Figure 1.5A, B) is one of the most predominate products generated by the reaction between hydroxyl radicals and DNA bases (van Loon et al., 2010). Hydroxyl radicals are first added to certain carbon atoms positioned on the main ring structure and following the formation of the guanine radical, multiple pathways exist by which the ultimate 8-oxoG molecule can be formed (Boiteux et al., 1992; Kasai et al., 1992; Doetsch et al., 1995; Cooke et al., 2003; Jena and Mishra, 2005). It is not only the guanine bases within DNA, though, that are susceptible to oxidation; dGTP can be modified as well and, if left in the nucleotide pool and selected for incorporation during DNA synthesis, can produce the same net effect as if the guanine bases of the DNA were damaged directly.

The presence of 8-oxoG within DNA is of notable biological relevance due to its remarkable propensity to rotate around the glycosidic bond from the standard *anti* conformation within the DNA helix to the *syn* position which facilitates its pairing with adenine (Figure 1.5C) that can lead to the fixation of a G → T mutation in subsequent rounds of DNA replication (Wood et al., 1990; Shibutani et al., 1991; Cheng et al., 1992). As a result

of this, in concert with the fact that the presence of ROS is unyielding, there has been significant interest in quantifying the concentration of 8-oxoG lesions with cells and current measurements estimate the number of lesions to be on the order of 10^3 per cell in normal tissues with elevated levels present in cancer cells (Yamaguchi et al., 1996; Gedik et al., 2005; van Loon et al., 2010).

As with uracil, the persistence of 8-oxoG within DNA elevates the risk of mutagenesis and so DNA glycosylases able to remove oxidized guanine bases in effort to preclude mispairing with adenine during replication exist. In humans, three enzymes coordinate individual activities to prevent the introduction of G → T mutations (Barnes and Lindahl, 2004). First, in what might be thought of as the most traditional way in which the cell repairs damage, the DNA glycosylase OGG1 catalyzes the cleavage of 8-oxoG from its sugar opposite a correctly paired cytosine base, which allows for the pairing of an undamaged guanine with the cytosine during resynthesis by pol β, pol δ or pol ε (Radicella et al., 1997). Interestingly, another glycosylase is present that, rather than excise the damaged base, removes an incorrectly paired adenine opposite the oxidized guanine base, 8-oxoG. MutY glycosylase homologue (MYH), recognizes 8-oxoG paired with adenine and initiates the base excision repair process ultimately allowing the resynthesis polymerase another opportunity to correctly incorporate dCTP opposite the damaged guanine base and also another opportunity for OGG1 to act on the 8-oxoG·C pair (Slupska et al., 1996). The fact that this somewhat peculiar repair pathway exists suggests the extraordinary frequency with which 8-oxoG is mispaired with adenine. In addition to the DNA glycosylases present within the cell, MTH1, the 8-oxoG-dGTPase, also acts to preserve nucleotide sequence. Its function

is to hydrolyze dGTP to dGMP, which eliminates it from the nucleotide pool (Sakumi et al., 1993). Altogether, these complementary enzymes provide a comprehensive strategy to protect the genome from the possible deleterious effects of 8-oxoG. In support of the importance of the 8-oxoG repair system is the finding that familial inheritance of germline mutations in the *MYH* gene that result in reduced adenine glycosylase activity can give rise to somatic inactivating mutations in the adenomatous polyposis coli (*APC*) gene that may result in the development of colorectal adenomas and carcinoma. Multiple studies have uncovered that the *APC* mutations are overwhelmingly G → T transversions (Al-Tassan et al., 2002; Jones et al., 2002; Sieber et al., 2003).

Ultraviolet radiation. Likely the most ubiquitous mutagen to which humans are exposed is solar UV radiation. More energetic than visible radiation (visible light), but less than X-ray radiation (X-rays), UV comprises UVA (320–400 nm), UVB (280–320 nm) and UVC (200–280 nm). The interaction between UV and the tissue of the skin, cells and DNA is complicated. The wavelength of UV is both indirectly proportional to the energy it carries and directly proportional to the depth with which it can penetrate the skin. Thus, for example, UVA delivers the least amount of energy but penetrates into the dermis. UVB is more energetic that UVA, but only penetrates into the epidermis (Figure 1.6) (Krutmann and Schroeder, 2009). Furthermore, the wavelength also determines the way in which UV interacts with cellular components. Absorption by DNA peaks at 260 nm and is inversely proportional to wavelength. Therefore, DNA more efficiently absorbs UVB than UVA, however UVA is absorbed by other cellular components that can result in the generation of ROS and oxidative stress. Lastly, the composition of UV that reaches the Earth's surface is

not uniformly composed of all three UV types. The ozone layer of the Earth's stratosphere filters most wavelengths above 300 nm and of the remaining UV that reaches the Earth's surface, UVA is much more prevalent (Pfeifer et al., 2005; Friedberg et al., 2006; Garibyan and Fisher, 2010).

Cyclobutane pyrimidine dimers. For over 50 years it has been recognized that exposure to UV can result in the dimerization of adjacent thymine residues as well as the generation of other photoproducts consisting of cytosine and thymine bases (Wacker et al., 1964; Setlow, 1966). Since then, many details have been identified. Specifically, the absorption of UVC and UVB by B-form DNA results most frequently in the dimerization of sequential pyrimidine residues in the form of *cis-syn* cyclobutane pyrimidine dimers (CPD) (Figure 1.7A, B) and, to a lesser degree, pyrimidine-pyrimidone (6-4) photoproducts [(6-4)PP] (Figure 1.7C, D) (Wacker et al., 1964; Pfeifer et al., 2005; Friedberg et al., 2006; Yoon et al., 2010). CPDs are characterized by the formation of a four-member ring between the carbons at positions five and six of adjacent pyrimidine residues (Figure 1.7A) and while six diastereomers are possible, only the *cis-syn* and *trans-syn* forms are generated within DNA due to steric constraints. Moreover, the *cis-syn* form is predominant; the *trans-syn* form is found only in single-stranded or denatured DNA (Ravanat et al., 2001). (6-4)PPs are linked by a single bond between the carbon at position four of one pyrimidine base and that at position six of the next pyrimidine base (Figure 1.7B). CPDs in particular are problematic as a result of their relative abundance, slow repair, propensity to result in mispairing and ability to participate in damage bypass by translesion synthesis polymerases (Pfeifer, 1997; Johnson et al., 2000a; Pfeifer et al., 2005; Biertümpfel et al., 2010).

It has been shown that CPDs occur at specific pyrimidine sequences with varying frequency. Specifically, TT > CT > TC > CC at a ratio of 68:13:16:3 was calculated for plasmid DNA irradiated with UV of 254 nm (Mitchell et al., 1992; Tornaletti et al., 1993). Furthermore, methylation of cytosine amplifies the degree to which UVB is absorbed and results in a 1.7-fold increase in the frequency of CPDs generated at dipyrimidine dimers containing 5mC (Rochette et al., 2009).

While TTDs are by far the more commonly generated CPD, cytosine-containing CPDs are more prone to mutagenesis. *in vitro* studies using *E. coli, S. cerevisiae* and human cells, have consistently demonstrated that irradiation with both UVB and UVC light results in mutations at CPD sequences and that C → T mutations as the result of single base substitution errors are preferentially generated (Miller, 1985; Brash, 1988; Hsia et al., 1989; Armstrong and Kunz, 1990). These findings have been supported by numerous studies to provide a clear causative correlation between UVB exposure and non-melanoma skin cancer (reviewed in Kraemer, 1997; de Gruijl, 1999; Pfeifer et al., 2005; Markovitsi et al., 2013). Unfortunately, however, the chemical synthesis of cytosine containing CPDs has proven exacting due to their instability and while recent advances in developing a synthetic pathway have been made (Peyrane and Clivio, 2013), a completely synthesized product is not yet available.

DNA damage, helix distortions and replication. The presence of DNA lesions such as 8-oxoG and CPDs are problematic for cell survival. During DNA replication the overwhelming majority of DNA synthesis is performed by two replicative polymerases, pol δ and pol ε (Hubscher et al., 2002). These polymerases are able to catalyze nucleotide

incorporation with tremendous accuracy (high-fidelity) and while several factors influence polymerase fidelity, one requirement appears to be the ability to efficiently incorporate correct Watson-Crick base paired nucleotides while rejecting mispaired nucleotides. Pol δ and pol ε, specifically, both possess binding spaces that exclude nucleotides that do not conform to the geometry of the canonical Watson-Crick base pairs, A·T and G·C. While this promotes selectivity in nucleotide pairing during DNA replication, any damage to nucleotides increases the possibility that steric clashes between the nucleotide pair and protein surface will be introduced (Kool, 2002; Kunkel, 2004).

CPDs in particular introduce severe distortions not only to base structure, base chemistry and base-pairing characteristics as discussed previously, but the DNA helix as well. A bend approaching 30° towards the major groove is introduced to the axis and the helix is unwound by approximately 9° (Park et al., 2002). Furthermore, though structural studies of TTDs have revealed that the DNA helix does adapt somewhat to the presence of the lesion and allow for limited hydrogen bonding between the thymine and paired adenine bases when in the *cis-syn* form (Taylor et al., 1990), CPDs still produce significant interruption to canonical B-form DNA.

In contrast, the structural changes in double-stranded DNA due to the presence of 8-oxoG are much more muted. The 8-oxoG base itself is remarkably similar in size and shape to the corresponding undamaged base and retains its aromatic, planar character (Figure 1.5A, B). Early studies failed to identify any significant distortion to the overall structure of the DNA duplex, and base stacking and hydrogen bonding opposite cytosine also appeared essentially unmodified (Cho et al., 1990; Oda et al., 1991; Lipscomb et al., 1995; Plum et al.,

1995; Crenshaw et al., 2011). More recent studies, however, have suggested that subtle structural changes do occur. For example, in agreement with the helix structure observed in crystal structure studies of 8-oxoG damaged DNA in complex with MutM, the bacterial DNA glycosylase responsible for recognizing and excising 8-oxoG from DNA (Sung et al., 2012), it has been suggested that the helix in free double-stranded DNA is slightly unwound 5′ to the damaged base by approximately 7° (Dršata et al., 2013). Furthermore, mutation frequency at 8-oxoG has repeatedly been shown to be affected by sequence context and researchers have proposed that this could be the result of sequence-specific structural changes that affect the repair of and replication fidelity past 8-oxoG lesions (Kamiya et al., 1995; Hatahet et al., 1998; Watanabe et al., 2001). Thus, while the damaged 8-oxoG base clearly is not as destructive to the DNA helix structure as CPDs, it would appear that subtle effects on DNA structure are still plausible.

In total, the presence of damage to DNA bases results in several possible properties problematic to the binding pockets of replicative polymerases that are optimized to tightly fit normal DNA and canonical Watson-Crick base pairs. When replicative polymerases encounter DNA damage such as CPDs, they typically are unable to accommodate the damaged bases in their active sites and this event results in polymerase stalling (Kaufmann, 1989; O'Day et al., 1992). Without a mechanism to facilitate DNA synthesis in the presence of DNA damage, complete genome replication and the necessary transference of genetic information to successive generations would be impossible.

Translesion Synthesis

The evolution of that mechanism, now referred to as translesion synthesis (TLS), seems obvious. Life evolved in the presence of unremitting insult to the genome by DNA damaging agents and while numerous repair mechanisms have also evolved to remove damaged bases from the genome, DNA damaging events can occur at any time including during the process of replication when repair may be difficult or impossible. Now recognized to be a damage tolerance mechanism, an overwhelming amount of effort has contributed to detailing the molecular mechanisms of TLS (Friedberg et al., 2006). Yet, many specifics still remain unclear.

Understanding TLS through in vitro assays. In mammalian cells, while several *in vitro* approaches have been used to establish the presence of TLS activity, many early studies incorporated the innovative use of viral vectors (Williams and Cleaver, 1978; Sarasin and Hanawalt, 1980; Stacks et al., 1983; Clark and Hanawalt, 1984). For example the presence of replication past CPDs was demonstrated using the SV40 infected TC7 cells. By radioactively labeling SV40 infected cells with [^{3}H]dT prior to irradiation with 254 nm UV and then density labeling the same cells with bromodeoxyuridine (BUdR), viral DNA of interest composed of ^{3}H labeled parent strands and ^{3}H-BUdR labeled daughter strands could be recovered by a CsCl density gradient. The labeled DNA was then incubated with T4 endonuclease V, which recognizes CPDs and catalyzes a single-strand break at the 5′ base of the dimer. After separation, the presence of two bands representing both supercoiled and linear DNA from irradiated cells compared to the presence of only supercoiled DNA from

control cells strongly suggested the existence of replication past CPDs after UV exposure (Stacks et al., 1983).

As the use of viral vectors continued to mature, more detailed data became available. With the introduction of *supF* and *lacZ* reporter genes into the SV40 shuttle vector, it was possible to calculate mutant frequencies and detect the introduction of mutations after UV treatment. Sequencing of replication products revealed that G·C → A·T transversions at dipyrimidine sequences predominate and also that CC → TT tandem base substitutions were generated (Carty et al., 1993; Thomas and Kunkel, 1993). In even further evolution, site-specific damage was introduced (Svoboda and Vos, 1995) and most recently, the use of a reporter gene in concert with the introduction of a damaged base in a synthesized DNA oligo and purified proteins made it possible to specifically calculate the rate of polymerase nucleotide misincorporation opposite several types of DNA damage (Kokoska et al., 2003; McCulloch et al., 2004b; McCulloch and Kunkel, 2006; McCulloch et al., 2009). Altogether, the totality of *in vitro* data has provided many important details about the TLS process.

Proposed TLS models. A comprehensive understanding of the TLS process thus far, however, has been elusive and several models have been proposed for the way in which lesions are bypassed (Figure 1.9A-D). In addition to the two replicative polymerases pol δ and pol ε, 15 other enzymes with DNA polymerase activity have been described in humans of which six appear to be predominately in control of TLS. Those polymerases are pol η, pol ι, pol κ and Rev1, which belong to the Y-family polymerases (Figure 1.8) and pol ζ, which belongs to the B-family polymerases (Hubscher et al., 2002; Gan et al., 2008; Sale, 2012; García-Gómez et al., 2013; Sale, 2013). Two models exist to describe the way in which a

damaged base is bypassed. In the first model (Figure 1.9A), a TLS polymerase acts alone to perform both nucleotide insertion opposite the damaged base as well as extension from the damaged base-base pair, presumably to leave a primer-template pair from which pol δ or pol ε can resume synthesis. The most well understood polymerase to operate in this way is likely pol η during the bypass of CPDs (Masutani et al., 1999a; Johnson et al., 2000b; Stary et al., 2003; Cruet-Hennequart et al., 2010; Livneh et al., 2010). It has also been proposed, however, that two or more polymerases may coordinate activities to bypass damaged bases within DNA. In this model (Figure 1.9B) one polymerase is responsible for incorporating a nucleotide opposite a damaged base, while a second extends the initial incorporation (Johnson et al., 2000a; Zhao et al., 2006; Shachar et al., 2009; Livneh et al., 2010; Jansen et al., 2015).

In addition to the two models proposed for the mechanism of lesion bypass, two models have also been proposed for the way in which TLS is integrated into the entire replication process. It has been advanced that TLS may occur directly following the stalling of the replication fork as DNA damage is encountered or, alternatively, via a gap-filling, post-replication mechanism. In the former, responsibility for DNA synthesis is transferred from the replicative polymerase to a TLS polymerase at the replication fork (Figure 1.9C). Using the damaged base as the template, the TLS polymerase then catalyzes DNA synthesis past the damage. After completion of that task, the TLS polymerase disengages and the replicative polymerase continues with replication of the undamaged DNA (Frank et al., 2002; Rechkoblit et al., 2002; McCulloch et al., 2004a; 2004b; 2004c; Wood et al., 2007). In the latter model (Figure 1.9D), a lesion is encountered by a replicative polymerase that

precipitates polymerase stalling. As replication cannot proceed past the lesion, it is restarted beyond the lesion, leaving a gap to be filled in later (Rupp and Howard-Flanders, 1968; Lehmann, 1972; Meneghini, 1976; Heller and Marians, 2006; Lehmann and Fuchs, 2006; Lopes et al., 2006). Important is that while multiple models exist for both the TLS process itself as well as the timing of that process, it is likely that all are important and occur in cooperation to achieve complete replication of the genome.

DNA Polymerase η

Of the TLS polymerases, pol η is probably the most broadly studied and most well understood due to the fact that lack of functional pol η results in the familial cancer syndrome xeroderma pigmentosum variant (XPV) characterized by an increased sensitivity to sunlight and skin cancer (Lin et al., 2006). Further, it is the only member of the Y-family polymerases for which a physiological function has been assigned. Despite that difference, pol η shares several characteristics with the other polymerases of the Y-family. They all lack 3′→5′ proofreading activity, possess low processivity and are, relative to replicative polymerases, error-prone. In addition, the Y-family polymerases share structural homology. Crystal structure solutions exist for each and that homology becomes evident when images of their catalytic cores are generated and aligned (Figure 1.8).

Polymerase η structure, domains and regulatory regions. Pol η is the protein product encoded by the *POLH* (*RAD30*, *XPV*) gene. At 713 amino acids in length and 78 kDa, it comprises an N-terminal catalytic core of 413 amino acid residues as well as a regulatory region in which several protein domains and motifs are located. The catalytic core consists of

four subdomains, three of which (finger, palm and thumb) are components of all DNA polymerases and fourth 'little finger' domain, which is found only in Y-family polymerases (Yang and Woodgate, 2007; Biertümpfel et al., 2010; Yang, 2014). Several contacts located in the thumb and little finger subdomains interact extensively with the DNA substrate while the active site is located within the palm subdomain. Relative to the replicative polymerases, the active site is large, allowing it to accommodate the substantial lesions that characterize DNA damage including TTDs (Biertümpfel et al., 2010; Silverstein et al., 2010).

The C-terminal portion of the polymerase encompasses two PCNA interacting peptides (PIP), a Rev1 interacting region (RIR), an ubiquitin-binding zinc domain (UBZ) and a nuclear localization signal. The PIP domains allow pol η to interact with the eukaryotic DNA clamp/processivity factor, PCNA, which stimulates the activity of the polymerase (Haracska et al., 2001; Yang and Woodgate, 2007; Hishiki et al., 2009; Yang, 2014). To facilitate interaction with ubiquitylated PCNA, the UBZ located at amino acids 628-662 binds ubiquitin and has been shown to be required for the localization of pol η to replication machinery after exposure to UV. Moreover, transfection of XPV cells with pol η possessing a mutated UBZ domain did not successfully rescue cell survival after UV treatment, underscoring the importance of the interaction between pol η and ubiquitylated PCNA to TLS (Bienko et al., 2005; Yang and Woodgate, 2007; Yang, 2014). Evidence suggests that Rev1 is central to TLS and may act primarily as a scaffolding protein and has been shown to interact with each of the primary TLS polymerases, pol η, pol ι, pol κ and pol ζ as well as PCNA (Guo et al., 2009; Waters et al., 2009; Sale et al., 2012). The RIR at amino acid residues 524-539 promotes the interaction between pol η and Rev1 (Pozhidaeva et al., 2012).

The exact function of the pol η-Rev1 interaction remains unclear however, as while XPV cells transfected with a Rev1-interaction deficient form of pol η exhibited an increase in spontaneous mutation rate compared to cells transfected with wild-type polymerase, a change in mutation rate following UV exposure was not observed. This suggests that while a pol η-Rev1 interaction may be important for bypass of spontaneous DNA damage, it is nonessential for UV induced TLS (Akagi et al., 2009).

Discovery of human polymerase η. Pol η was the first human TLS polymerase to be purified and identified. In the early 70's it became appreciated that DNA repair in cells from patients with XP was impaired and that although XP patients displayed similar symptoms, there were differences in the disease phenotype. Further, the rate of DNA repair in the primary cells cultured from patients varied (de Weerd-Kastelein et al., 1972). As complementation studies began to show definitively that XP was, in fact, a group of disorders caused by several related, but distinct deficiencies in excision repair (de Weerd-Kastelein et al., 1972; 1973; 1974; Paterson et al., 1974; Robbins and Kraemer, 1974) there still remained a cohort of patients that presented with classical XP symptoms, but whose excision repair activity appeared intact.

In 1975, however, evidence was generated supporting the idea that a deficiency in what was presumed at the time to be post-replication repair imparted the XPV phenotype. Lehmann et al. carried out pulse-chase analysis using normal, classical XP and XPV cell lines and were able to show that XPV cells were impaired in their ability to convert low molecular weight DNA to high molecular weight DNA after treatment with UV. Moreover, the effect observed was significantly amplified in the presence of caffeine. While the authors

quite clearly stated, “At this stage we do not know the nature of the defective enzyme in the XP variants.”, they did entitle their missive “Xeroderma Pigmentosum Cells with Normal Levels of Excision Repair Have a Defect in DNA Synthesis after UV-Irradiation”. Whether deliberate or not, the title would foreshadow what was to come (Lehmann et al., 1975).

It wasn’t until nearly 25 years later that pol η would be conclusively identified and cloned from the *POLH* gene. Late in the 1990’s, *in vitro* studies using cell-free extracts from XPV cell lines demonstrated the incompetence of XPV extracts for TTD bypass leading to the conclusion that the XPV phenotype was due to the lack of or alteration to TTD TLS (Cordeiro-Stone et al., 1997; Svoboda et al., 1998). Subsequently, pol η was isolated from HeLa cells that complemented the deficiency observed in XPV cell extracts (Masutani et al., 1999a) and shortly thereafter the *POLH* gene was identified and recombinant pol η was generated (Johnson et al., 1999; Masutani et al., 1999b).

Damage bypass by human polymerase η. Since then, a clearer understanding of pol η activity and function has emerged. *In vitro*, it is highly efficient when copying past TTDs and, remarkably, is more efficient when copying TTD damaged DNA than undamaged DNA (McCulloch et al., 2004c). However, it is rather error prone, relative to the replicative polymerases, and has been shown to generate single base substitutions approximately once for every 30 nucleotides synthesized when copying undamaged DNA (Matsuda et al., 2000; 2001). Another interesting feature of TTD bypass is the presence of what has been described as a molecular switch after the observation using *in vitro* lesion bypass reactions that pol η processivity is reduced two nucleotides beyond the 5′T of the TTD. It was suggested that this could be due to steric clashes of the lesion with the polymerase after the lesion moves

downstream of the binding pocket, prompting the disengagement of the polymerase from the DNA substrate (McCulloch et al., 2004c). As the way in which pol η is regulated to prevent excessive mutation introduction is unknown, this was an intriguing finding. In addition to TTD bypass, the polymerase has also been shown to be able to bypass several other lesions including O^6-methylguanine, cisplatin-induced intrastrand crosslinks (cisplatin-GG) and 8-oxoG (Masutani et al., 2000; Haracska et al., 2000a; Zhang et al., 2000a; Haracska et al., 2000b; Levine et al., 2001; Kusumoto et al., 2002; Vaisman et al., 2012). The relevance of *in vitro* bypass data to *in vivo* activity, though, remains unresolved.

The bypass of 8-oxoG by pol η in particular has been the subject of particular interest as the way in which it may be bypassed during replication is unclear. Several polymerases have been shown to be capable of TLS *in vitro*, however the efficiency with which they bypass the damaged base under what would approximate physiological conditions has rarely been determined. Adding further complication is that many human polymerases studied appear to misincorporate dATP frequently which would appear to be incompatible with the large number of 8-oxoG lesions currently proposed to be created per cell, per day (Zhang et al., 2000a; Haracska et al., 2000b; Zhang et al., 2000b; 2001; Haracska et al., 2002; McCulloch et al., 2009; Locatelli et al., 2010). Pol η, specifically, is able to carry out replication past oxidized guanine with greater efficiency than past the corresponding undamaged base, however fidelity studies in which the polymerase is allowed to catalyze DNA synthesis in the presence of all four dNTPs would suggest that, in the absence of any mitigating conditions, the polymerase misincorporates dATP once for every two lesions copied (McCulloch et al., 2009). This is in apparent conflict with some cell-based studies that

suggest pol η is important to mutagenesis suppression. Using human skin fibroblasts and a *supF* shuttle vector treated with methylene blue and visible light to introduce 8-oxoG lesions, it was demonstrated that mutant frequencies increased two-fold compared to control when cells were transfected with siRNA targeting pol η or alternatively, when carrying out the same experiment in pol η deficient XPV cells. Interestingly, though, in the absence of pol η there was not any appreciable change in G → T mutations, nor was there any significant change in the overall mutation spectra, which might be expected should 8-oxoG be bypassed by an alternative pathway with a distinct fidelity profile (Lee and Pfeifer, 2008). Thus, despite the attention 8-oxoG bypass has received, uncertainty remains.

Research Hypotheses and Rationale

While it is patently understood that pol η is responsible for the bypass of TTD and possibly 8-oxoG *in vivo*, the specific details of the process are unclear and the disparity between ostensible poor polymerase fidelity *in vitro* and its clear function in mutation suppression *in vivo* has not been explained. In response, this work provides insight into how the structure of the polymerase stabilizes damaged DNA templates and contributes to its remarkable damage bypass capability as well as how abnormal conditions in which pol η may be operating could affect polymerase activity and function. The intent is to provide greater understanding of DNA damage bypass, pol η fidelity and mechanisms of mutagenesis.

The hypotheses that have guided this work follow:

1. The highly conserved little finger β-strand of polymerase η is important to lesion bypass fidelity and that modification of amino acid residues will result in an increase in polymerase error rate opposite TT dimer and 8-oxoG lesions.
2. The open active site of polymerase η is poor in its ability to discriminate against incorrect nucleotide pairing and thus will be highly sensitive to changes in nucleotide pool concentrations resulting in a change in mutation spectrum when completing lesion bypass.

Figures

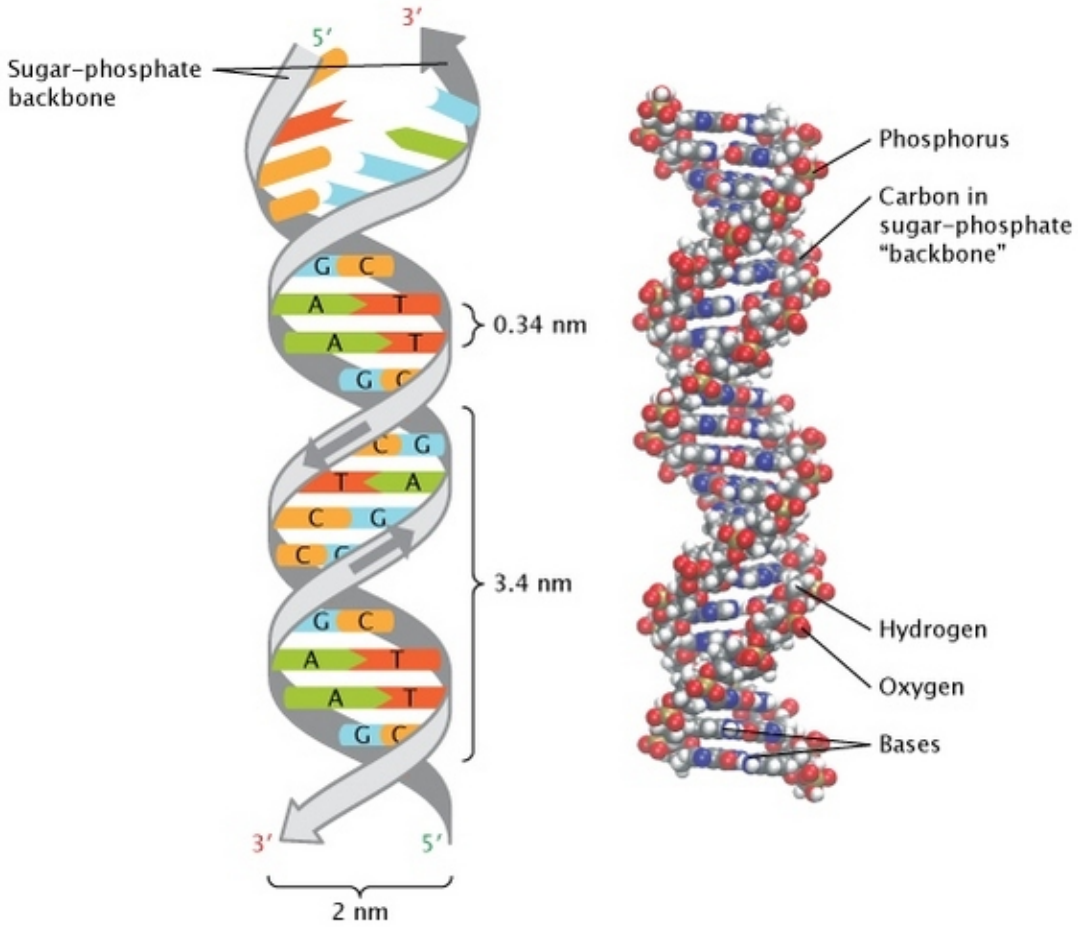

Figure 1.1 Double helical structure of DNA.

Cartoon on the left represents a simplified illustration of the DNA double helix structure. The sugar-phosphate polymer backbone is represented in grey. The 5′ end of one strand is paired to the 3′ end of the other strand. Because of this the strands are antiparallel to one another. Between the sugar-phosphate backbone sit the 4 bases (adenine, A, green; cytosine, C, yellow; guanine, G, blue; thymine, T, red). Image on the right represents a space-filling model of the DNA double helix structure. Hydrogen atoms represented by white spheres, oxygen atoms represented by red spheres, carbon atoms represented by grey spheres, phosphorous atoms represented by gold spheres and nitrogen atoms represented by blue spheres. Legend adapted and image reprinted by permission from Pray, L. A. Discovery of DNA Structure and Function: Watson and Crick. *Nature Education* **2008**, *1*, 100. Copyright 2013 Nature Education. (Pray, 2008).

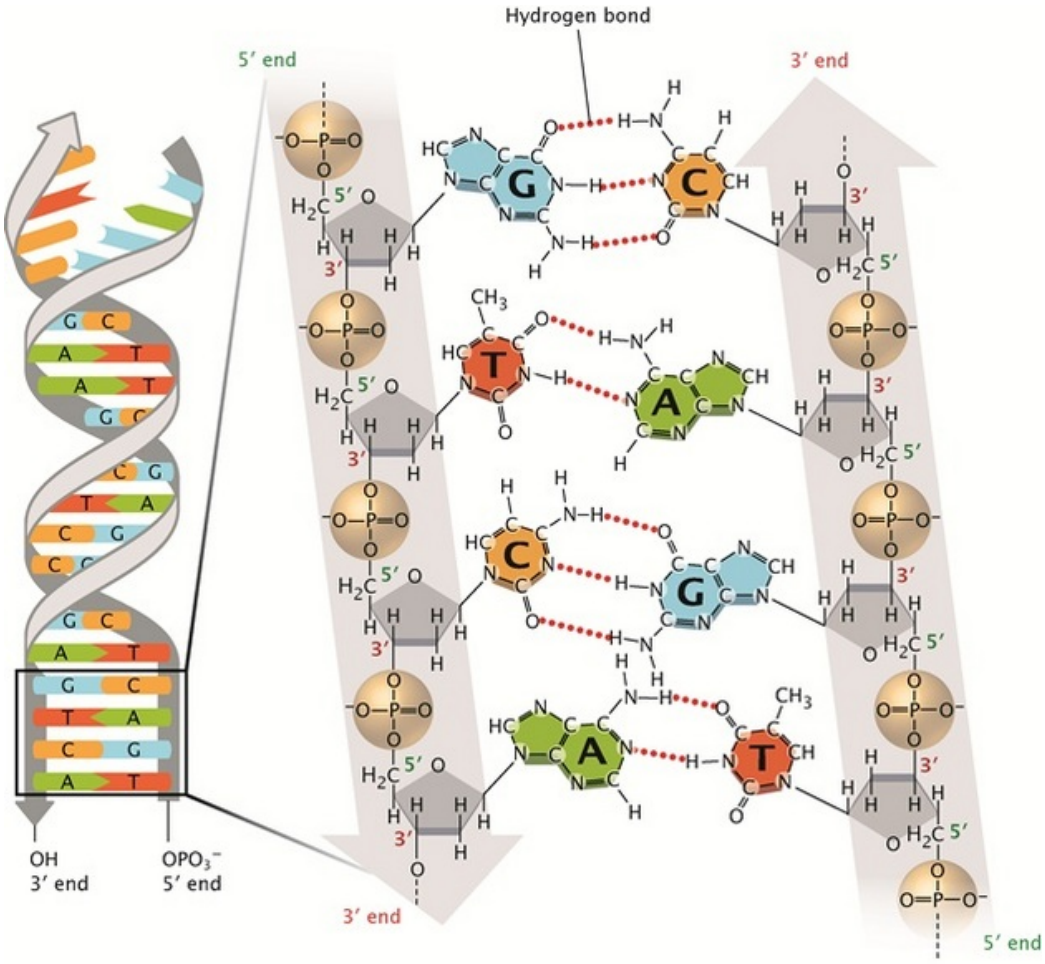

Figure 1.2 Watson-Crick base pairing and hydrogen bonding.

Cartoon on the left represents a simplified illustration of the DNA double helix structure. The sugar-phosphate polymer backbone is represented in grey. The 5′ end of one strand is paired to the 3′ end of the other strand. Because of this the strands are antiparallel to one another. Between the sugar-phosphate backbone sit the 4 bases (adenine, A, green; cytosine, C, yellow; guanine, G, blue; thymine, T, red). Cartoon on the right represents a magnified view of the flattened section from the image on the left and the structural formula of the DNA molecule. Phosphorous are atoms represented by gold spheres, sugars by grey pentagons, bases are colored as follows: adenine, A, green; cytosine, C, yellow; guanine, G, blue; thymine, T, red. Hydrogen bonds represented by dashed red lines. Canonical Watson-Crick base pairs comprise adenine hydrogen bonded with thymine and guanine hydrogen bonded with cytosine. Legend adapted and image reprinted by permission from Pray, L. A. Discovery of DNA Structure and Function: Watson and Crick. *Nature Education* **2008**, *1*, 100. Copyright 2013 Nature Education. (Pray, 2008).

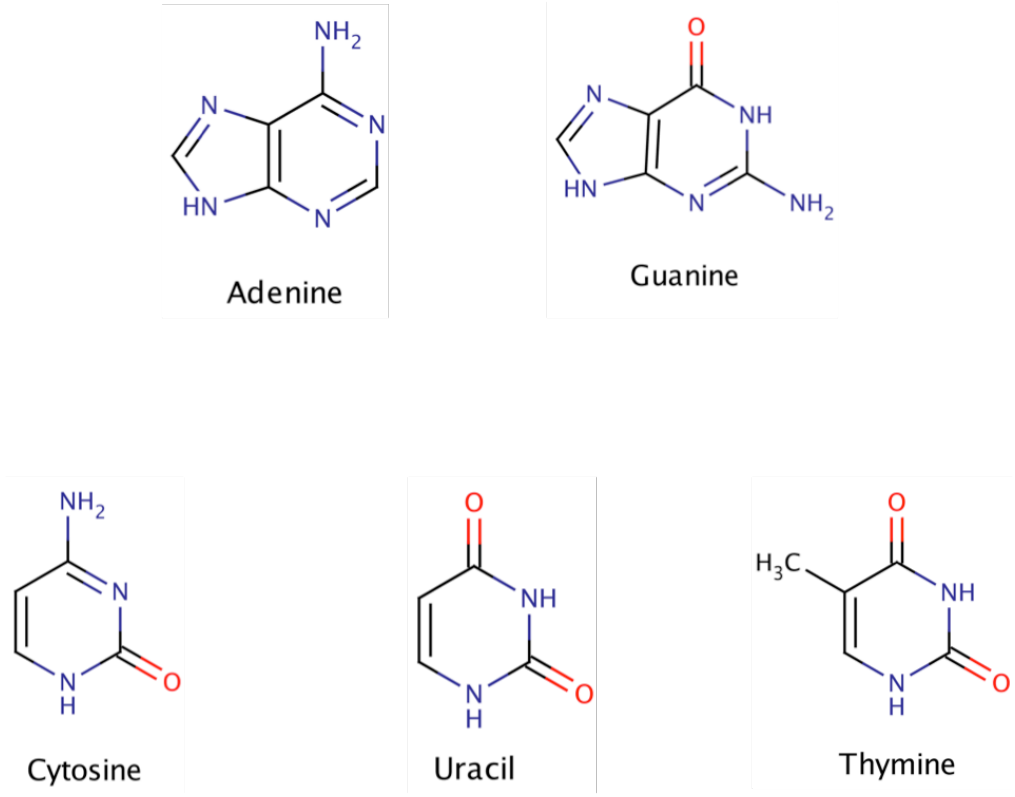

Figure 1.3 Skeletal formulas of DNA bases.

Canonical bases of a DNA molecule include purines, adenine and guanine, and pyrimidines, cytosine and thymine. Uracil is a pyrimidine normally found only in RNA, however it can be found in DNA as a result of misincorporation by DNA polymerases or the deamination of cytosine. MarvinSketch was used for drawing and displaying chemical structures and reactions, MarvinSketch 5.12.1, 2013, ChemAxon (https://www.chemaxon.com/).

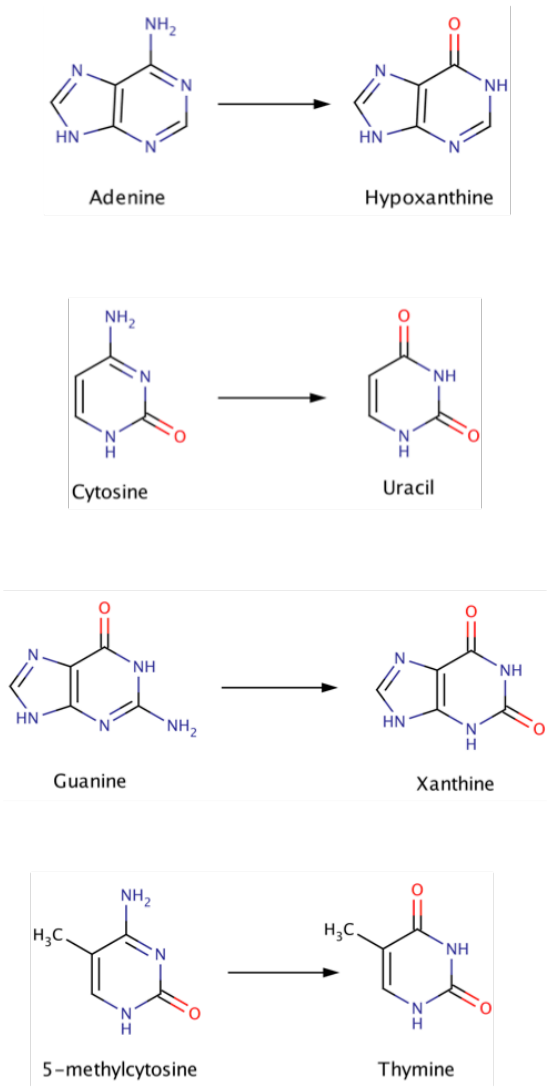

Figure 1.4 Base deamination products.

Adenine, cytosine, guanine and 5mC can undergo deamination reactions in DNA. The product of adenine deamination is hypoxanthine, the product of cytosine deamination is uracil, the product of guanine deamination is xanthine and the product of 5mC deamination is thymine. MarvinSketch was used for drawing and displaying chemical structures and reactions, MarvinSketch 5.12.1, 2013, ChemAxon (https://www.chemaxon.com/).

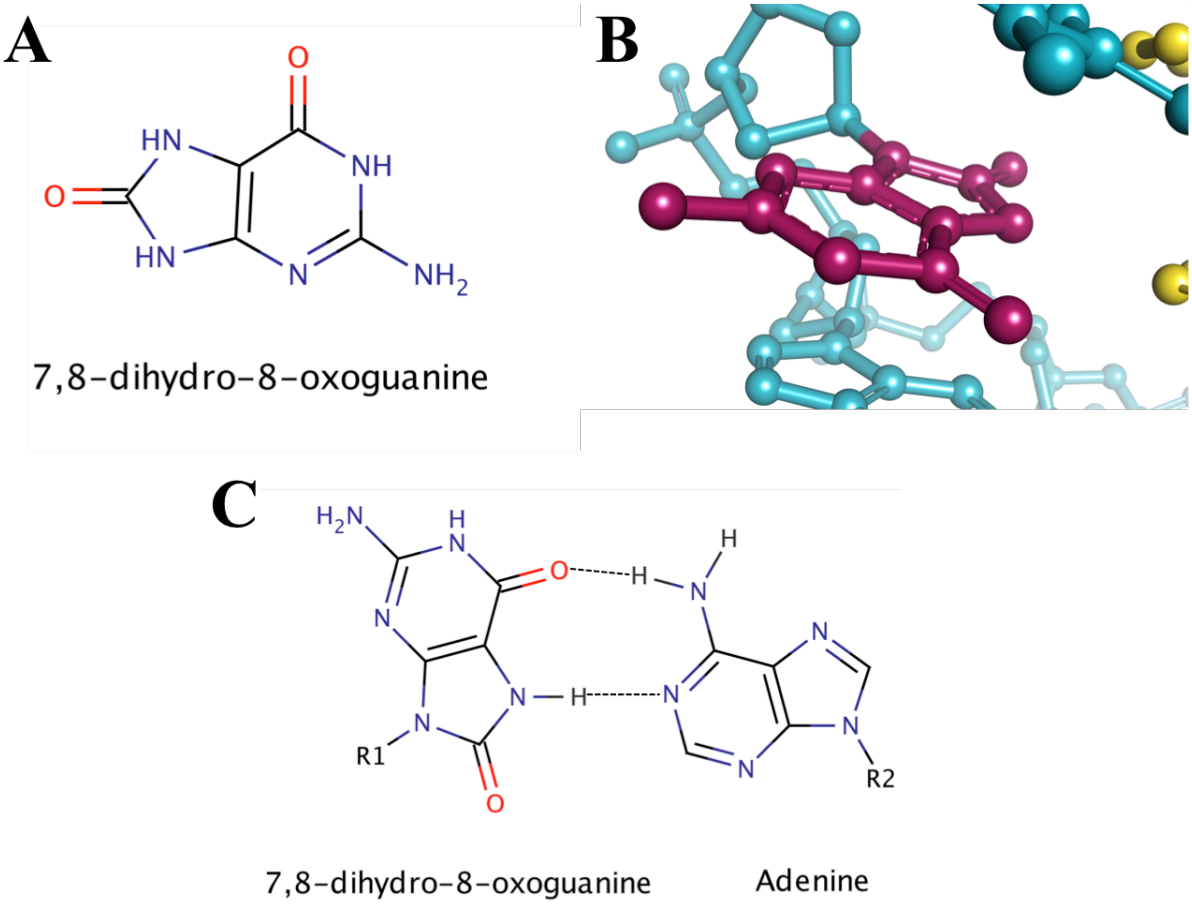

Figure 1.5 7,8-dihydro-8-oxoguanine.

A. Skeletal formula of 8-oxoG. **B.** Molecular structure of oligonucleotide containing chemically modified base 8-oxoG in complex with normal DNA. 8-oxoG is paired with adenine. In both (B) and (D), damaged bases are displayed in dark magenta with the remaining sugar-phosphate backbone and bases represented in cyan. Complementary strand represented in yellow. Image prepared from PDB entry 178D (McAuley-Hecht et al., 1994) using the PyMOL Molecular Graphics System, Version 1.3 Schrödinger, LLC (http://www.pymol.org/). **C.** Skeletal formula of 8-oxoG in *syn* conformation mispaired with adenine. MarvinSketch was used for drawing and displaying chemical structures and reactions, MarvinSketch 5.12.1, 2013, ChemAxon (https://www.chemaxon.com/).

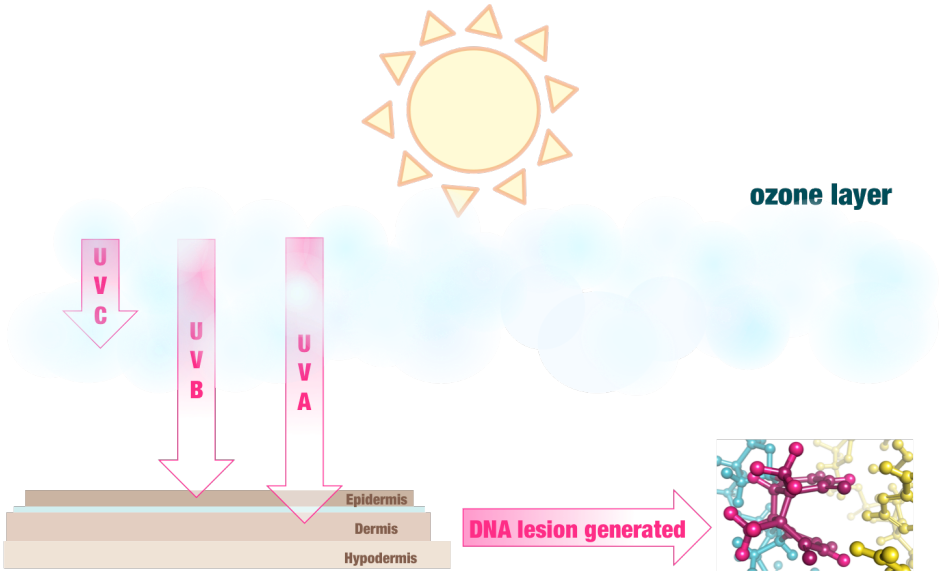

Figure 1.6 Ultraviolet light induces DNA damage.

Cartoon representation of the interaction of UV light with the Earth's atmosphere and human skin. High-energy short wave UVC is primarily filtered by the ozone layer in the stratosphere and therefore does not reach the Earth's surface. Organisms, however, are exposed to less energetic UVB and UVA. UVA delivers the least amount of energy but penetrates into the dermis. UVB is more energetic that UVA, but only penetrates into the epidermis. DNA damage can result from exposure to UV light. A TTD that can be generated from absorption of UVB by DNA is depicted. Damaged bases are displayed in dark magenta with the remaining sugar-phosphate backbone and bases represented in cyan. Complementary strand represented in yellow. Image adapted by permission from Kevin Patton: Lion Den Slide Collection, "UV penetration" (http://www.lionden.com), copyright 1988-2015 Kevin Patton. Image of molecular structure prepared from PDB entry 1TTD (McAteer et al., 1998) using the PyMOL Molecular Graphics System, Version 1.3 Schrödinger, LLC (http://www.pymol.org/).

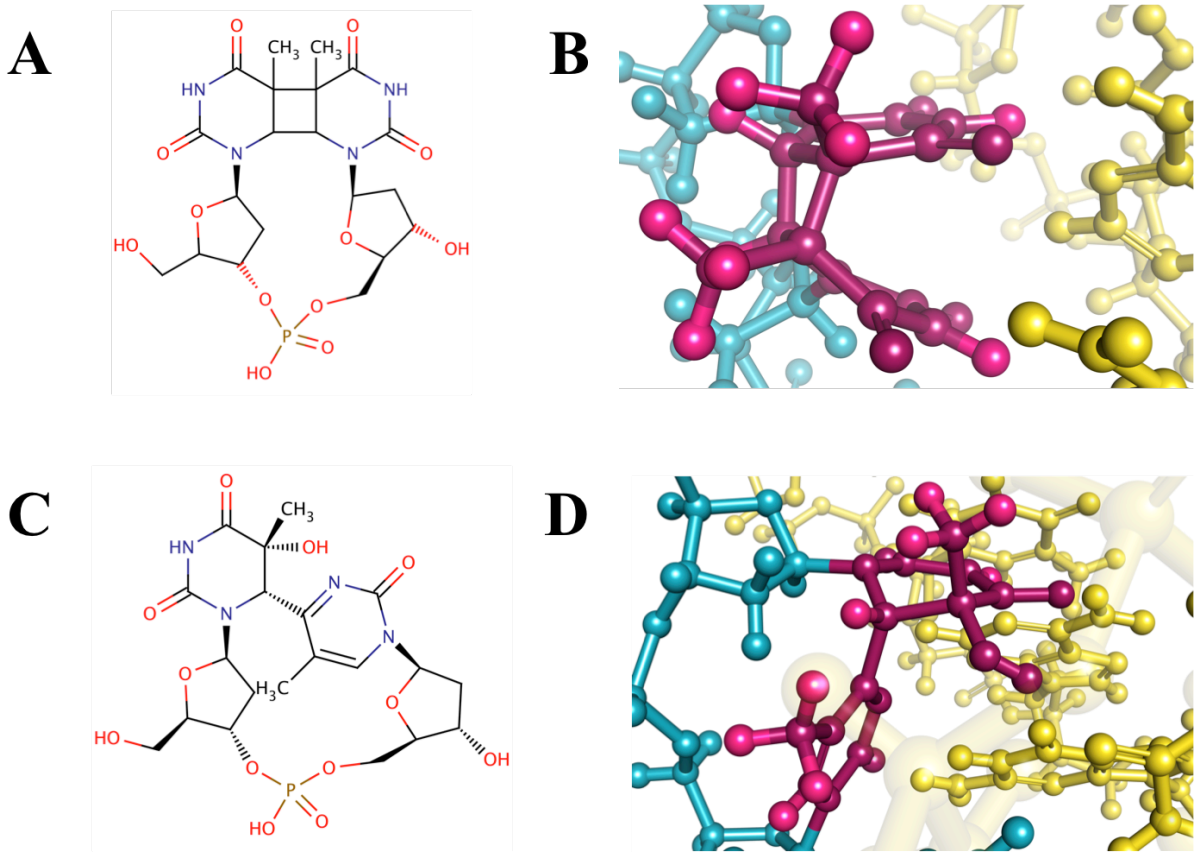

Figure 1.7 UV-induced DNA damage.

A. Skeletal formula of a *cis-syn* thymine-thymine CPD. **B.** Molecular structure of oligonucleotide containing chemically modified base TTD in complex with normal DNA. TTD is paired with two adenine bases. In both (B) and (D), damaged bases are displayed in dark magenta with the remaining sugar-phosphate backbone and bases represented in cyan. Complementary strand represented in yellow. **C.** Skeletal formula of a pyrimidine-pyrimidone (6-4) photoproduct. MarvinSketch was used for drawing and displaying chemical structures and reactions, MarvinSketch 5.12.1, 2013, ChemAxon (https://www.chemaxon.com/). **D.** Molecular structure of oligonucleotide containing chemically modified base (6-4)PP in complex with normal DNA. (6-4)PP is paired with a 3′ thymine base and a 5′ guanine base. Images of molecular structures prepared from PDB entry 1TTD (B) (McAteer et al., 1998) and 1CFL (D) (Lee et al., 1999) using the PyMOL Molecular Graphics System, Version 1.3 Schrödinger, LLC (http://www.pymol.org/).

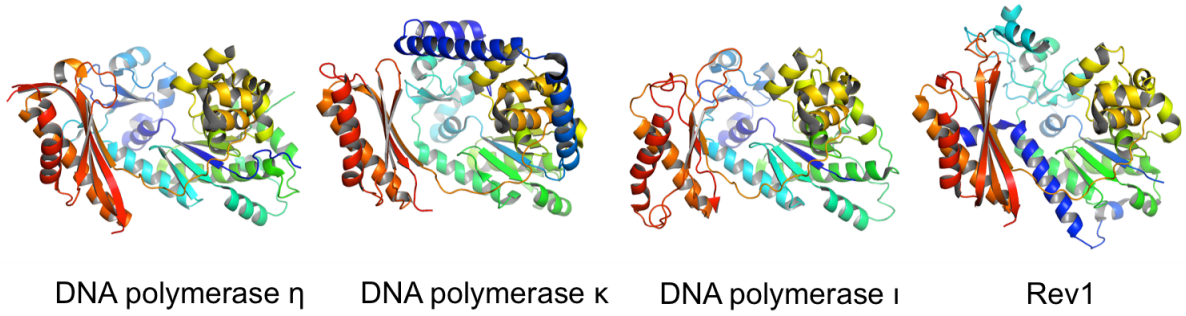

Figure 1.8 Y-family polymerases.

Aligned cartoon images representing structures of human Y-family polymerase catalytic cores generated from crystal structure solution coordinates. Peptide backbones are displayed in rainbow spectra with the N-terminal end displayed in red and the C-terminal end displayed in blue. Images prepared from PDB entry 3MR2 (pol η) (Biertümpfel et al., 2010), 3IN5 (pol κ) (Vasquez-Del Carpio et al., 2009), 1T3N (pol ι) (Nair et al., 2004) and 3GQC (Rev1) (Swan et al., 2009) using the PyMOL Molecular Graphics System, Version 1.3 Schrödinger, LLC (http://www.pymol.org/).

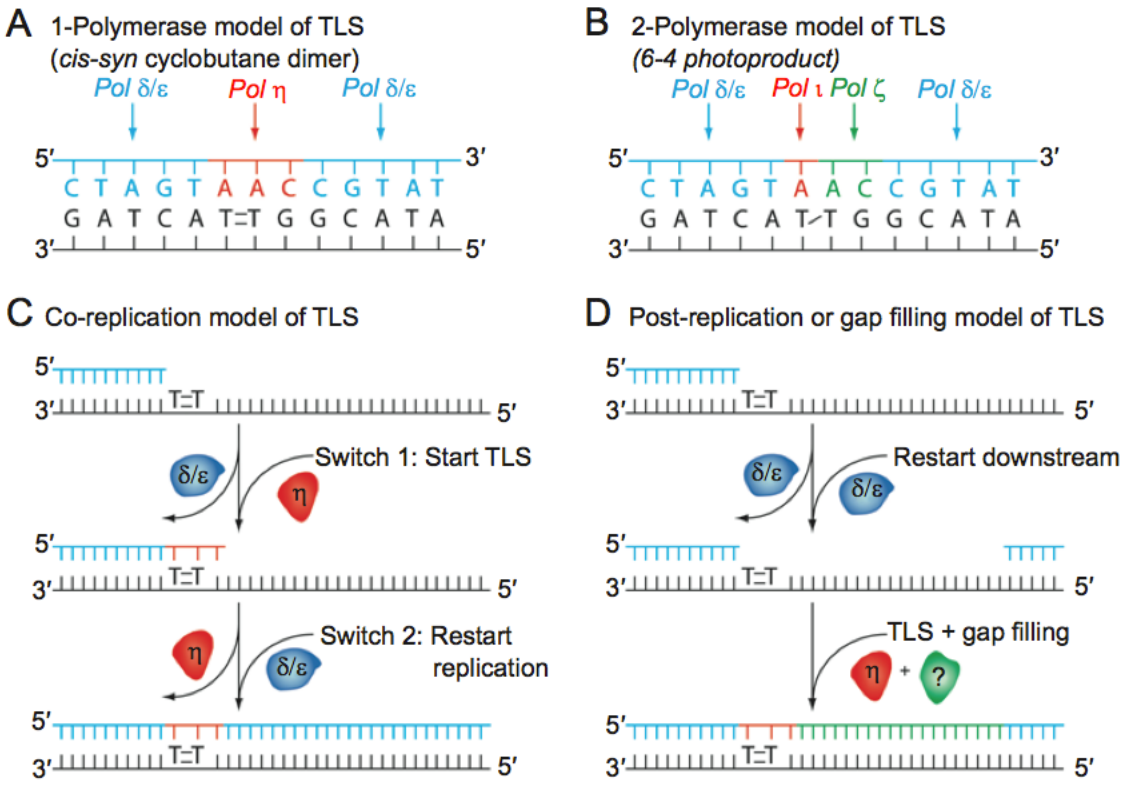

Figure 1.9 Proposed translesion synthesis models

A. 1-polymerase model of TLS. A single TLS polymerase incorporates a nucleotide opposite the damaged base and also extends the damaged base-base pair. **B.** 2-polymerase model of TLS. Two or more polymerases act together to bypass damaged bases. In the example depicted, pol ι is responsible for nucleotide incorporation opposite the 3′T followed by extension/nucleotide incorporation opposite the 5′T as well additional extension beyond the danaged site by pol ζ. **C.** Co-replication model of TLS. A single polymerase binds a primer terminus at a stalled replication fork at a damaged base site. The TLS polymerase completes bypass presumably leaving an undamaged base pair from which a replicative polymerase can resume synthesis. **D.** Post-replication or gap filling model of TLS. Upon the encounter of a damaged base, the replication machinery stalls. Replication is subsequently reprimed downstream, leaving a gap that is replicated thereafter. Note that models represented in both (C) and (D) are compatible with either model depicted in (A) or (B). In addition, the models depicted are not necessarily inconsonant with one another, rather it is likely that they coexist and act together to complete genome replication. Legend adapted and image reprinted by permission from Macmillan Publishers Ltd: Cell Research McCulloch, S. D.; Kunkel, T. A. The Fidelity of DNA Synthesis by Eukaryotic Replicative and Translesion Synthesis Polymerases. *Cell Res* **2008**, *18*, 148–161, copyright 2008. (McCulloch and Kunkel, 2008).

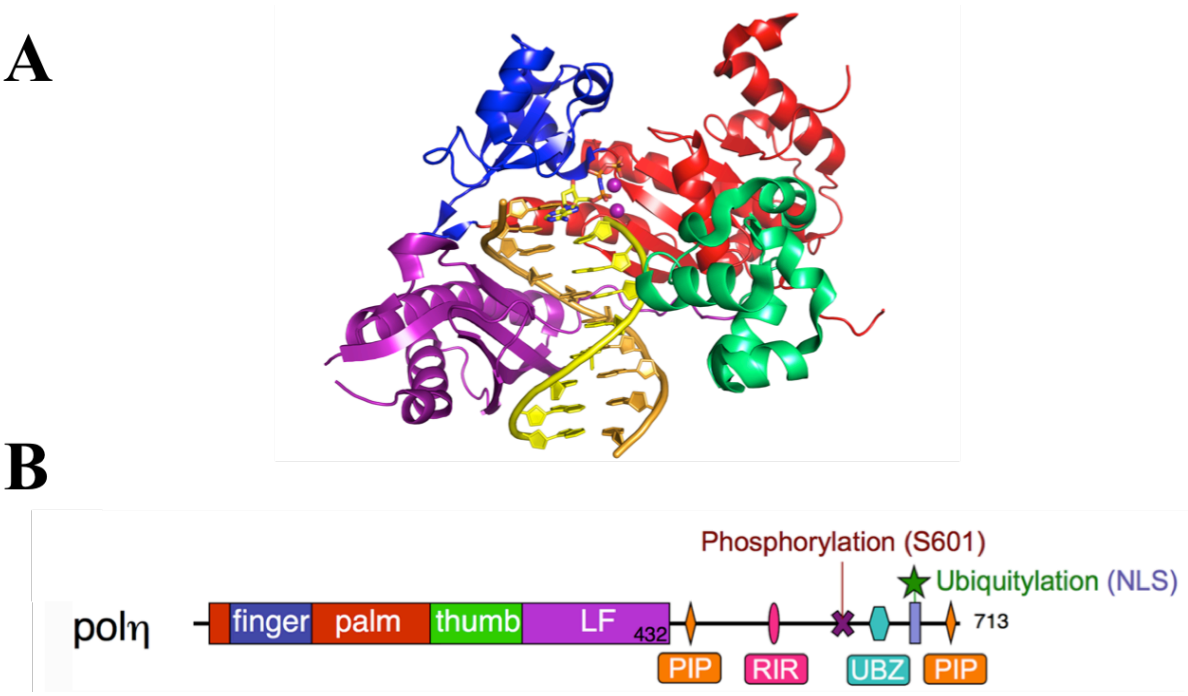

Figure 1.10 Human pol η structure, domains and motifs.

A. Cartoon of human pol η catalytic core structure in complex with normal DNA and incoming dNTP. Finger subdomain represented in blue, palm subdomain represented in red, thumb subdomain represented in green and little finger subdomain represented in purple. DNA template strand is represented in yellow and the primer strand is represented in orange. Incoming dNTP is displayed as sticks (carbon atoms: yellow, nitrogen atoms: blue, oxygen atoms: red, phosphorous atoms: orange) and magnesium atoms are represented as spheres in purple. Images from PDB entry 3MR2 using the PyMOL Molecular Graphics System, Version 1.3 Schrödinger, LLC (http://www.pymol.org/). **B.** Linear representation of functional domains and motifs of human pol η. Legend adapted and image reprinted with permission from Yang, W. An Overview of Y-Family DNA Polymerases and a Case Study of Human DNA Polymerase η. *Biochemistry* **2014**, *53*, 2793–2803.

CHAPTER 2: DNA-POL η LITTLE FINGER DNA CONTACTS ALTER FIDELITY

Originally published as:

Mutation of the Little Finger Domain in Human DNA Polymerase η Alters Fidelity when Copying Undamaged DNA (Beardslee et al., 2013)

Renee A. Beardslee[§], Samuel C. Suarez[§], Shannon M. Toffton[§], Scott D. McCulloch[§⌘]

[§] Department of Environmental and Molecular Toxicology

[⌘]Center for Human Health and the Environment

North Carolina State University, Raleigh, NC 27695

http://onlinelibrary.wiley.com/doi/10.1002/em.21807/abstract

Abstract

DNA polymerase η (pol η) synthesizes past cyclobutane pyrimidine dimer and possibly 7, 8-dihydro-8-oxoguanine (8-oxoG) lesions during DNA replication. Loss of pol η is associated with an increase in mutation rate, demonstrating its indispensable role in mutation suppression. It has been recently reported that β-strand 12 (amino acids 316–324) of the little finger region correctly positions the template strand with the catalytic core of the enzyme. We hypothesized that modification of β-strand 12 residues would disrupt correct enzyme-DNA alignment and alter pol η's activity and fidelity. To investigate this, we purified the catalytic core of the polymerase containing single amino acid changes within β-strand 12 and evaluated them for their DNA synthesis properties. Lesion bypass efficiencies and replication fidelities when copying DNA containing *cis-syn* cyclobutane thymine-thymine dimer and 8-oxoG lesions were determined and compared to the corresponding values for the wild type polymerase. The results confirm the importance of the β-strand in polymerase function and show that fidelity is most often altered when undamaged DNA is copied. Additionally, we show that DNA-protein contacts distal to the active site can significantly affect the fidelity of synthesis.

Introduction

DNA polymerase η (pol η) functions to suppress mutations after exposure to ultraviolet light (Masutani et al., 1999a; 1999b). This is remarkable because its fidelity is low when copying DNA and bypassing the cyclobutane pyrimidine dimers (CPD) created by UV exposure (Matsuda et al., 2000; Johnson et al., 2000b; Matsuda et al., 2001; Washington et

al., 2001a; McCulloch et al., 2004c). In addition to CPDs, biochemical studies demonstrate that pol η can bypass a variety of other lesions, for which the fidelity is varied and poor compared with that of replicative polymerases copying undamaged DNA (Masutani et al., 2000; Zhang et al., 2000a). For example, the in vitro error rate of pol η approaches 50% when replicating past 7,8-dihydro-8-oxoguanine (8-oxoG), a ubiquitous oxidative lesion, despite in vivo evidence that it suppresses mutations caused by the lesion (Zhang et al., 2000a; Maga et al., 2007; Lee and Pfeifer, 2008; McCulloch et al., 2009).

High quality crystal structures of yeast and human pol η bound to undamaged DNA as well as DNA containing *cis-syn* thymine dimers or cisplatin adducts have recently been described and provide a basis for the proclivity of pol η to bypass lesions that stall other polymerases. Specifically, two structural attributes of pol η may contribute to the highly efficient bypass observed (Vaisman et al., 2000; McCulloch et al., 2004c). First, the polymerase possesses a large catalytic center capable of accommodating two template bases simultaneously (Biertümpfel et al., 2010; Silverstein et al., 2010; Zhao et al., 2012; Ummat et al., 2012a). High fidelity polymerases are unable to accomplish this as they kink the phosphate backbone of template DNA 3′ to the template base (Beese et al., 1993; Sawaya et al., 1997; Doublié et al., 1998). This action is impossible with the adjacent bases of CPDs and 1,2-intrastrand cisplatin lesions due to their cross-linked nature. Therefore, while these lesions are unsuitable substrates for the high fidelity polymerases they can be proficiently copied by pol η due to its expansive catalytic site. Second, several intra- and intermolecular forces throughout the catalytic core exist that provide pol η with the unique ability to straighten and maintain DNA in B-form conformation (Biertümpfel et al., 2010). This

buttressing action positions the 3′ hydroxyl so that it is ready for catalysis despite the presence of distortion inducing lesions. Appropriately, Biertümpfel et al. described pol η as a "molecular splint" and linked several xeroderma pigmentosum variant (XPV) mutations to the disruption of this binding surface.

Human pol η β-strand 12, comprising amino acids 316–324, provides several important contacts that contribute to the splinting action of pol η (Boudsocq et al., 2002; Biertümpfel et al., 2010). Located in the Y-family polymerase-specific little finger domain (also called the polymerase associated domain, or PAD) (Trincao et al., 2001), this β-strand is situated almost parallel to the template strand and helps to orient the DNA into the active site by extensively interacting with template strand DNA. Hydrogen bonds extend from both the hydroxyl group of Thr 318 and the amine group of Lys 317, as well as from main chain amide groups to DNA template phosphate residues (Biertümpfel et al., 2010). These interactions reach to template strand DNA that has already been copied (Figure 2.1A). In total, the pol η little finger β-strand has direct contact with 5 template strand bases of newly synthesized DNA downstream of the active site, indicating that it would interact with damaged bases even when the active site is 1–4 nucleotides upstream. We have previously shown the polymerase to preferentially dissociate from DNA 2–4 bases beyond a thymine dimer site after lesion bypass and proposed that this dissociation could be the result of a conformational change (McCulloch et al., 2004c). This is now supported by structural data demonstrating that, when the CPD is located at the -3 position, lesion induced DNA distortion leads to steric clashing and hydrogen bond loss that may be responsible for the

release of polymerase from DNA. These unpropitious interactions provide a mechanism for limiting the activity of such a low fidelity enzyme during replication.

In addition to the interactions between the β-strand and template DNA, hydrogen bonds between Pro 316 and Arg 361 secure the position of the β-strand within the protein. The identification of an R361S missense mutation in a XPV patient highlights the significance of this interaction (Broughton et al., 2002). Because of the apparent importance of β-strand 12 to polymerase function, we performed site-directed mutagenesis to modify several amino acids within this section of the pol η little-finger domain. We studied the effect of these changes on polymerase activity and determined the lesion bypass efficiencies and fidelities of the mutated versions of the polymerase. We have used the results of these biochemical experiments to further characterize the relationship between the structure and function of pol η as well as to impart insight into the molecular mechanism by which pol η performs translesion synthesis (TLS).

Materials and Methods

Materials. Reaction buffer for all assays consisted of 40 mM Tris (pH 8.0), 250 μg/mL bovine serum albumin, 10 mM dithiothreitol, 10 mM magnesium chloride, 60 mM potassium chloride and 1.25% glycerol. Polymerase activity, lesion bypass efficiency and reversion mutation assays were supplemented with all four dNTPs to a final concentration of 0.1 mM each. The gap-filling forward mutation assay was supplemented with each dNTP to a final concentration of 1.0 mM. All cell lines, bacteriophage and reagents for lesion bypass fidelity and forward mutation assays have been previously described (Bebenek and Kunkel,

1995; McCulloch and Kunkel, 2006). DNA sequencing was performed by Genewiz, Inc. (South Plainfield, NJ). Oligonucleotides were purchased from Integrated DNA Technologies, Inc. (Coralville, IA) and The Midland Certified Reagent Company, Inc. (Midland, TX). Nucleotides and restriction enzymes were obtained from New England Biolabs, Inc. (Ipswich, MA).

Expression and Purification of Pol η Little Finger β-strand Mutants. The seven forms of pol η (wild type, P316A, T318A, G320A, G320P, S322A, N324A) were overexpressed and purified as previously detailed (Suarez et al., 2013). Briefly, the vector pET21b-XPV, which codes for the catalytic core amino acids 1-511 of human pol η and includes a C-terminal 6x histidine tag, was utilized. The truncated pol η catalytic core has been shown to retain the same TLS activity as the full-length polymerase (Kusumoto et al., 2002; Biertümpfel et al., 2010). Amino acid substitutions were introduced by use of a QuikChange II XL Site-Directed Mutagenesis Kit (Agilent Technologies, Inc.) and targeted changes were validated by sequencing. Proteins were overexpressed in *E. coli* BL21(DE3) cells and the protein product was purified by affinity chromatography using $NiSO_4$ charged HiTrap™ Chelating HP (GE Healthcare) with subsequent application of pol η enriched fractions to Mono S™ (GE Healthcare) as described (Suarez et al., 2013).

Measurement of Polymerase Activity. Polymerase activity assays were performed as previously described (Nick McElhinny et al., 2007). All reagents were pre-chilled to 4 °C and maintained at 4 °C throughout the assay. Reaction mixtures (60 μL) containing 1.5 μg activated calf thymus DNA (GE Healthcare) and ~10 μCi ^{32}P-α-dCTP (PerkinElmer, Inc.) were initiated by the addition of 150 nM polymerase and incubated at 37 °C for 30 minutes.

11 μL aliquots of reaction mixture were terminated by the addition of an equal volume of 50 mM EDTA and 20 μg glycogen (Roche Diagnostics). 10 μL of stopped reaction mixture was processed in duplicate by the addition of 40 μL ultrapure water and 500 μL 10% trichloroacetic acid (TCA). After incubating on ice for 15 minutes, 500 μL of 5% TCA, 1% sodium pyrophosphate ($NaPP_i$) solution was added and precipitate was collected by vacuum filtration through Whatman GF/C glass fiber filters that were pre-soaked in cold 5% TCA, 1% NaPPi. The precipitate was subsequently washed three times with 5 mL cold 5% TCA, 1% NaPPi and one time with 5 mL 95% cold ethanol by passing the wash solutions through the filters. The filters were removed and dried under a heat lamp. Liquid scintillation counting was used to quantify the amount of ^{32}P-α-dCTP incorporated.

Measurement of Lesion Bypass Efficiency. Lesion bypass efficiency assays have been previously described in detail (Kokoska et al., 2003). Two DNA lesions were assayed: *cis-syn* cyclobutane thymine-thymine dimer (TT dimer/TTD) and 8-oxoG. Substrates used for the bypass efficiency analysis were created by annealing a Cy5-labeled primer strand to a template strand (5′-Cy5-AATTTCTGCAGGTCGACTCCAAAGGC-3′ to 5′-CCAGCTCGGTACCGGGTTAGCCTTTGGAGTCGACCTGCAGAAATT-3′ for TT/TT dimer reactions where the underlined TT is either a thymine pair or a TT dimer and 5′-Cy5-GCAGGTCGACTCCAAAG-3′ to 5′-TCGGTACCGGGTTAxCCTTTGGAGTCGACCTGC-3′ for G/8-oxoG reactions where x represents either guanine or 8-oxoG). Reaction mixtures (30 μL) containing 670 nM DNA substrate were initiated by the addition of polymerase and incubated at 37 °C. Concentration of polymerase in reaction mixtures varied from 1.7–67 nM in G/8-oxoG reactions and 2.2–

110 nM in TT/TT dimer reactions. 6 μL aliquots of reaction were removed at 2, 4 and 6 minutes, quenched by adding an equivalent volume of 95% formamide, 25 mM EDTA (formamide loading dye) and separated by electrophoresis on a denaturing 10% polyacrylamide gel. Products were imaged with a Storm™ 865 imager (GE Healthcare) and quantified using Image Quant™ TL software (GE Healthcare). Values for termination probabilities, bypass probabilities and efficiencies and primer utilization were calculated as described elsewhere (Kokoska et al., 2003).

Reversion Mutation Assay and Analysis for Fidelity of Lesion Bypass. Analysis of lesion bypass fidelity was carried out as reported previously (McCulloch and Kunkel, 2006). Two DNA lesions were assayed: TT dimer and 8-oxoG. Substrates used for the lesion bypass assay were created by annealing a primer strand to a template strand (5′-Cy5-AATTTCTGCAGGTCGACTCCAAAGGC-3′ to 5′-AGGAAACAGCTATGACCATGATTACGAATTCCAGCTCGGTACCGGGTTAGCCTTTGGAGTCGACCTGCAGAAATT-3′ for TT/TT dimer reactions where the underlined TT is either a thymine pair or a TT dimer and 5′-Cy5-AATTTCTGCAGGTCGACTCCAAAG-3′ to 5′- CCAGCTCGGTACCGGGTTAxCCTTTGGAGTCGACCTGCAGAAATT-3′ for G/8-oxoG reactions where x represents either guanine or 8-oxoG). Reaction mixtures (30 μL) containing 330 nM DNA and ~50 μCi ^{32}P-α-dCTP were initiated with 170 nM polymerase and incubated for 30 minutes at 37 °C. The 75-mer reaction products (TT/TT dimer) were digested with *Pst*I and *Eco*RI and the 45-mer reaction products (G/8-oxoG) were digested with *Pst*I. An equal volume of formamide loading dye was added to prepare the samples for separation by electrophoresis on a denaturing 10% polyacrylamide gel. Newly synthesized

strand was recovered and annealed to M13 gapped circular DNA. Annealed DNA was transformed into *E. coli* strain MC1061 cells and plated in a soft agar overlay atop a layer of CSH50 cells. The lesions are located within an amber stop codon in the *lacZα* gene sequence. Correct synthesis results in preservation of the amber stop codon and thus complementation of the N-terminally truncated *lacZ* gene in CSH50 does not occur, which generates plaques with a light blue phenotype. Errors generated when copying the stop codon result in a functional *lacZα* gene and dark blue plaques are produced. Plaques were counted and assessed for color phenotype to determine mutant frequencies and DNA from individual colonies was amplified using Illustra™ TempliPhi (GE Healthcare) and sequenced to determine the spectrum of changes. Error rates were calculated as described (Kokoska et al., 2003; McCulloch and Kunkel, 2006).

Gap-filling Forward Mutation DNA Synthesis Reactions. The creation of the M13mp2 (WT2) gapped DNA and the gap-filling assay were carried out as detailed previously (Bebenek and Kunkel, 1995). Reactions (20 μL) contained 3.9 nM gapped M13mp2 (WT2) DNA. Polymerase concentrations varied from 75 nM to 1.3 μM. Reactions were incubated at 37 °C for 1 hour and products were separated by 0.8% agarose gel electrophoresis to verify complete filling. DNA from reactions was transformed into *E. coli* strain MC1061 cells and plated as described above. Errors in synthesis by pol η result in the inability of the *lacZα* translated gene product to provide complementation to the LacZα deficient cells, causing a change from dark blue to light blue or colorless plaques. Resultant plaques were counted and scored for color phenotype to determine mutant frequency. DNA

from individual plaques was amplified and sequenced as described above. Error rates were calculated as described (Bebenek and Kunkel, 1995).

Results

Generation of Pol η Little Finger β-strand Mutants. Amino acids in the β-strand (β-strand 12; residues 316–324) in the little finger region of pol η were selected for mutation based on the observation that this region of the polymerase is important to correctly position the DNA template strand with the catalytic core of the enzyme (Biertümpfel et al., 2010; Ummat et al., 2012b). This β-strand interacts extensively and assumes a nearly parallel alignment with the DNA template strand via hydrogen bonds including those that extend from amide hydrogen atoms in the protein backbone to oxygen atoms of DNA template phosphate groups (Biertümpfel et al., 2010) (Figure 2.1A). To study the role of this β-strand in polymerase function, we purified a truncated fragment of human pol η (amino acids 1–511) that was overexpressed in *E. coli*. We generated wild type enzyme and individual single amino acid substitutions at residues Pro 316, Thr 318, Gly 320, Ser 322 and Asn 324. At each position, alanine was substituted for the wild type residue. We also generated a sixth variation in which Gly 320 was replaced with proline, hypothesizing that such a drastic change in the middle of the β-strand would significantly affect polymerase function. In each case, the protein purification resulted in the production of an abundantly pure protein (Figure 2.1B). All seven protein preparations were assayed for both polymerase and exonuclease activity. As pol η is an exonuclease-deficient polymerase, uncontaminated purifications should not exhibit any exonuclease activity. As expected, none of the purified samples

displayed any detectable mismatched (A:G) primer terminus exonuclease activity (data not shown).

Activity of Pol η Little Finger β-strand Mutants. The overall polymerase activity of each preparation of pol η was measured using incorporation of ^{32}P-α-dCTP during in vitro DNA synthesis on activated calf thymus DNA, followed by TCA precipitation and scintillation counting. Although most of the mutated forms of pol η retained ample activity, we observed a decrease relative to that of wild type in all cases (Table 2.1). The activities of P316A, G320A, S322A and N324A were 56–66% of the wild type value. The activity of T318A was further diminished (33% activity compared to wild type), while the activity of G320P was nearly abolished (7% activity compared to wild type). Because of the exceedingly low activity of G320P, the results of further analysis of this mutant is not presented.

Bypass Efficiency of Pol η Little Finger β-strand Mutants Past TTD and 8-oxoG. Next we measured the efficiencies with which the wild type and mutated forms of pol η bypassed both TTD and 8-oxoG lesions. To do this, we used an *in vitro* primer extension assay (Figure 2.2A) in which the substrate was in sufficient excess to ensure that when a given substrate molecule was extended by polymerase, additional extension events on the same substrate did not occur. Thus, the assay allows for analysis of a single interaction between substrate and polymerase. By performing running-start reactions with both undamaged and damaged templates, we can determine the efficiency with which pol η copies damaged DNA. Pol η exhibits very low processivity. At the 6-minute time point all forms evaluated had incorporated no more than 5–8 nucleotides when bypassing the TTD and 7–12

nucleotides when bypassing 8-oxoG (Figure 2.2B, C). The efficiency with which wild type pol η was able to bypass the TTD lesion was 140% (Table 2.1). These data indicated that wild type pol η was more likely to bypass the lesion than it was to copy equivalent undamaged DNA. This is similar to published results for full-length pol η (McCulloch et al., 2004c). All the β-strand mutants also bypassed the TTD lesion with greater than 100% efficiency (Table 2.1). To consider a lesion bypass efficiency value materially different from that of wild type, we require, at minimum, a two-fold change. None of our mutants were significantly different from wild type by this measure. So while these mutants do have reduced overall activity, their ability to bypass a TT dimer remains unaffected.

The efficiency with which wild type pol η was able to bypass an 8-oxoG lesion was 93% (Table 2.1). This is only slightly lower than published results using full-length pol η (McCulloch et al., 2009). The efficiencies of P316A and S322A were 150% and 180%, respectively (1.6 and 2.0 fold increases compared to wild type), which would suggest that these forms bypass this lesion better than wild type polymerase. N324A bypassed 8-oxoG with approximately the same efficiency as wild type (92%; no change) and T318A and G320A showed slightly decreased bypass efficiencies compared to wild type (75%, 80%; 0.8 and 0.9 fold changes, respectively). These values indicate that bypass efficiencies of 8-oxoG by the mutated forms of pol η remain effectively equivalent to that of the wild type polymerase. That is, bypass remains robust despite overall reduced polymerase activity. In total, we find that none of the pol η mutants presented in this bypass efficiency analysis displayed any significant change in their TTD or 8-oxoG lesion bypass ability when compared to wild type polymerase.

Fidelity of Pol η Little Finger β-strand Mutants when Copying TTD and 8-oxoG. To determine the fidelities with which the mutated forms of pol η bypass TTD and 8-oxoG lesions we used an in vitro reversion mutation assay. The substrate sequence matched that used in the efficiency assay and corresponded to a portion of the *lacZα* gene. A premature stop codon that contained the lesion under investigation was present within the sequence. Insertion of the correct nucleotide opposite the lesion preserved the stop codon, while an incorrect insertion at the lesion resulted in reversion to a viable *lacZα* sequence. After extension by the polymerase, the synthesized strand was recovered, annealed to gapped M13mp18 DNA and transformed into E. coli. Resultant M13 phage plaques containing DNA in which replication errors were made at the stop codon were identified by their dark blue phenotype. DNA from these plaques was then amplified and sequenced to determine polymerase error rates and spectrums.

The error rates calculated for the bypass of both TTD and 8-oxoG indicate that the mutated forms of pol η can be broadly categorized into two distinct groupings (Figure 2.3A-D). The first includes mutants that showed no appreciable difference in fidelity when copying either lesion and also had error rates essentially the same as wild type when copying the corresponding undamaged DNA sequence. For this assay, we define an error rate as unchanged when the rate of the mutated polymerase exhibits a fold change of less than 2 when compared to that of wild type (i.e. 50% to 200% the wild type rate). In contrast, a second group of pol η β-strand mutants had error rates unchanged from wild type when bypassing either lesion, but their fidelities were substantially altered when copying the comparable undamaged sequence. Surprisingly, all of these mutants had better fidelities than

the wild type protein. Thus, modification of certain amino acid residues in the little finger β-strand did in fact affect the fidelity of the polymerase, but the effect was limited to the replication of undamaged DNA and surprisingly resulted in an increase in fidelity.

T → C Transitions at the 3′T of TTD. Misincorporation of dGMP opposite thymine (either as part of a TT dimer or as undamaged DNA) causing a T → C mutation is the most frequent error made by pol η (Matsuda et al., 2000; Johnson et al., 2000b; Matsuda et al., 2001; McCulloch et al., 2004c). The error rates for T → C at the 3′T of the dimer sequence by wild type polymerase for either TTD or corresponding undamaged templates were comparable (220 and 270 × 10^{-4}, respectively) (Figure 2.3A, B), in agreement with the values observed using full-length pol η (McCulloch et al., 2004c). The mutated forms of pol η with amino acid changes proximal to the active site, S322A and N324A, exhibited error rates that were not appreciably different when copying past either damaged or undamaged thymine bases (Figure 2.3A, B). The error rates for S322A copying TTD and undamaged templates were 0.9 fold and 0.6 fold the wild type rate while for N324A they were 0.8 and 0.8 fold the wild type rate (TTD and undamaged templates, respectively).

When the amino acid changes were distal to the active site, the mutated polymerases exhibited error rates that were comparable to wild type for TTD bypass. The TTD 3′ T → C error rates were essentially unchanged compared to wild type for P316A, T318A and G320A (0.9, 0.7 and 1.1 fold changes, respectively), with the greatest effect on TTD bypass fidelity for any of the mutated forms of pol η occurring when residue T318 was altered. But unlike S322A and N324A, when copying undamaged DNA the error rates for these mutants were decreased compared to wild type. That is, their fidelities were much better. The undamaged

3′ T → C error rates for P316A (83×10^{-4}), T318A (79×10^{-4}) and G320A (67×10^{-4}) were all reduced at least 3 fold compared to wild type (Figure 2.3A, B).

G → T Transversions at 8-oxoG. While T → C changes are common with pol η, G → T (misinsertion of dAMP opposite G) changes when copying undamaged DNA are much less frequent, but increase markedly when copying 8-oxoG (Zhang et al., 2000a; McCulloch et al., 2009). The rate of dAMP misincorporation opposite G was 14×10^{-4} for wild type polymerase (Figure 2.3D). When bypassing the corresponding oxidized base, 8-oxoG, the error rate increased to 3900×10^{-4} (Figure 2.3C). The overall trend in error rates observed for the bypass of 8-oxoG by the mutated forms of pol η was very similar to that observed for TTD bypass. Changes in amino acid residues closest to the active site did not have a significant effect on the fidelity of the polymerase when copying either the damaged or the undamaged base. In the case of 8-oxoG bypass, this included not only S322A and N324A, but also G320A. When bypassing 8-oxoG, we observed only a slight increase in error rates for these forms of pol η (1.4, 1.1 and 1.2 fold changes for G320A, S322A and N324A, respectively). The rates of misincorporation opposite guanine did not differ significantly from that of wild type (0.7, 0.5 and 0.8 fold changes for G320A, S322A and N324A, respectively). Similar to what we observed with TTD bypass, amino acid changes distal to the active site resulted in no change in fidelity when copying 8-oxoG, but did affect synthesis of undamaged DNA. The error rate for P316A opposite 8-oxoG was slightly increased (5100×10^{-4}, 1.3 fold change compared to wild type) and slightly decreased for T318A (3300×10^{-4}, 0.8 fold change). However, when copying G, the error rates for both forms of pol η were distinctly decreased (3.0×10^{-4}, 0.2 times the wild type rate for both).

Single Base Substitutions at Undamaged Stop Codon. Because of the unexpected increase in fidelity on undamaged DNA by certain pol η mutants, we also calculated error rates for total single base substitutions at the undamaged TAG stop codon as well as all other individual single base substitutions detectable by this assay. The total overall base substitution error rate for wild type pol η was 400×10^{-4} (Figure 2.3E). The mutated forms of pol η exhibited a similar trend as was observed for the T → C and G → T single base substitutions. That is, S322A and N324A had error rates that were not significantly different from wild type (0.6 and 0.9 fold changes, respectively). However, significant changes in fidelities were observed for the forms of pol η that possessed amino acid residue changes distal to the active site. The overall error rates for P316A, T318A and G320A were 130, 92 and 100×10^{-4} (0.3, 0.2 and 0.3 the rate of wild type, respectively). It is interesting that while changes in pol η fidelity were not observed when bypassing either lesion, we did consistently observe changes when the polymerase was acting on undamaged DNA. Furthermore, the effect was most remarkable when the changes in amino acid residues were located in the region of the DNA that stabilizes the newly synthesized duplex, rather than the region stabilizing the template near the incoming dNTP.

This trend in error rates for the mutated forms of pol η when compared to wild type generally held for all other possible single base substitutions. The error rates for P316A, T318A and G320A were reduced by 50% or more compared to wild type for all combined nucleotide mispairs at A, at G and at T (G·dTMP mispairs are not detected by this assay as they result in a TAA ochre stop codon). The error rates for the remaining forms, S322A and N324A, did not deviate significantly from wild type. We did observe that the change in

fidelity was most often the greatest for T318A (Table 2.2). The T318A error rate for all combined mispairs at A was 0.2 that of the wild type rate, 0.1 for mispairs at G and, as previously noted, 0.2 for total overall single base substitutions. For combined mispairs at T, G320A had the greatest decrease; the error rate was 0.2 that of the wild type rate. For the same changes, the error rate for T318A was 0.3 times the wild type rate.

Generation of Single Base Substitutions During Gap-Filling DNA Synthesis. To further understand how mutating residues in β-strand 12 of the little finger region of pol η affects fidelity, we used a forward mutation assay that can evaluate all possible single base substitutions as well as insertions, deletions and other complex errors made by the polymerase. In this assay, the polymerase replicates a 407 base gap located in the *lacZα* complementation sequence present in bacteriophage M13 DNA. Upon transformation into *E. coli* containing non-functional N-terminally deleted LacZ protein, faithful replication of the template sequence results in dark blue plaques while low fidelity replication results in a light blue or colorless phenotype. A colorless phenotype is usually the result of frameshift mutations, but can also correspond to multiple mutations made by the polymerase during synthesis of a single gapped molecule. By selecting mutant plaques for sequencing we are able to observe the types of mutations created by the polymerase and calculate error rates. Although the overall differences observed between the mutated forms of pol η and wild type were not as great as those from the reversion assay, the same trends appear. That is, when changes in amino acid residues in the β-strand occur farther away from the active site, a greater decrease in error rate was generally observed. Of the 5 mutated forms of pol η that were able to fill the gap, P316A and T318A had the greatest decreases in overall single base

substitution error rate (0.7 and 0.6 fold changes, respectively) (Figure 2.4A). G320A, S322A and N324A had fold changes of 0.8, 0.9 and 0.9, respectively. T318A exhibited the greatest decrease in error rate at each individual template base when compared to wild type in nearly all cases. The error rate at A was 0.5 times the wild type rate, 0.8 times at G and 0.7 times at T. For mispairs at C, P316A had the greatest decrease (0.4 times the wild type rate).

Tandem Base Substitutions, Complex Mutations, Insertions and Deletions. The forward mutation assay also allowed us to calculate error rates for a variety of other replication errors. A common replication error made by pol η is the incorporation of 2 sequential mispairs resulting in a tandem base substitution (Matsuda et al., 2000; 2001). Like full-length pol η, we observed these types of errors in all of the mutants studied. As has been already described, we found that the greatest reductions in error rates were observed when amino acid residues distal to the active site were altered. The tandem base error rate for the wild type polymerase was 6.9×10^{-4} (Figure 2.4B). We observed a 0.1 and 0.3 fold change in error rates for P316A and T318A, respectively, a 0.8 fold change for G320A and a 1.7 and 1.4 fold increase for S322A, and N324A, respectively, when compared to wild type. The results for other complex error rates were similar. We define complex errors to include insertions and deletions of two or more bases, single base substitutions separated by one correctly copied base, two or more consecutively mispaired bases and/or any combination thereof. The complex mutation error rate for the wild type polymerase was 15×10^{-4} (Figure 2.4C). The observed error rates for P316A and T318A were significantly decreased (0.2 and 0.3 fold changes, respectively), while the rate for G320A was unchanged compared to the wild type polymerase. Surprisingly, when amino acid residues S322 and N324 were mutated,

there was a nominal increase in the number of complex mutations detected. We calculated a 1.6 fold increase in the error rate for S322A and a 1.9 fold increase for N324A relative to wild type polymerase.

In general, we did not observe any significant change in the rate of insertions or deletions made by the mutated forms of pol η compared to wild type (Figure 2.4D, E). The only notable observation was the insertion error rate of T318A. As noted for other types of changes made by the mutated forms of pol η, the decrease in error rate for insertions was greatest for T318A. The wild type insertion error rate was 6.1×10^{-4}, while the rate of the T318A form was 1.0×10^{-4}.

Discussion

Mutating residues in the little finger β-strand 12 of pol η that stabilizes the DNA template strand provides clues to help understand the ability of the polymerase to bypass lesions. Specifically, our results show that the polymerase is able to tolerate minor alterations in its structure and still perform lesion bypass robustly. The observation that the fidelity of bypass is still relatively low (error frequencies of 3-5% for TT dimer; 50% for 8-oxoG) suggests two things. One, pol η seems ideally suited for performing bypass of these lesions because its structure not rigidly constrained to a single conformation. And two, its propensity for introducing errors during lesion bypass is a result of this same flexibility.

Of the residues tested, Thr 318 appears to be distinct and especially important to pol η fidelity. It was somewhat surprising that mutating T318 and adjacent residues affected fidelity as they did, given their distant location from the polymerase active site. Considering

the importance of pol η in lesion bypass, it was also unexpected to observe that mutating residues in this region had a much greater effect on polymerase fidelity when copying undamaged DNA than was observed when the polymerase bypassed either TT dimer or 8-oxoG lesions. The results may provide additional insight regarding both the behavior of pol η as well as the remarkable aptitude of pol η for DNA lesion bypass.

Thr 318 and Pol η Fidelity. Using two distinct assays for fidelity, we find the T318A mutant consistently makes a variety of errors with less frequency than the wild type polymerase. That is, the fidelity is better than wild type when copying undamaged DNA, although we did see a modest increase in the bypass fidelity for both TT dimer and 8-oxoG as well. When copying A, G, or T bases, 8-oxoG and the 3′T of TTD, T318A had the lowest error rates. Thr 318 provides a hydrogen bond from its side-chain hydroxyl group to a template phosphate oxygen imparting stability to the newly formed DNA duplex (Figure 2.5A). Noting that mutations occur when a mispaired nucleotide is stable enough to be both incorporated and extended by the polymerase, it is possible that the replacement of threonine with alanine disrupts the hydrogen bonding and engenders a slight shift in the template strand position. The conformational adjustments rendered by pol η presumably destabilize the incorrect base pairing. That a residue residing at least 3 bases downstream of the active site (Figure 2.1A) can so drastically alter fidelity is surprising.

Little finger β-strand in other Y-family polymerases. Crystal structures of not only human pol η, but of *S. cerevisiae* pol η and the other human Y-family members ι, κ and Rev1 have provided a wealth of information that has helped to elucidate the functional domains of these enzymes (Nair et al., 2004; 2005a; Lone et al., 2007; Biertümpfel et al., 2010;

Silverstein et al., 2010). The β-strand and the way in which it interacts with the template DNA is conserved across nearly all of the Y-family polymerase structures. This suggests that β-strand 12 is essential to polymerase function. Our result that distal amino acid residue T318 appears to be particularly important to fidelity is compelling considering that T318 is not a conserved residue (Figure 2.5B) (Boudsocq et al., 2002; Biertümpfel et al., 2010). In many other Y-family polymerases, serine occupies this position and we wonder if its modification would affect fidelity and function in a similar manner. In addition, it will be interesting to test a pol η T318S mutant using the assays described here.

β-strand Significance to Polymerase Fidelity. In addition to the effect observed when mutating Thr 318, the error rate was also suppressed when Pro 316 was mutated and, to a lesser extent, when Gly 320 was mutated. These findings support the hypothesis that interactions between the region of the β-strand distal to the active site and the newly synthesized duplex DNA are influential to pol η fidelity. This is consistent with previous observations regarding these amino acids (Biertümpfel et al., 2010; Zhao et al., 2012; Ummat et al., 2012a) and this work extends those observations to a large number of types of errors. Crystal structures of human pol η reveal four hydrogen bonds that extend from the side chain of Arg 361. Two reach to the main chain oxygen of Pro 316 and two to the side chain of Asp 355. These construct a web of hydrogen bonds that provide additional stability to the β-strand (Biertümpfel et al., 2010). G1083T has been established as a missense mutation in an XPV patient (Broughton et al., 2002), leading to the amino acid change R361S. The patient in whom the homozygous G1083T change was identified presented with a fairly mild XPV phenotype (at age 57 with less than 10 tumors (Broughton et al., 2002)). It has been proposed

that the disruption of the hydrogen bond between Arg 361 and Pro 316 leads to the XPV phenotype due to subsequent interruption of the polymerase-DNA interaction (Biertümpfel et al., 2010). Because the results of our current study support the hypothesis that modification to amino acid residues contributing to the positional integrity of the little finger β-strand affect pol η function, an in vitro characterization of the R361S form of the polymerase would be insightful, as would be an investigation of the in vivo phenotype of P316A.

Lesion bypass and mutation suppression. We have recently reported on other pol η mutants that affected undamaged and damaged DNA replication fidelity differentially and we believe these reports are the first to describe this phenomenon (Suarez et al., 2013). In that report, two different active site residues, R61 (interacts with the incoming dNTP) and S62 (contacts the DNA one base upstream of the template base), were changed to alanine (R61, S62) or glycine (S62). These forms displayed increased fidelity when copying undamaged G but not when copying 8-oxoG. Additionally, mutation of Q38 (interacts with the template base) to alanine resulted in an increase in fidelity when copying both G and 8-oxoG, but a decrease in fidelity when copying a TT dimer.

In this new work, the finding that the identity of amino acid residues providing hydrogen bonds from the backbone of β-strand 12 is sometimes inconsequential to pol η bypass efficiency and fidelity was not altogether unexpected as the interactions likely remain in place in the mutated forms of the polymerase. This emphasizes the importance of the β-strand main chain-DNA interactions. Nonetheless, it was somewhat unexpected that when certain residues were mutated, fidelity was affected when copying undamaged DNA but not when bypassing DNA lesions. As pol η is likely evolutionarily optimized for TLS, it is

reasonable to find that fidelity of lesion bypass appears to function at a given fidelity and efficiency. However, the extent to which these properties are unyielding in addition to the fact that some mutated forms of the polymerase seem unable to accommodate undamaged DNA in the same way as damaged DNA was unanticipated. It could be suggested that, under initial consideration, these results are not relevant to pol η function in vivo. Indeed, the most widely accepted role of pol η is the bypass of cyclobutane pyrimidine dimers and other lesions (Prakash et al., 2005). However, the exact molecular mechanism of TLS by pol η is not clear and evidence suggests that short stretches of undamaged DNA both upstream and downstream of the lesion are also copied by the polymerase (McCulloch et al., 2004a). It is interesting that each mutant tested displayed overall activity that was lower than that of the wild type enzyme (Table 2.1). This fits our hypothesis that, in vivo, it is the entire TLS process that is relevant to mutation suppression. This would include at minimum: bypass efficiency and fidelity by the polymerase, overall ability to synthesize DNA, proofreading in trans of errors and the effects of accessory proteins. In addition, pol η has been shown to participate in multiple DNA metabolism pathways, not all of which involve damaged DNA (Rogozin et al., 2001; Zeng et al., 2001; Kawamoto et al., 2005; Kamath-Loeb et al., 2007; Bétous et al., 2009; Rey et al., 2009), making study of its properties when copying undamaged DNA relevant.

That modifying residues important to stabilize and align the DNA for correct nucleotide incorporation did not appreciably alter the fidelity of the polymerase opposite DNA lesions demonstrates just how exceptional pol η is as a lesion bypass polymerase. It is clearly able to accommodate slight alterations to protein-DNA alignment without affecting

its TLS function. Furthermore, the fact that this was the case not only for the bypass of TT dimer, but also for 8-oxoG, might imply that pol η is equally suited to bypass the 8-oxoG lesion as well. Whether the same holds true for lesions not bypassed as readily (i.e. AP site, 2-hydroxyadenine) (Kokoska et al., 2003; Barone et al., 2007) will be interesting to investigate, as will the properties of lesions with crystal structure information (i.e. cisplatin adducts) (Zhao et al., 2012; Ummat et al., 2012a).

We acknowledge that the in vitro properties of the various mutated forms of pol η described here may not translate to phenotypic changes in vivo and that post-translational modifications to the polymerase and other protein-protein interactions that may affect the TLS process are not considered in this biochemical analysis. To address this, we propose to investigate whether or not these forms of pol η are able to provide complementation to XPV cells and to determine if these mutants behave similarly in vivo. We do assert, however, that even in absence of in vivo analysis, the type of biochemical data that we have presented here provides indispensible information regarding the relationship between polymerase structure and function and molecular mechanism. Accordingly, we believe it will be valuable to characterize the forms of full-length pol η predicted to possess amino acid substitutions from the various identified XPV mutations (Broughton et al., 2002) for their properties in vitro. Compilation of such results with existing biochemical data will provide important insight to help further understand the unique aptitude of pol η for lesion bypass and its other possible functions within the cell.

Statement of Author Contributions

R.A. Beardslee designed and conducted experiments, analyzed data, and prepared the manuscript. S.C. Suarez helped design experiments and provided technical assistance and input. S.M. Toffton provided technical assistance with experiments. S.D. McCulloch designed experiments, provided intellectual input, and made final edits to the manuscript. All authors approved the final manuscript. R.A Beardslee and S.D. McCulloch had complete access to the study data. All authors declare no conflicts of interest.

Acknowledgements

We thank Drs. Robert C. Smart (North Carolina State University), James Bonner (North Carolina State University) and Thomas A. Kunkel (National Institute of Environmental Health Sciences) for critical reading of the manuscript, helpful conversations and materials. This work was supported by the National Institute of Environmental Health Sciences of the National Institutes of Health [R01 ES016942] (SM) and [T32 ES007046] (SM, SS, RB) and the College of Agriculture and Life Sciences at North Carolina State University (ST).

Figures

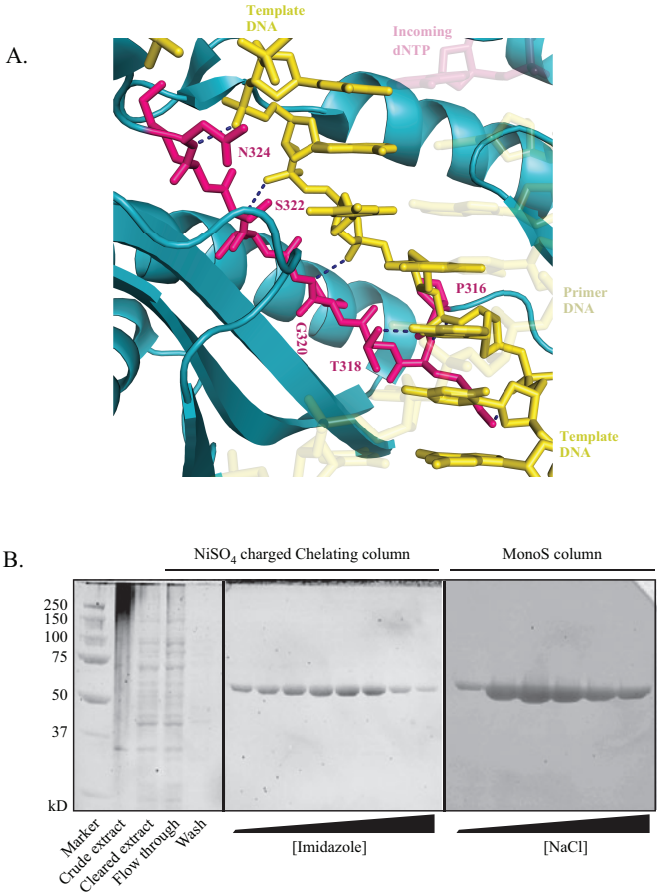

Figure 2.1 Pol η structure and protein purification.

A. Magnified view of the little finger domain β-strand of human pol η in complex with undamaged DNA. Image prepared from PDB entry 3MR2 (Biertümpfel et al., 2010)using the PyMOL Molecular Graphics System, Version 1.3 Schrödinger, LLC (http://www.pymol.org/). Amino acid residues 316-324 are displayed in magenta with remaining polymerase ribbon displayed in cyan. DNA template is displayed in yellow, incoming dNTP displayed in transparent magenta and the newly synthesized primer strand in transparent yellow. Hydrogen bonds are represented by dark blue dashed lines. **B.** Representative SYPRO-RED stained SDS-PAGE gels from purification of *E. coli* expressed proteins. Peak fractions eluted from a HiTrap™ Chelating HP (GE Healthcare) column using an imidazole gradient and from a Mono S™ (GE Healthcare) column using a NaCl gradient are shown. Protein fractions analyzed in gels were selected based on absorbance readings at 280 nm.

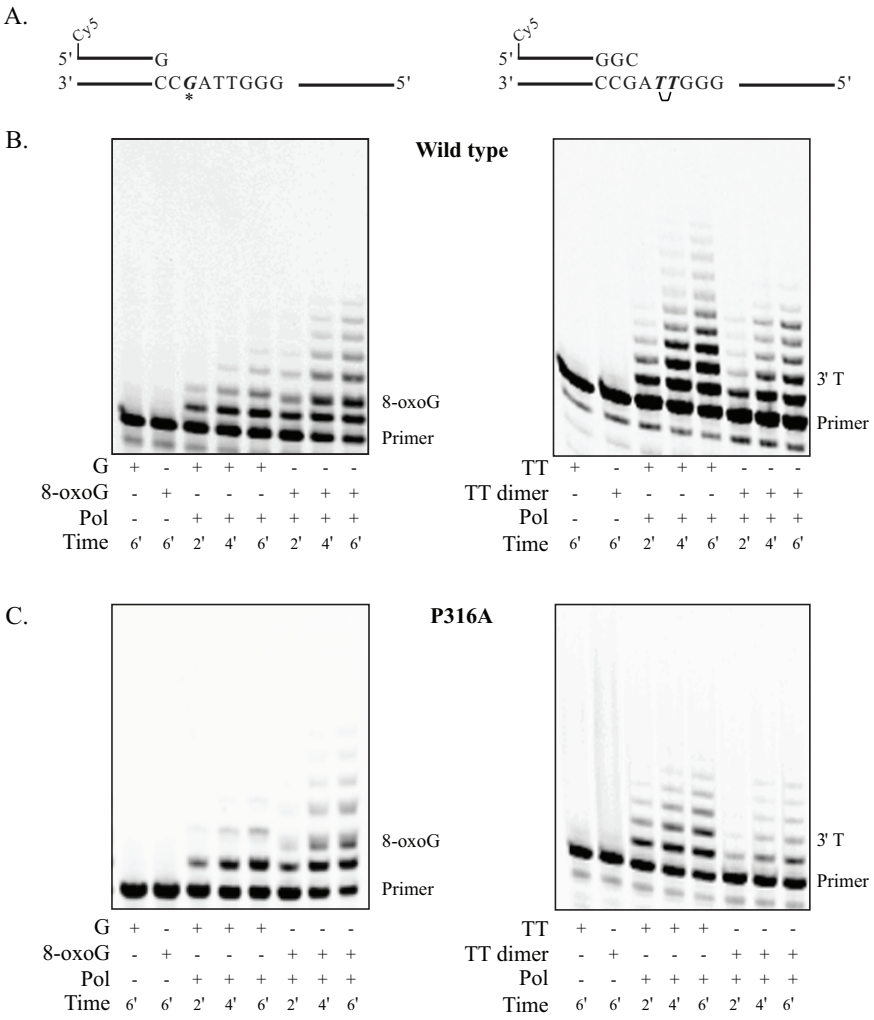

Figure 2.2 Bypass efficiency of TTD and 8-oxoG DNA lesions by human pol η.

A. Schematic diagrams for G/8-oxoG (33-mer template, 17-mer primer) and TT/TT dimer (45-mer template, 26-mer primer). All substrates cause a 'running start' reaction, with the 3′ end of the primer at the -2 position with respect to the damaged base (3′ cross-linked thymine for the TT dimer substrate). **B.** Wild type polymerase lesion bypass efficiency reaction product separation by denaturing polyacrylamide gel electrophoresis. Analysis of band intensity (Image Quant™ TL software from GE Healthcare) verified that reactions to be under single interaction conditions as judged by having constant termination probability over time in reactions that contain a large substrate excess with respect to polymerase (TT dimer: 250:1 for wild type, 150:1 for P316A; 8-oxoG: 400:1 for wild type, 200:1 for P316A) (Lesion bypass efficiency values were calculated as previously described (Kokoska et al., 2003). **C.** Representative β-strand mutant (P316A) lesion bypass efficiency reaction product separation.

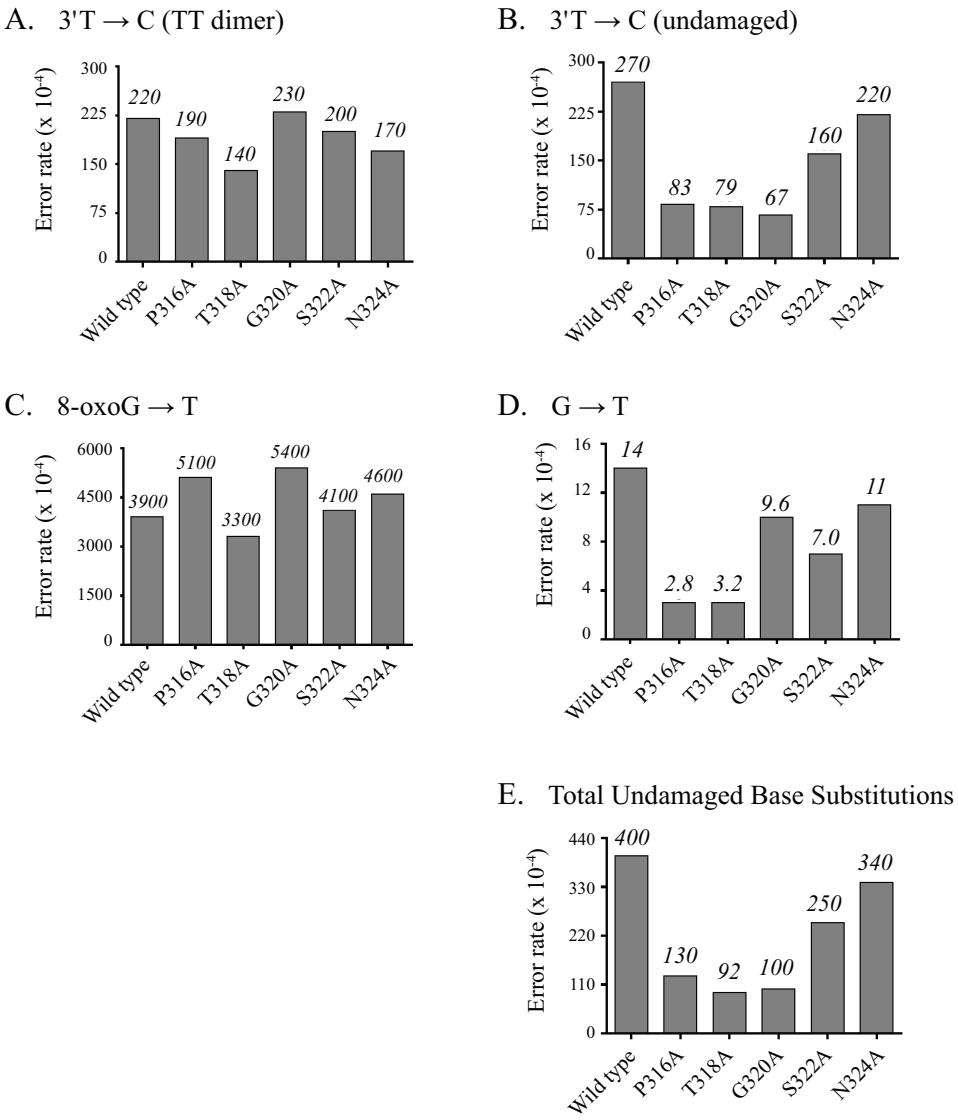

Figure 2.3 Mutating pol η differentially affects fidelity.

A. TTD 3′T → C error rates for reversion mutation assay. **B.** T → C error rates for reversion mutation assay. **C.** 8-oxoG → T error rates for reversion mutation assay. **D.** G → T error rates for reversion mutation assay. **E.** Total detectable single base substitution error rates at stop codon for reversion mutation assay. Although a significant change in fidelity was not observed for any of the mutated forms of pol η when copying either TTD or 8-oxoG lesions, the error rates opposite the corresponding undamaged bases were repeatedly observed as markedly suppressed for certain mutated forms of pol η.

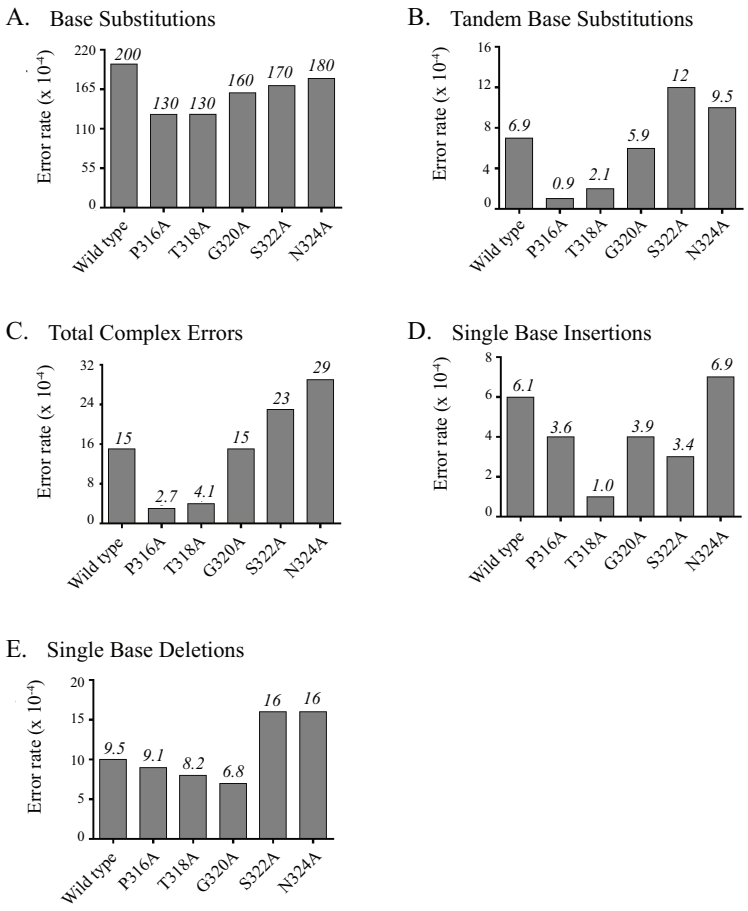

Figure 2.4 Forward mutation assay results support reversion mutation assay observations.

A. Total single base substitution error rates for gap-filling forward mutation assay. **B.** Tandem base substitution error rates for gap-filling forward mutation assay. **C.** Complex error rates for gap-filling forward mutation assay. Complex errors include insertions and deletions of two or more bases, single base substitutions separated by one correctly copied base, two or more consecutively incorrectly copied bases and/or any combination thereof. Amino acid substitutions in pol η little finger β-strand generally result in a suppression of erroneous base substitution compared to wild type. When substitutions are distal to the active site, the effect is amplified. **D.** Insertion error rates for gap-filling forward mutation assay. **E.** Deletion error rates for gap-filling forward mutation assay. Significant changes for insertion and deletion fidelity generally not observed. The only notable exception is the decrease in insertions made by T318A compared to wild type.

A.

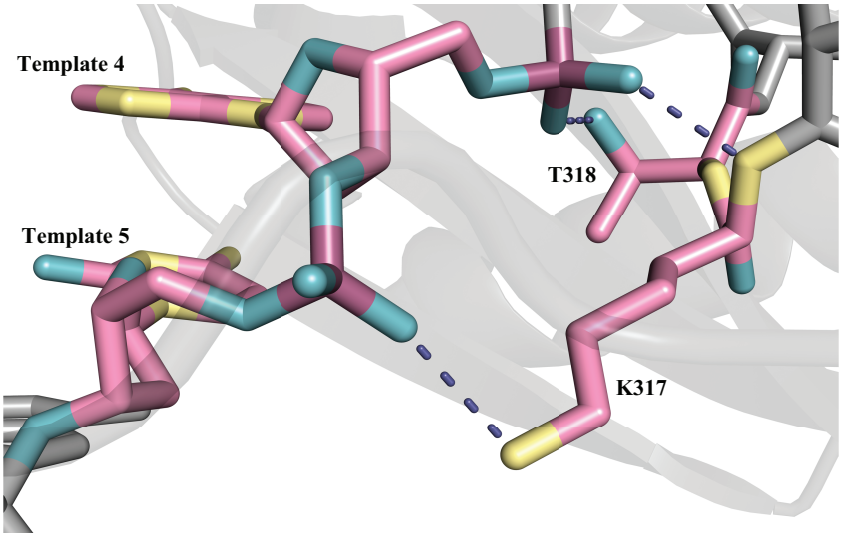

B.

Hs	pol η	301	EHDPVKPRQL**PKTIGCSKN**FPGKTALA
Mm	pol η	300	EHDPVKPRQL**PKTIGCSKN**FPGKTALA
Xl	pol η	300	EDEPVKPRQL**PKSIGCSKN**FPGKTSLS
At	pol η	296	SGEEVQGRLL**PKSHGSGKT**FPGPRALK
Ce	pol η	299	CDEPVRPRKE**SSSIAVSKN**FPGKLSIR
Sc	pol η	377	YGLPLSSRPV**VKSMMSNKN**LRGKSC-N
Hs	pol ι	309	DNSPVILSGP**PQSFSEEDS**FKKCSS--
Hs	pol κ	398	GSTHLTRDGE**RKSMSVERT**FSEINKA-
Hs	Rev1	694	DDRPVRTEKE**RKSVSAEIN**YGIRFT--

Figure 2.5 Pol η and the T318 residue.

A. Magnified view of pol η little finger β-strand that stabilizes the DNA template strand. Hydrogen bonds (violet dashed lines) from amino acid residues K317 and T318 are shown interacting with the template strand of recently copied DNA (the fourth and fifth bases away from the templating base:incoming dNTP pair). Light pink – carbon; dark pink – phosphorus; yellow – nitrogen; cyan – oxygen. Only hydrogen bonds from K317 and T318 are shown with the remaining protein and DNA atoms represented in gray. Image prepared from PDB entry 3MR2 (Biertümpfel et al., 2010) using the PyMOL Molecular Graphics System, Version 1.3 Schrödinger, LLC (http://www.pymol.org/). **B.** Amino acid sequence alignment of pol η from multiple species and the other human Y-family polymerases. Hs, *Homo sapiens*; Mm, *Mus musculus*; Xl, *Xenopus laevis*; At, *Arabidopsis thaliana*; Ce, *Caenorhabditis elegans*; Sc, *Saccharomyces cerevisiae*. Letters in bold indicate β-strand 12 residues. Alignment was created using Clustal Omega (Sievers et al., 2011).

Tables

Table 2.1 Activity and lesion bypass efficiency of β-strand mutants of human pol η.

Activity values in comparison to wild type (average of two experiments). Variability in relative values between experiments was less than 15%. Incorporation of ^{32}P-α-dCTP into activated calf thymus DNA was determined by scintillation counting of TCA precipitable material after a 30-minute incubation. Wild type polymerase activity was 7.9 nmoles dCTP incorporated/fmole polymerase/minute. Bypass efficiencies are the average of three time points (2, 4, 6 minutes) ± standard deviation. Substrate:polymerase ratios for TTD containing template varied from 60:1 (T318A) to 300:1 (S322A and N324A) and 100:1 (T318A) to 400:1 (wild type) for 8-oxoG containing template. Values in parentheses are relative to wild type. ND, not determined.

Mutant	Relative Polymerase Activity	Bypass Efficiency			
		TTD		8-oxoG	
Wild type	100%	140 ± 8%		93 ± 29%	
P316A	57%	240 ± 53%	(1.7X)	150 ± 54%	(1.6X)
T318A	33%	150 ± 47%	(1.1X)	75 ± 20%	(0.8X)
G320A	56%	140 ± 43%	(1.0X)	80 ± 21%	(0.9X)
G320P	7.1%	ND		ND	
S322A	66%	110 ± 16%	(0.8X)	180 ± 78%	(2.0X)
N324A	61%	160 ± 16%	(1.1X)	92 ± 15%	(1.0X)

Table 2.2 Error rates copying undamaged DNA by little finger β-strand mutants of pol η.

Total base substitutions at the three template bases of the stop codon (8 of 9 possible errors are detected in this assay. G → A changes generate an ochre stop that cannot be detected by plaque phenotype). The error rates for wild type are: A, 47 x 10^{-4}; G, 51 x 10^{-4}; T, 300 x 10^{-4}; Total, 400 x 10^{-4}. Each value comes from sequence analysis of a minimum of 103 mutant plaques. Error rates expressed as fold change compared to wild type. Values less than one represent error rates less than wild type (i.e. higher fidelity); values greater than one represent error rates greater than wild type (i.e. lower fidelity). Values in bold indicate the β-strand mutant for which the greatest suppression in error rate was observed.

Fold Change in Error Rate Relative to Wild Type						
Template base	**Wild type**	**P316A**	**T318A**	**G320A**	**S322A**	**N324A**
A	1.0	0.5X	**0.2X**	0.3X	1.3X	1.8X
G	1.0	0.5X	**0.1X**	0.3X	0.5X	0.6X
T	1.0	0.3X	0.3X	**0.2X**	0.6X	0.8X
Total	1.0	0.3X	**0.2X**	0.3X	0.6X	0.9X

CHAPTER 3: CHANGING dNTP POOLS ALTER FIDELITY

Abstract

DNA polymerase η (pol η) is responsible for the bypass of both cyclobutane pyrimidine dimers (CPDs) and 7,8-dihydro-8-oxoguanine (8-oxoG) during DNA replication. Loss of pol η is associated with an increase in mutation rate, demonstrating its indispensable role in mutation suppression, yet when copying DNA pol η is error-prone and frequently misincorporates incorrect nucleotides contributing to mutagenesis and genomic instability. As relative dNTP concentrations can affect the rate of nucleotide misincorporation, we have investigated the role of changing dNTP concentrations on pol η function and fidelity and hypothesized that nucleotide concentrations that attempt to approximate mammalian physiological ratios would alter certain rates of single base substitutions when copying both undamaged and damaged DNA. To study the effect of these mutations, we expressed the catalytic core of wild type human pol η in *E. coli*. Overexpressed protein was purified by chromatography and purified protein fractions and DNA oligomers were used in *in vitro* assays to evaluate DNA synthesis and fidelity opposite templates with and without *cis-syn* thymine-thymine CPD and 8-oxoG lesions. Results demonstrate that the efficiency of primer elongation is limited when dNTP concentrations approximate physiological concentrations and that these concentrations modify the error rates and mutation spectrum observed. Because dNTP concentrations vary throughout the cell cycle, we propose that these results suggest that the fidelity of pol η is dynamic. Further, dysregulated pol η and dNTP pool concentrations are both associated with cancer cells and, in concert, could contribute to the mutator phenotype proposed to be significant to cancer progression.

Introduction

Human polymerase η (pol η) is responsible for replication past ultraviolet light-induced cylobutane pyrimidine dimers (CPD) *in vivo* (Masutani et al., 1999a; 1999b). Pol η deficient cells accumulate mutations at CPD sites (Maher et al., 1976; Patton et al., 1984; Wang et al., 1991; 1993; Waters et al., 1993; Choi and Pfeifer, 2005) and, in humans, lack of functional pol η results in the autosomal recessive cancer syndrome, xeroderma pigmentosum (XPV), which is characterized by increased sensitivity to sunlight and skin cancer incidence. While the apparent function of the pol η *in vivo* is UV-induced mutation suppression, *in vitro* biochemical studies have indicated that pol η is prone to nucleotide mispairing when copying both undamaged DNA and *cis-syn* thymine-thymine CPDs (TTD) (Matsuda et al., 2000; Johnson et al., 2000b; Matsuda et al., 2001; Washington et al., 2001a; McCulloch et al., 2004c). In addition to replication past CPDs, pol η has also been implicated in the bypass of 7,8-dihydro-8-oxoguanine (8-oxoG) (Zhang et al., 2000b; Maga et al., 2007; Lee and Pfeifer, 2008; McCulloch et al., 2009).

Crystal structure solutions of human pol η revealed a large open active site that is characteristic to all the members of the Y-family polymerases and conserved across species (Nair et al., 2004; 2005b; Lone et al., 2007; Biertümpfel et al., 2010; Silverstein et al., 2010). This distinctive structural feature is essential to TLS polymerase function as it allows the enzyme to accommodate bulky DNA lesions including TTDs and 8-oxoG within its active site and facilitate nucleotide pairing with, and DNA synthesis past those lesions. While this imparts the replication process with a strategy to avoid stalling of the replicative polymerases, replication fork collapse and cell death, it simultaneously increases the

opportunity for the incorporation of incorrectly paired nucleotides and the introduction of fixed mutations within the genome as the consequence of an active site that is less discriminatory against mispaired nucleotides than those of the replicative polymerases, pol δ and pol ε (Arana et al., 2008).

In addition to the responsibility of the polymerase binding pocket to distinguish correctly paired nucleotides from those paired in error, various *in vitro* studies have underscored the importance of individual dNTP pool concentrations to polymerase error rates (reviewed in Kunkel, 1992; Mathews and Ji, 1992; Martomo and Mathews, 2002). Recently, studies using *in vivo* models have revealed that *E. coli* and *S. cerevisiae* strains possessing mutant ribonucleotide reductase enzyme, which results in perturbations to nucleotide pool concentrations, have displayed an increase in mutation rate as well a direct relationship between dNTP concentrations and individual mutation rates (Kumar et al., 2011; Ahluwalia et al., 2012; Schaaper and Mathews, 2013). As nucleotide species are in competition with one another for incorporation at the polymerase active site, it would be anticipated, and computational studies have predicted that there exists a relationship between the probability of incorporation for a given nucleotide and the local concentration of that nucleotide at the replication fork (Arias-Gonzalez, 2012). Given the permissive nature of the pol η active site and its propensity for misincorporation of dNTPs and the lack of fidelity data available for pol η in the presence of dNTP concentrations that attempt to approximate physiological conditions, we carried out several assays to assess what implications changing dNTP pools may have for pol η function and fidelity.

Materials and Methods

Materials. Reaction buffer for all assays consisted of 40 mM Tris (pH 8.0), 250 μg/mL bovine serum albumin, 10 mM dithiothreitol, 10 mM magnesium chloride, 60 mM potassium chloride and 1.25% glycerol. Both equimolar and unequal reaction mixtures were supplemented with all four dNTPs to total final concentrations varying from 25 μM to 400 μM. Individual dNTP concentrations were 25% of the total concentration in equimolar reactions. In unequal reaction mixtures, dATP was 16% of the total dNTP concentration, dCTP was 11%, dGTP was 10% and dTTP was 63%. All cell lines, bacteriophage and reagents for the lesion bypass fidelity assay have been previously described (McCulloch and Kunkel, 2006). All DNA sequencing was performed by Genewiz, Inc. (South Plainfield, NJ). Oligonucleotides were purchased from Integrated DNA Technologies, Inc. (Coralville, IA) and The Midland Certified Reagent Company, Inc. (Midland, TX). Nucleotides and restriction enzymes were obtained from New England Biolabs, Inc. (Ipswich, MA).

Expression and Purification of Wild Type Pol η. Wild type (WT) polymerase η (pol η) was overexpressed and purified as previously detailed (Suarez et al., 2013). Briefly, the vector pET21b-XPV, which codes for the catalytic core amino acids 1-511 of human pol η and includes a C-terminal 6x histidine tag, was utilized. Protein was overexpressed in *E. coli* BL21(DE3) cells and the protein product was purified by affinity chromatography using HiTrap™ Chelating HP (GE Healthcare) with subsequent application of pol η enriched fractions to Mono S™ (GE Healthcare) as described (Suarez et al., 2013)

Primer Extension Assay - Substrates were created by annealing a 5′-Cy5-labeled DNA primer strand to a 1.1x molar excess of complementary template strand in 100 mM sodium chloride and 20 mM Tris (pH 8.0). 24-mer primer sequence 5′-Cy5-AATTTCTGCAGGTCGACTCCAAAG-3′ and 45-mer template sequences 5′-CCAGCTCGGTACCGGGTTAGCCTTTGGAGTCGACCTGCAGAAATT-3′ (TTAG), 5′- TCCGCGCTACGGGCATGCGATCTTTGGAGTCGACCTGCAGAAATT-3′ (CGAT), 5′- CGACCGGTTTCACCGGGGCTACTTTGGAGTCGACCTGCAGAAATT-3′ (GCTA), were used. Regions paired with primer are underlined. Reaction mixtures containing 330 nM DNA substrate were initiated by the addition of 33 nM polymerase, incubated at 37 °C for 20 minutes and quenched by adding an equivalent volume of 95% formamide, 25 mM EDTA (formamide loading dye). Reaction products were separated by electrophoresis on a denaturing 10% polyacrylamide gel, imaged with a Storm™ 865 imager (GE Healthcare) and quantified using Image Quant™ TL software (GE Healthcare).

Reversion Mutation Assay and Analysis for Fidelity of Lesion Bypass. Fidelity of lesion bypass analysis was carried out as reported previously (Kokoska et al., 2003; McCulloch and Kunkel, 2006). Two DNA lesions were assayed: *cis-syn* cyclobutane thymine-thymine dimer (TT dimer/TTD) and 7,8-dihydro-8-oxoguanine (8-oxoG). Substrates used for the lesion bypass assay were created by annealing a primer strand to a template strand (5′-Cy5-AATTTCTGCAGGTCGACTCCAAAG-3′ to 5′-CCAGCTCGGTACCGGGTTAGCCTTTGGAGTCGACCTGCAGAAATT-3′ for TT dimer reactions where the underlined TT is either a thymine pair or a TT dimer and 5′-Cy5-AATTTCTGCAGGTCGACTCCAAAG-3′ to 5′-

CCAGCTCGGTACCGGGTTAxCCTTTGGAGTCGACCTGCAGAAATT-3′ for G/8-oxoG reactions where x represents either guanine or 8-oxoG). Reaction mixtures (30 μL) containing 330 nM DNA and ~50 μCi ^{32}P-α-dCTP were initiated with 170 nM polymerase and incubated for 30 minutes at 37 °C. The reaction products were digested with *Pst*I. An equal volume of formamide loading dye was added to prepare the samples for separation by electrophoresis on a denaturing 10% polyacrylamide gel. Newly synthesized strand was recovered and annealed to M13 gapped circular DNA. Annealed DNA was transformed into *E. coli* strain MC1061 cells and plated in a soft agar overlay atop a layer of CSH50 cells. The lesions are located within an amber stop codon in the *lacZα* gene sequence. Correct synthesis results in preservation of the amber stop codon and thus complementation of the N-terminally truncated *lacZ* gene in CSH50 does not occur, which generates plaques with a light blue phenotype. Errors generated when copying the stop codon result in a functional *lacZα* gene and produce dark blue plaques. Plaques were counted and assessed for color phenotype to determine mutant frequencies as outlined previously (McCulloch and Kunkel, 2006). DNA from individual colonies was amplified using illustra™ TempliPhi (GE Healthcare) and sequenced to determine the spectrum of changes. Error rates were calculated as described (McCulloch and Kunkel, 2006).

Results

Primer extension by pol η in the presence of equimolar and unequal dNTP pools

To select dNTP concentrations that were representative of *in vivo* pool ratios, we used values from a recent report in which a newly developed assay that employs high performance

liquid chromatography coupled with tandem mass spectroscopy was used for dNTP concentration analysis. In this study all dNTPs and rNTPs were measured in four distinct human cancer cell lines (H23, PANC1, HepG2 and H1975) and data were reported in pmoles per million cells (Zhang et al., 2011). We determined the μM concentration of each dNTP by using the cell volume reported in the study and averaged the values across the four cell lines to establish relative dNTP concentrations for use in our reactions in which unequal dNTP concentrations were used. The calculated values were: dATP 2.24 μM, dCTP 1.50 μM, dGTP 1.48 μM and dTTP 9.02 μM. Of the total dNTP concentration, dATP represented approximately 16% of the total, dCTP 11%, dGTP 10% and dTTP 63%. Although discrepancies in dNTP measurements exists due to possible variation in tissue and/or cell type as well as experimental approach, these values are consistent with other published data. Reported individual dNTP concentrations determined by experimental methods range from 0.3 to 39 μM (Traut, 1994). In addition, there is consistency in the relative level of each dNTP to the others. In general, [dGTP] < [dCTP] < [dATP] < [dTTP] (Leeds et al., 1985; Mathews and Ji, 1992; Martomo and Mathews, 2002).

Because we felt that attempting to imitate exact *in vivo* conditions with respect to absolute dNTP concentrations was not only impossible, but also would have still remained an artificial experimental environment, we elected to emphasize the effect a change in relative concentrations of dNTP pools at variety of total dNTP concentrations would have on pol η primer extension activity. To do this, we carried out *in vitro* primer extension assays at varied total dNTP concentrations with both equal and unequal dNTP pools in a variety of experimental conditions. For reactions in which equal dNTP concentrations were used, each

dNTP represented 25% of the total concentration. For reactions in which unequal dNTP concentrations were used, the total dNTP pool was composed of the percentages previously described as calculated from the literature.

Total dNTP concentrations affect primer extension. We first carried out primer extension reactions (Figure 3.1A) to determine what effect decreasing total dNTP concentrations in the presence of equimolar dNTP pools would have on extension by pol η (Figure 3.1B,C). Historically, these reactions with pol η have been carried out at 400 μM total dNTP and thus this was selected as the maximum total dNTP concentration for this set of reactions. Reactions with total dNTP concentrations of 300 μM, 200 μM, 100 μM, 50 μM and 25 μM were also carried out (Figure 3.1B, Table 3.S.1). In general, a large change in primer utilization was not observed as the total dNTP concentration decreased. Only when the total dNTP concentration was dropped to 25 μM was a decrease evident. The effect, however, was subtle; there was only a 10% reduction in utilization compared to that of the reaction in which 400 μM dNTP concentration was used.

While total dNTP concentration did not affect primer utilization, there was however a clear difference in extension profiles (Figure 3.1B). Impaired extension was observed at intermediate nucleotides as total dNTP concentrations declined. To assess the extent to which pol η primer extension activity decreased we divided the template sequence into four sections and evaluated and compared band intensity over those sections (Table 3.S.1). The template sequence was split nearly equally into quarters. Quarter one comprised incorporation opposite the first template nucleotide through the 5th template nucleotide. Quarter two

included template nucleotides 6–10, quarter three included template nucleotides 11–15 and the last quarter included the final six nucleotides.

For reactions in which the total dNTP concentration was 400 μM, 11% of the reaction products terminated after the incorporation of less than six nucleotides, while 65% of reaction products were extended by at least 16 nucleotides (Table 3.S.1). In contrast, for reactions in which the total dNTP concentration was 25 μM, 64% of reaction products were extended by less than six nucleotides (5.8x change over equimolar reaction), while only 1% were extended by 16 or more nucleotides (0.02x change). For reactions of intermediate total dNTP concentration, the fraction of products with impaired extension increased as the total dNTP concentration decreased.

Corresponding reactions with unequal dNTP pools were carried out to determine whether or not the concentrations of the individual dNTPs have an effect on primer extension (Figure 3.1C, Table 3.S.2). Results of the equimolar reactions revealed that full-length extension began to taper when the total dNTP concentration was between 200 μM and 100 μM. We established the maximum total dNTP concentration for these unequal molar reactions by setting dGTP, the nucleotide experimentally determined to be at the lowest concentration *in vivo* to 25 μM, equal to the concentration of dGTP in the 100 μM equimolar reaction. As a result, the reaction with the greatest total dNTP concentration for this set of primer extension reactions contained a total dNTP concentration of 240 μM. Reactions with total dNTP concentrations of 200 μM, 100 μM and 50 μM were completed so that comparisons could be made between the equimolar and unequal molar reactions, in additional to a fifth reaction with a total dNTP concentration of 39 μM.

In general, the same trend was observed for the unequal molar reactions as was observed for the equimolar reactions. As total dNTP concentration decreased, full-length primer extension was impaired (Figure 3.1B, C). For the reaction in which the total dNTP concentration was 240 μM, only 16% of reaction products were terminated after the addition of less than six nucleotides, while 43% of reaction products were terminated after the addition of at least 16 nucleotides (Table 3.S.2). The inverse was observed when the total dNTP concentration was 39 μM. For that reaction, 72% of the reaction products were terminated after less than six nucleotides were incorporated (4.5x change). Reaction products with the incorporation of 16 or more nucleotides were undetectable.

Ratios of individual dNTP concentrations affect primer extension. Because our primary interest in this project was to determine how unequal dNTP pools modify the activity and fidelity of pol η, we compared the extent of primer extension in unequal dNTP pool reactions to that in reactions with equal dNTP pools for matching total dNTP concentrations (Figure 3.1B, C). For example, the results from paired equimolar and unequal molar reactions in which the total dNTP concentration was 200 μM reveal an increase in impaired extension in the reaction with unequal dNTP pools. While 57% of extension products had 16 or more nucleotides incorporated in the equimolar reaction, only 23% of the products in the unequal molar reaction exhibited the same (0.4x change) (Table 3.S.1, Table 3.S.2). 13% of reaction products in the equimolar reaction terminated after the incorporation of less than six nucleotides. This percentage increased to 22% for the reaction with unequal molar dNTP pools (1.7x change). The presence of unequal pools inhibited extension by pol η earlier in the template sequence and reduced the amount of full-length product polymerized.

The result was the same for total dNTP concentrations of 100 μM and 50 μM (Figure 3.1B, C). For the 100 μM equimolar reaction, 18% of the reaction products were the result of the incorporation of less than six nucleotides, while 37% were the result of the incorporation of greater than 15 nucleotides (Table 3.S.1, Table 3.S.2). For the reaction in which the dNTP pools were unequal, however, there was an increase in products with less than six nucleotides incorporated (30%, 1.7x) and a decrease in products with more than 15 nucleotides incorporated (8%, 0.2x) as was observed for the reactions with 200 μM total dNTPs. Similarly, for the 50 μM reactions, the increase in products with less than 6 nucleotides incorporated was 1.3x (36% and 46%, equimolar and unequal molar reactions, respectively) and the decrease in products with more than 15 nucleotides incorporated was 0.2x (5% and 1%, equimolar and unequal molar reactions, respectively).

The identity of the template base can affect extension by pol η. An increase in band intensity was observed at the same bands consistently for both the equimolar and unequal molar reactions. Upon inspection of the template base that corresponded to those bands of increased intensity, it was observed that those template bases often directly preceded template guanine bases (Figure 3.1B, C). To determine if this was an artifact of the template sequence or rather a phenomena related to the presence of a template guanine and/or the incorporation of dCTP opposite the guanine, two ancillary template sequences were generated (CGAT and GCTA) in addition to our standard template, TTAG (Figure 3.2). The composition with respect to total oligomer length and number of each species of base present was maintained, but the order in which they were present in the template was changed.

For the TTAG template, a template guanine is located at the second position in the sequence, a series of template guanines are situated at the sixth, seventh and eighth positions as well as at the 13th and 14th positions, and a single final guanine sits near the end of the template at the 18th position (Figure 3.2A). The impaired extension observed is illustrated by the pattern of band intensity at positions 12, 13 and 14 for the reaction in which the total dNTP concentration was 100 μM. The intensity of the band that corresponded to the total incorporation of 12 nucleotides represented 9.6% of the total reaction products (Table 3.S.4). That which corresponded to the incorporation of 13 nucleotides represented 7.4% of the total reaction products. Furthermore, of all the reaction product bands, these were among the top five in greatest intensity. In contrast, however, the band that corresponded to the incorporation of 14 total nucleotides represented only 2.6% of the total reaction products. This could suggest that there was impaired extension after the incorporation of the 12th and 13th nucleotide, which both directly precede guanines located at bases 13 and 14 in the template. However, as the template base at the 15th position was a cytosine and thus required the incorporation of dGTP, once the G·C pair at position 13 was polymerized, pol η could more easily extend the primer thus resulting in weaker band intensity.

The same phenomenon was observed, perhaps to an even greater extent, for the reaction in which the dNTP pools were unequal. With a total dNTP concentration of 66 μM, large increases in impaired extension were observed after the incorporation of the first and fifth bases that directly precede the incorporation of dCTP opposite template guanines at positions two and six (Figure 3.2A). The band corresponding to the incorporation of a nucleotide opposite the first template base represented 22.5% of the total reaction products,

while the following band which represents the incorporation opposite the first template guanine in the sequence, had an intensity that constituted only 7.4% of the total reaction products (Table 3.S.4). This corresponds to a 66% decrease in band intensity between the first and second incorporations. The band corresponding to the incorporation of a nucleotide opposite the fifth template base directly preceding the guanine at position six in the template represented 17.5% of the reaction products, while the band representing the next incorporation represented only 8.8% of the and the band representing nucleotide incorporation opposite the third template guanine in this stretch represented only 3.5% of the total reaction products. This could again suggest that the incorporation of dCTP opposite a guanine template base may be impaired for pol η and that extension kinetics prior to the incorporation of dCTP opposite a template guanine are not favorable. However after successful nucleotide incorporation opposite the template guanine, further extension is likely.

Similar patterns were observed when reactions were carried out using the alternative template sequences, CGAT and GCTA (Figure 3.2B, C). In the CGAT template, there are guanine bases situated at the third and fifth positions as well as a string of three consecutive guanine bases at positions nine, ten and eleven (Figure 3.2B). The string of three guanine bases appeared to particularly contribute to impaired extension. For the equimolar reaction in which the total dNTP concentration was 100 μM, the band intensity that corresponded to a nucleotide opposite the eighth base in the sequence represented 7.8% of the total reaction products (Table 3.S.4). The band intensity at the next two positions represented 7.6% and 9.8% of the total, respectively. In contrast, though, the band that represents dNTP incorporation opposite the last guanine in the series of three constitutes only 3.1% of the total

reaction products. For the unequal molar reaction, the same pattern was observed. The band intensity at position eight was 11.1% of the total, 13.0% and 10.1% at positions nine and ten, respectively and yet only 2.9% at position 11.

The template sequence for the final template used, GCTA, also possesses seven template guanines including four template guanines in succession at positions four, five, six and seven (Figure 3.2C). Our hypothesis was that if incorporation of dCTP opposite a template guanine was indeed problematic for pol η, the presence of four template guanines near the beginning of the sequence would greatly impair extension. That is, in fact, what was ultimately observed. For the equimolar reaction, the band intensity at position three was 6.5% of the total (Table 3.S.4). At positions four through seven, the intensities were 5.1%, 23.6%, 21.5% and 4.7% of the total, respectively. For the unequal molar reaction, the intensities for the same bands were 27.8%, 11.8%, 18.3%, 5.8% and 1.5%. In both cases, a large increase in band intensity was observed either directly prior to or within the string of four template guanines.

To provide further information as to whether or not dCTP was the limiting dNTP in these reactions and a contributing factor to the impaired extension observed, 100 μM of each individual dNTP was supplemented to individual reactions in which the total concentration of unequal dNTP pools was 50 μM (Figure 3.1D, Table 3.S.3). Stimulation of primer extension was observed only for when supplemental dCTP was added to the reaction. For the reaction in which dNTPs were not added, only 1% of the reaction products were the result of the incorporation of more than 15 nucleotides (Table 3.S.2). For the reaction in which dATP was added, 2% of the reaction products were the result of the incorporation of more than 15

nucleotides (Table 3.S.3). The corresponding result for dGTP was 1% and there were no detectable reaction products that were the result of the addition of greater than 15 nucleotides when dTTP was added to the reaction. However, when 100 μM of dCTP was added to the reaction, 13% of the reaction products represented the incorporation of the same number of nucleotides (13x change). Interestingly, not only did the addition of dATP, dGTP and dTTP fail to yield an increase in polymerization beyond 15 nucleotides, they appeared to also inhibit incorporation of the first five nucleotides during primer extension. For the reaction in which additional dNTPs were not added, 46% of the reaction products were the result of the incorporation of less than six nucleotides (Table 3.S.2). Corresponding values for reactions with the addition of 100 μM dATP, dGTP and dTTP were 55%, 67% and 65%, respectively (1.2x, 1.5x, 1.4x) (Table 3.S.3). Extension impairment was not observed for the reaction in which dCTP was supplemented; there was no change (46%) in the percentage of total reaction products that were the result of less than six nucleotides.

Pol η fidelity in the presence of equimolar and unequal dNTP pools

The primary objective of this study was to assess the effect of unequal dNTP pools on the fidelity of replication and DNA damage bypass past TTD and 8-oxoG lesions by pol η. To accomplish this we used an *in vitro* reversion mutation assay. In this assay, pol η was allowed to fill a primer-template substrate whose sequence corresponds to a portion of the *lacZα* gene. Within the sequence a premature stop codon was present in which a lesion or corresponding undamaged nucleotides were located. Accurate replication retained the stop codon within the sequence, while insertion of an incorrect nucleotide(s) resulted in reversion

to a viable *lacZα* sequence. After substrate extension was complete, the synthesized strand was recovered and annealed to M13mp18 gapped DNA. The annealed plasmid was transformed into *E. coli* and M13 plaques that contained DNA in which incorrect nucleotides were incorporated at the stop codon were able to be distinguished by their dark blue phenotype from those that possessed DNA that was faithfully replicated. DNA from those dark blue plaques was then amplified and sequenced to determine polymerase error rates and spectrums.

Unequal dNTP pools do not appreciably affect total single base substitution error rate. The error rates calculated indicate that there is not an appreciable difference in total single base substitutions detected by this assay between reactions in which equimolar dNTP pools were present and those in which unequal dNTP pools were present. We regard an appreciable difference as a fold change of two or greater (i.e. less than 0.5x or greater than 2x change).

We first compared reactions in which the total dNTP concentration was 240 μM. Three comparisons were made. First, we carried out paired reactions using undamaged DNA substrate. The total single base substitution error rate for reactions in which equimolar dNTPs were present was 540×10^{-4} (Table 3.1). For those in which unequal dNTP pools were used, the error rate was 530×10^{-4} (no change). The same paired reactions were also completed using 8-oxoG and TTD damaged substrates. There was not a significant change in error rate during bypass of either lesion. For nucleotide insertion opposite 8-oxoG, the error rate for equimolar dNTP reactions was 4600×10^{-4} while the error rate for unequal dNTP reactions

was 4800×10^{-4} (no change). For TTD, the error rate increased slightly from 410×10^{-4} to 620×10^{-4} (1.5x change, equimolar and unequal molar dNTPs, respectively).

We were curious as to whether or not the total dNTP concentration would affect these results. The total dNTP concentration was doubled to 480 μM and the same sets of paired reactions were completed. The results were similar; there was generally not an overwhelming difference between the reactions in which equimolar dNTP pools were used and the reactions in which unequal dNTP pools were used. For reactions in which pol η was allowed to catalyze DNA synthesis on undamaged substrate, the error rate decreased only slightly from the equimolar reactions to the unequal molar reactions: 660×10^{-4} (equimolar dNTPs) compared to 380×10^{-4} (unequal dNTPs, 0.6x change) (Table 3.1). The error rate also changed only slightly for reactions in which 8-oxoG was present in the template: 4300×10^{-4} (equimolar dNTPs) compared to 6300×10^{-4} (unequal dNTPs, 1.5x change). For reactions in which TTD was bypassed, the error rate was essentially the same: 600×10^{-4} to 670×10^{-4} (1.1x change, equimolar and unequal molar dNTPs, respectively).

Unequal dNTP pools alter base substitution spectrum. While we did not observe a change in total single base substution error rate, we did find that the spectrum of misincorporated nucleotides was altered when unequal dNTP pools were used (Figure 3.3). For reactions using both undamaged and damaged substrates, we observed changes to the rate of nucleotide misincorporation for certain specific errors including T → C transitions, and T → A and G → T transversions.

First, because the incorrect pairing of template thymine with dGTP has been reported as the most recurrent misincorporation made by pol η, the error rates leading to a T → C

transition were calculated for reactions in which both equimolar and unequal molar dNTPs were present (Matsuda et al., 2000; Johnson et al., 2000b; Matsuda et al., 2001; McCulloch et al., 2004c). For reactions in which the total dNTP concentration was 240 μM, the error rate for T → C changes decreased slightly from 360×10^{-4} when dNTP pools were of equal size to 210×10^{-4} when unequal pools were used (0.6x change) (Figure 3.3A). Using a total dNTP concentration of 480 μM resulted in a decrease as well; the error rate for reactions in which equimolar dNTPs were present was 360×10^{-4}, while the rate for the corresponding unequal molar dNTP reactions was 180×10^{-4} (0.5x change).

As pol η is well understood to be responsible for the bypass of TTD DNA lesions (Masutani et al., 1999a; 1999b), the error rate for the misincorporation of dGTP opposite the 3′T of the TTD CPD was also calculated (Kokoska et al., 2003; McCulloch and Kunkel, 2006). For both 240 μM and 480 μM reactions, a reduction in error rate was observed (Figure 3.3B). For the reactions in which the total dNTP concentration was 240 μM, the error rate decreased from 160×10^{-4} to 110×10^{-4} (0.7x change, equimolar and unequal molar, respectively). For the reactions in which a total dNTP concentration of 480 μM was present, the error rate decreased from 270×10^{-4} for the equimolar reactions to 78×10^{-4} for the unequal molar reactions, which corresponds to a 0.3x change.

When comparing equimolar and unequal molar reaction error rates, the misincorporation for which the greatest changes were observed was the mispairing of dTTP with both undamaged and damaged template thymine bases. Resulting in a T → A transversion mutation, the error rate consistently increased when comparing equimolar to unequal molar reactions for those with both 240 μM and 480 μM total dNTPs (Figure 3.3C).

For the 240 μM reactions the error rate when copying the undamaged base increased from 58×10^{-4} to 140×10^{-4} (2.4x change, equimolar and unequal molar reactions, respectively). For reactions in which the total dNTP concentration was 480 μM, it similarly increased from 31×10^{-4} to 65×10^{-4} (2.1x change, equimolar and unequal molar reactions, respectively).

Opposite the 3′T of a TTD the rate of mispairing with dTTP increased from 54×10^{-4} to 350×10^{-4} for the reactions in which the total dNTP concentration was 240 μM, which corresponds to a 6.5x increase (Figure 3.3D). For the corresponding reactions at twice the total dNTP concentration, there was also an increase: 120×10^{-4} to 300×10^{-4} (2.5x change, equimolar and unequal molar dNTPs, respectively). Interestingly, while the misincorporation of dGTP leading to a TTD 3′T → C change was more common in the reactions for which the dNTPs were equimolar, the misincorporation of dTTP leading to a TTD 3′T → A change was more common in the reactions for which the dNTPs were of unequal concentration.

Opposite an undamaged guanine base, the rate of nucleotide misincorporation by pol η is relatively infrequent. However when a guanine base is oxidized to 8-oxoG in the presence of ROS, the damaged base is readily mispaired with dATP, which can result in a G → T transversion mutation (Zhang et al., 2000a; McCulloch et al., 2009). The error rates calculated for the bypass of both undamaged guanine and damaged 8-oxoG bases by pol η suggest that the effect of unequal dNTP pools may be greater for the former (Figure 3.3E, F). When copying the undamaged base in reactions with total dNTP concentration of 240 μM, the error rate for reactions in which the dNTPs were equimolar was 12×10^{-4} (Figure 3.3E). The error rate for the corresponding unequal molar dNTP reactions was 55×10^{-4} (4.6x change). When the total dNTP concentration was doubled, the error rate for dATP

misincorporation was 31×10^{-4} when the dNTP pools were equimolar, while the rate was 45×10^{-4} for reactions in which the dNTP pools were unequal (1.5x change).

When copying the oxidized base, 8-oxoG, the error rates were significantly elevated over those resulting from the replication past an undamaged guanine and generally in agreement with previously published data (McCulloch et al., 2009; Suarez et al., 2013). However, a large change in error rate for reactions in which the total dNTP concentration was 240 μM was not observed when comparing those with equimolar dNTPs to those with unequal molar dNTPs. The error rate for the former was 4000×10^{-4}, and 4400×10^{-4} for the later which equates to only a 1.1x change (Figure 3.3F). A slightly larger 1.6x increase was calculated when the total dNTP concentration was 480 μM. The error rate when the dNTPs were equimolar was 3600×10^{-4} and 5800×10^{-4} for reactions with unequal dNTP pools.

Discussion

Total dNTP concentration as well as individual dNTP pool concentration affects primer extension by pol η. It was not altogether surprising to observe a reduction in the ability of pol η to catalyze primer extension as the result of a reduction in total dNTP concentrations. The concentrations at which impaired extension began to be detected, however, were greater than anticipated. For the equimolar reaction, impairment in extension was observed at a total dNTP concentration of between 200 μM and 100 μM. The individual dNTP concentrations for these reactions were 50 μM and 25 μM, respectively. For the equimolar reaction, impairment was observed at a total dNTP concentration of 240, in which

individual nucleotide concentrations were 38 μM dATP, 25 μM dCTP, 25 μM dGTP and 150 μM dTTP.

For both the 100 μM equimolar reaction and the 240 μM unequal molar reaction, dCTP and dGTP concentrations were 25 μM. As dTTP was greatly elevated to 150 μM in the unequal molar reaction, it would seem that dTTP is not a likely candidate for the cause of the extension impairment observed. While dATP is only slightly elevated to 38 μM in the unequal molar reaction and therefore could be limiting polymerization in some way, the additional observation that primer extension reaction products consistently revealed impaired extension immediately prior to guanine bases in all the template sequences assessed suggests that the incorporation of the base opposite to template guanine bases, which presumably would be dCTP, is the culprit for the extension impairment observed. That only the addition of dCTP to the 50 μM unequal molar reaction resulted in any appreciable stimulation of extension provides additional evidence that dCTP is the limiting nucleotide in these reactions.

The findings from the extension reactions on the alternate templates, CGAT and GCTA, would also appear to support that low dCTP concentrations result in reduction of pol η extension activity. As stated, we consistently observed impaired extension immediately prior to guanine bases. The effect was reliably amplified in the unequal molar reactions in which the dCTP concentration was 6.9 μM compared to the equal molar reactions in which the dCTP concentration was 25 μM, suggesting that dCTP concentration is important to efficient polymerase activity.

Interestingly, while dCTP concentration in the equimolar reactions is low (11% of the total dNTP concentration), dGTP concentration is comparable at 10% of the total dNTP concentration. In spite of the essentially equally reduced concentrations, no discernable extension impairment was observed at template cytosine bases, nor did the addition of dGTP to the 50 μM reaction provide any stimulation in primer extension. This would indicate that the basis for effects observed by altered dNTP pools is not simply the reduction of a single dNTP concentration but the identity of that dNTP as well.

Kinetic analysis of human pol η has been conducted and K_m values have been measured for incorporation of both correct and incorrect nucleotides opposite undamaged and TTD damaged DNA as well as for extension from those same base pairs (Matsuda et al., 2000; Johnson et al., 2000b; Washington et al., 2001a; 2001b). Values vary widely however. For example, opposite a template thymine base, K_m values of both 31 ± 6 μM (Matsuda et al., 2000) and 0.13 ± 0.02 (Johnson et al., 2000b) have been reported for the incorporation of the correctly paired nucleotide, dATP. Furthermore, results from within the same lab also appear to differ (Washington et al., 2001a; 2001b). Because of the uncertainty generated by the differing values as well assay variation, it is difficult to draw correlations between our observations and the published values available. However, published K_m values for correct nucleotide incorporation by pol η would appear to support the observation that, of the four possible correct nucleotide pairs, dCTP incorporation could be especially problematic. Steady state kinetic study calculated the K_m of correct dCTP incorporation to be 0.44 ± 0.0.6 μM, while the K_m values for correct dATP, dGTP and dTTP were 0.13 ± 0.02 μM, 0.23 ± 0.06 μM and 0.27 ± μM, respectively (Johnson et al., 2000b). Thus, dCTP incorporation

requires the highest concentration to reach its half-maximal reaction rate and these values could provide a partial explanation to the preferential impaired extension observed prior to dCTP incorporation. We do note that the concentrations at which our reactions were carried out are significantly higher than the K_m values cited, however the sensitivity of the steady state kinetic assays used to derive those values are distinct from that of the TLS assay employed herein and we would assert that it is the relative values that are central here.

Unequal dNTP pools affect pol η single base substitution error rates. Three changes in error rates were primarily observed for the reactions in which the dNTP pools were unequal; two were at template thymine bases while one was at a template guanine base. Notably, though the same changes were observed at both undamaged and damaged bases, the magnitude of change appeared to vary. Nevertheless, the relative concentrations of correct and incorrect dNTPs available for pairing with the template bases appear to provide plausible justification for both the increases and decreases in error rates in all cases.

At thymine template bases, unequal dNTP pools resulted in both an increase in the incorporation of dTTP, which resulted in a corresponding increase of T → A changes, as well as a decrease in the incorporation of dGTP, which resulted in a commensurate decrease of T → C changes. As dATP and dGTP are reduced to 16% and 10%, respectively, in the unequal molar dNTP reactions and dTTP is increased to 63%, it would be reasonable to attribute the changes observed at least in part to dNTP concentration pool changes. Opposite TTD damaged bases, unequal dNTP pools had the same effect. Generally, it appeared that the magnitude of change in error rate was comparable between undamaged and TTD damaged substrates.

One change observed at the TTD modified base was of particular interest. As noted, the reduction in dGTP misincorporation with the coincident increase in dTTP misincorporation resulted in a shift of the most common change observed at the 3′T of a TTD from T → C to T → A. Opposite the 3′T, Johnson et al. determined the frequency of misincorporation (f_{inc}) of all possible mispairs using a single nucleotide, steady-state kinetic approach. The value of f_{inc} for dGTP misincorporation resulting in a 3′TTD → C change was 4.2×10^{-3}, while the value of f_{inc} for dTTP misincorporation resulting in a 3′TTD → A change was 1.1×10^{-2} (Johnson et al., 2000b). This would suggest that dTTP would be mispaired with the damaged base more frequently, however when propensity for extension was considered, it was asserted that, for the complete bypass event, misincorporation of dGTP was just slightly favored (Washington et al., 2001a). This explanation supported later *in vitro* studies that concluded the 3′T → C change was the most common error made by pol η at the TTD modified base (McCulloch et al., 2004c; Suarez et al., 2013). Those experiments, though, were carried out using equimolar dNTP pool concentrations at a total dNTP concentration of 400 μM. In contrast, the unequal dNTP pool conditions used here would suggest that previous observations and explanations presented may not detail the complexity of pol η fidelity and that, *in vivo*, polymerase fidelity may be rather plastic. As T → A mutations have been observed in skin cancer cells (Pleasance et al., 2010), we believe that the observations included here may provide a basis for those mutations.

In addition, at template guanine bases, an increase in error rate was measured for misincorporation of dATP leading to a G → T change, which can also be explained by the dNTP concentration changes in the unequal molar reactions. Specifically, a greater decrease

in the correct Watson-Crick pairing nucleotide, dCTP (11%) over the incorrect pairing, dATP (16%) in the unequal molar reactions is likely driving the G·A mispairing. At the corresponding damaged base, 8-oxoG, it appeared that the unequal nucleotide pools affected the error rate of dATP misincorporation to a lesser degree. As the oxidized guanine base readily assumes a syn conformation, it is possible that the properties associated with the *syn-anti* 8-oxoG·A basepair make the damaged base less responsive to changes in dNTP concentrations (McAuley-Hecht et al., 1994; Reynisson and Steenken, 2002; Cheng et al., 2005; Reynisson and Steenken, 2005).

Acknowledgements

We thank Drs. Robert C. Smart (North Carolina State University) and Thomas A. Kunkel (National Institute of Environmental Health Sciences) for helpful conversations and materials. This work was supported by the National Institute of Environmental Health Sciences of the National Institutes of Health [R01 ES016942] (SM) and [T32 ES007046] (SM, RB) and the College of Agriculture and Life Sciences at North Carolina State University (ST).

Figures

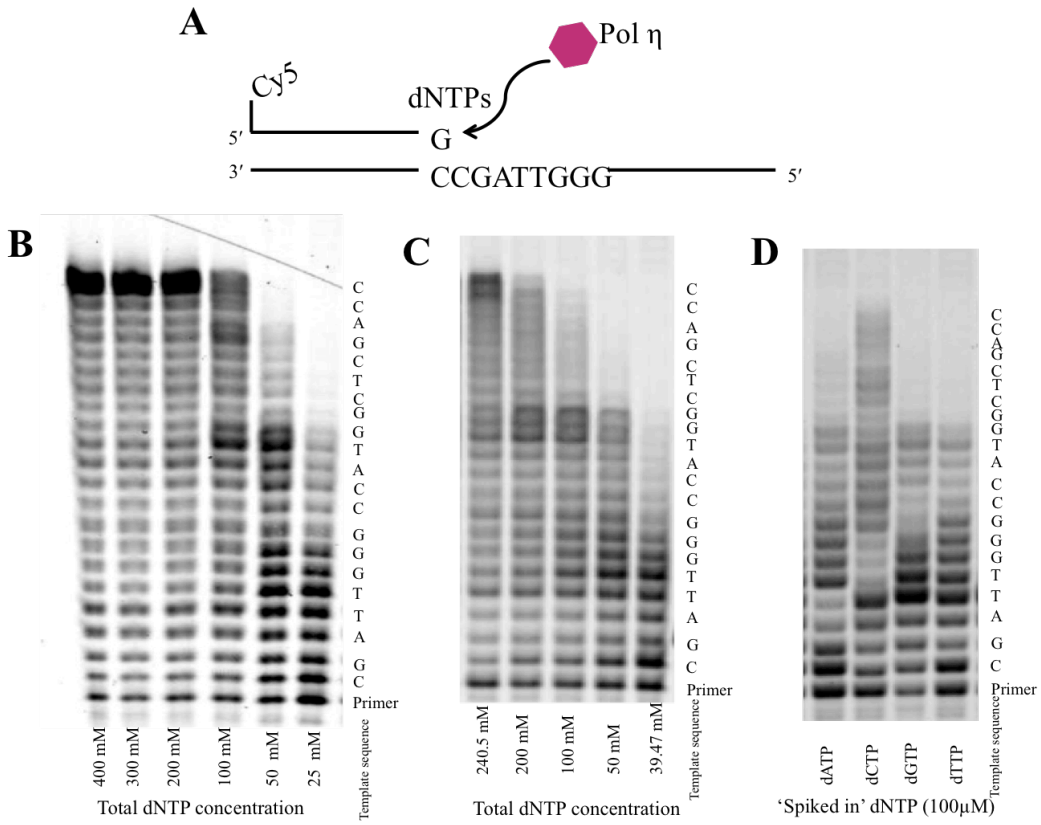

Figure 3.1 Primer extension in the presence of changing dNTP pools by pol η.

A. Schematic diagram of primer extension reactions (45-mer template, 24-mer primer). **B.** Polymerase extension reaction product separation by denaturing polyacrylamide gel electrophoresis. Individual dNTP pool concentrations were equimolar in these reactions (dATP 25%, dCTP 25%, dGTP, 25%, dTTP 25%). **C.** Polymerase extension reaction product separation by denaturing polyacrylamide gel electrophoresis. Individual dNTP pool concentrations were unequal molar in these reactions (dATP 16%, dCTP 11%, dGTP 10%, dTTP 63%). **D.** Polymerase extension reaction product separation by denaturing polyacrylamide gel electrophoresis. Total dNTP pool concentration was 50 μM (individual dNTP pool concentrations unequal) with a single additional dNTP spiked in at 100 μM. Labels denote the species of the spiked in dNTP. Quantification of all replication product bands and quadrants is presented in tables located in the Supplemental Information. 3.1.A Reprinted by permission from John Wiley and Sons: Environmental and Molecular Mutagenesis Volume 54, Issue 8, pages 638–651, October 2013. Copyright 2013 John Wiley and Sons.

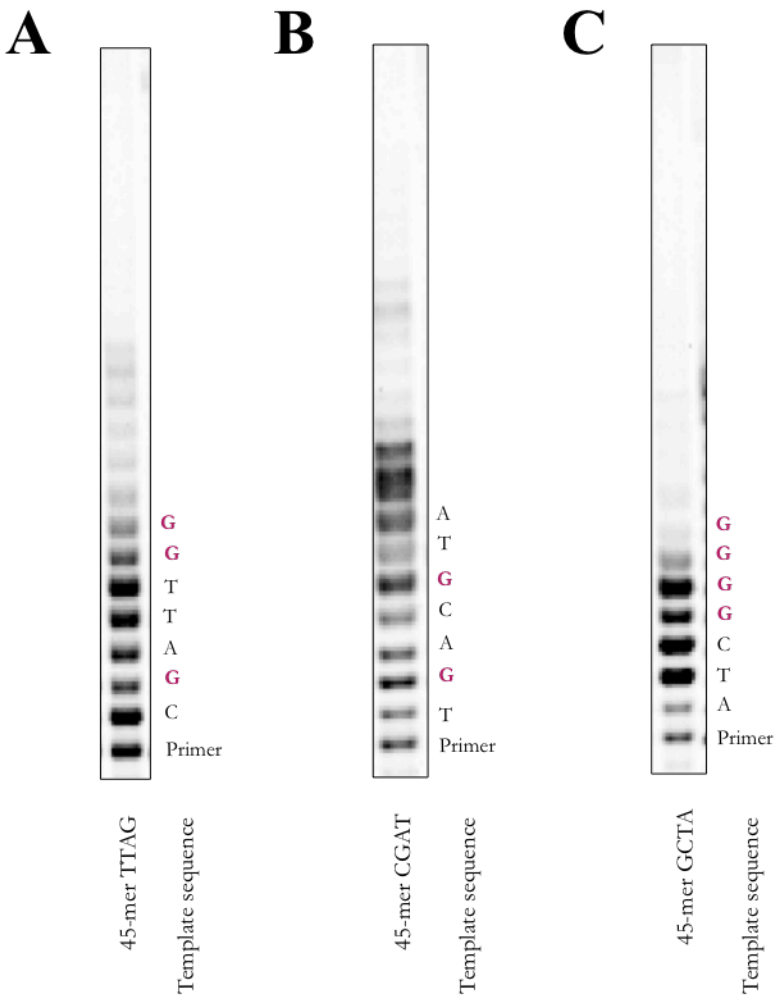

Figure 3.2 Pol η primer extension is affected by template sequence.

Representative polymerase extension reaction product separations by denaturing polyacrylamide gel electrophoresis. Total dNTP concentration in each reaction was 66 μM. Individual dNTP pool concentrations were unequal molar in these reactions (dATP 16%, dCTP 11%, dGTP 10%, dTTP 63%). **A.** TTAG template sequence. **B.** CGAT template sequence. **C.** CGTA template sequence. Quantification of all replication product bands and quadrants is presented in tables located in the Supplemental Information.

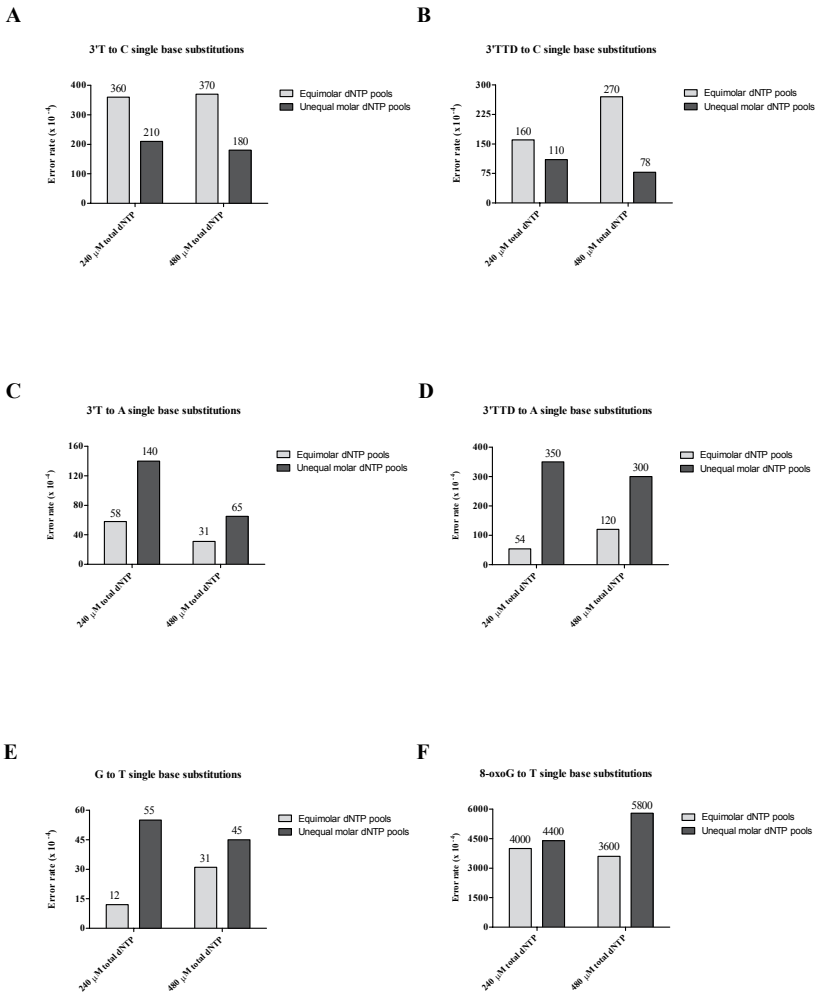

Figure 3.3 Changing dNTP pools affect pol η error rates.

A. T → C error rates for reversion mutation assay. **B.** TTD 3′T → C error rates for reversion mutation assay. **C.** T → C error rates for reversion mutation assay. **D.** TTD 3′T → A error rates for reversion mutation assay. **E.** G → T error rates for reversion mutation assay. **F.** 8-oxoG → T error rates for reversion mutation assay. An increase or decrease in concentration of an incorrect nucleotide results in an increase or decrease in error rate, respectively (direct relationship). Similarly, an increase or decrease in concentration of the correct nucleotide results in a decrease or increase in error rate, respectively (indirect relationship). Values for the following reactions are the average of two independent experiments: 240 μM, TTAG and TTA(8-oxoG), unequal molar; 240 μM, TTA(8-oxoG), equal molar; 480 μM, TTAG and TTA(8-oxoG), unequal molar. The remaining values are from single experiments.

Tables

Table 3.1 Total single base substitution error rates.

Total single base substitution error rates for reactions win which total dNTP concentrations were 240 μM and 480 μM using TTAG template sequence substrates containing undamaged DNA, TT dimer and 8-oxoG modified bases. Values for the following reactions are the average of two independent experiments: 240 μM, TTAG and TTA(8-oxoG), unequal molar; 240 μM, TTA(8-oxoG), equal molar; 480 μM, TTAG and TTA(8-oxoG), unequal molar. The remaining values are from single experiments.

	240 μM total dNTP concentration			480 μM total dNTP concentration		
	TTAG	(TTD)AG	TTA(8-oxoG)	TTAG	(TTD)AG	TTA(8-oxoG)
Equimolar dNTP reactions	540×10^{-4}	4600×10^{-4}	410×10^{-4}	660×10^{-4}	4300×10^{-4}	600×10^{-4}
Unequal molar dNTP reactions	530×10^{-4}	4800×10^{-4}	6200×10^{-4}	380×10^{-4}	6300×10^{-4}	670×10^{-4}
Change relative to equimolar reactions	no change	no change	1.5x	0.6x	1.5x	1.1x

Supplemental Information

Table 3.S.1 Equimolar extension reactions

Values represent raw data generated from the pixel density of 5′-Cy5-labeled DNA oligo primer bands imaged with a Storm™ 865 imager (GE Healthcare) and quantified using Image Quant™ TL software (GE Healthcare). Headings note the total dNTP concentration of the reactions. The top portion of the data represents pixel density of individual bands; the bottom portion comprises sums of certain sets of bands as detailed in the results section.

400 uM		300 uM		200 uM		100 uM		50 uM		25 uM	
Band No	Volume	Band No	Volume	Band No	Volume	Band No	Volume	Band No	Volume	Band No	Volume
21	33589689.8	21	33092156.1	21	29383236.6	21	9245086.3	21	123284.0	21	103140.4
20	4197440.3	20	4148436.6	20	4829992.3	20	4583501.2	20	156123.3	20	10325.0
19	2948015.1	19	3125560.2	19	3126041.8	19	4638577.8	19	722813.3	19	50814.0
18	3297776.4	18	3239997.7	18	3879281.6	18	6487697.7	18	829271.1	18	52939.5
17	2348722.5	17	2465428.2	17	2557959.9	17	3462205.7	17	966452.4	17	83769.3
16	2379441.0	16	2617219.5	16	2889046.7	16	3543217.6	16	1345306.2	16	137425.1
15	2575860.4	15	2642857.6	15	3284993.4	15	3641317.5	15	1378166.5	15	175969.9
14	1486340.7	14	1708650.9	14	1867886.7	14	2156354.6	14	1319683.9	14	219451.3
13	1834092.7	13	2056372.3	13	2292036.3	13	5112315.1	13	5021635.1	13	759485.4
12	2504100.7	12	2761568.8	12	3598175.4	12	8512773.5	12	9720977.8	12	1721418.5
11	2426038.7	11	2791625.5	11	3505025.0	11	4988025.5	11	6048455.0	11	1899512.8
10	1641272.5	10	1892014.7	10	2399083.3	10	3340550.0	10	5534100.3	10	2281681.2
9	1161179.7	9	1460331.6	9	1786098.9	9	2230780.9	9	3415483.7	9	1812808.3
8	1658094.1	8	1821631.0	8	2348461.0	8	3204103.9	8	4092790.9	8	2314319.8
7	1271342.6	7	1420814.7	7	1874215.9	7	3177131.8	7	7271585.6	7	4607105.1
6	1258580.0	6	1321549.5	6	1744098.1	6	2873723.9	6	6800674.0	6	5525658.0
5	1303007.4	5	1298959.6	5	1749983.7	5	3170450.6	5	10806922.2	5	11121759.3
4	2462609.4	4	2550043.3	4	3243163.5	4	4733138.2	4	7310961.4	4	7937549.7
3	2058046.2	3	2138888.7	3	2475511.9	3	3083510.5	3	4621174.6	3	5846426.6
2	1465477.0	2	1456958.2	2	1718184.5	2	2288326.3	2	3802085.5	2	5490845.6
1	1253798.4	1	1185023.6	1	1587058.0	1	2106206.7	1	4336209.4	1	8246638.5
Primer	2418537.2	Primer	2207691.7	Primer	2934470.3	Primer	3286234.9	Primer	4314523.1	Primer	11274873.6
Totals											
1-5	8542938.4	1-5	8629873.4	1-5	10773901.5	1-5	15381632.2	1-5	30877353.1	1-5	38643219.6
6-10	6990468.9	6-10	7916341.4	6-10	10151957.3	6-10	14826290.4	6-10	27114634.5	6-10	16541572.3
11-15	10826433.1	11-15	11961075.0	11-15	14548116.7	11-15	24410786.1	11-15	23488918.3	11-15	4775837.8
16-21	48761084.9	16-21	48688798.3	16-21	46665558.8	16-21	31960286.3	16-21	4143250.3	16-21	438413.3
1-21	75120925.2	1-21	77196088.2	1-21	82139534.3	1-21	86578994.9	1-21	85624156.2	1-21	60399043.0
Total	77539462.5	Total	79403779.9	Total	85074004.6	Total	89865229.8	Total	89938679.3	Total	71673916.6

Table 3.S.2 Unequal molar extension reactions.

Values represent raw data generated from the pixel density of 5′-Cy5-labeled DNA oligo primer bands imaged with a Storm™ 865 imager (GE Healthcare) and quantified using Image Quant™ TL software (GE Healthcare). Headings note the total dNTP concentration of the reactions. The top portion of the data represents pixel density of individual bands; the bottom portion comprises sums of certain sets of bands as detailed in the results section.

240.5 uM		200 uM		100 uM		50 uM		37.47 uM	
Band No	Volume	Band No	Volume	Band No	Volume	Band No	Volume	Band No	Volume
21	3025576.5	21	447878.6	21	31489.4	21	14500.7	21	18382.5
20	4007777.7	20	1949249.0	20	332189.1	20	12775.6	20	13746.5
19	1346396.0	19	1075983.8	19	353231.3	19	21484.0	19	7230.8
18	1051961.5	18	965550.2	18	375152.3	18	37973.7	18	5943.3
17	1083206.0	17	949763.0	17	450667.6	17	71793.4	17	7999.6
16	931649.9	16	917650.5	16	435543.3	16	100599.7	16	13901.1
15	950453.3	15	1020120.6	15	614492.5	15	187750.1	15	22596.3
14	1164715.6	14	1703852.5	14	1977855.7	14	949075.9	14	80075.9
13	1333092.3	13	2048165.4	13	1479194.7	13	881001.0	13	109758.4
12	1719607.2	12	2437019.8	12	2425965.6	12	1220793.4	12	179040.4
11	1090861.8	11	1227409.8	11	1137865.8	11	993109.6	11	225189.7
10	829884.8	10	926654.5	10	1100481.8	10	1209942.2	10	420753.8
9	825604.5	9	1049395.8	9	1256586.8	9	1341253.5	9	550911.2
8	1187746.4	8	1509429.4	8	1929619.9	8	2125571.1	8	1095838.1
7	932729.8	7	1349278.1	7	1986907.4	7	2681655.0	7	1589893.5
6	919160.3	6	1237690.9	6	2009363.8	6	2901460.9	6	2719463.2
5	1034223.5	5	1491608.6	5	2436123.9	5	4149978.4	5	4318464.0
4	1343051.9	4	1709509.4	4	2020645.6	4	2877480.7	4	3467202.0
3	570832.3	3	723764.7	3	880788.4	3	1481592.5	3	2392921.9
2	601575.4	2	789650.4	2	927464.5	2	1436771.1	2	2102788.3
1	710173.5	1	1310124.7	1	1418017.5	1	2552355.7	1	5478861.7
Primer	2454443.7	Primer	1909680.8	Primer	2108484.4	Primer	2664511.8	22	3713403.8
Totals									
1-5	4259856.6	1-5	6024657.8	1-5	7683039.9	1-5	12498178.4	1-5	17760237.9
6-10	4695125.7	6-10	6072448.7	6-10	8282959.7	6-10	10259882.7	6-10	6376859.8
11-15	6258730.2	11-15	8436568.1	11-15	7635374.2	11-15	4231730.0	11-15	616660.6
16-21	11446567.6	16-21	6306075.0	16-21	1978272.9	16-21	259127.1	16-21	67203.9
1-21	26660280.1	1-21	26839749.7	1-21	25579646.7	1-21	27248918.2	1-21	24820962.3
Total	29114723.8	Total	28749430.5	Total	27688131.1	Total	29913430.0	Total	28534366.1

Table 3.S.3 Unequal molar reactions with added 100 µM single dNTP.

Values represent raw data generated from the pixel density of 5′-Cy5-labeled DNA oligo primer bands imaged with a Storm™ 865 imager (GE Healthcare) and quantified using Image Quant™ TL software (GE Healthcare). Headings note the individual dNTP added to the reactions. The top portion of the data represents pixel density of individual bands; the bottom portion comprises sums of certain sets of bands as detailed in the results section.

dATP spike		dCTP spike		dGTP spike		dTTP spike	
Band No	Volume	Band No	Volume	Band No	Volume	Band No	Volume
21	37241.7	21	507452.5	21	18768.3	21	12027.7
20	43923.4	20	567678.3	20	10405.3	20	6968.1
19	73796.8	19	441616.3	19	39053.1	19	24041.9
18	128976.3	18	383526.8	18	43030.6	18	14738.6
17	189845.7	17	646118.5	17	54227.7	17	25522.3
16	196449.4	16	959899.5	16	140344.7	16	20861.9
15	194766.0	15	681245.1	15	172160.3	15	42803.5
14	301069.1	14	497350.7	14	688838.7	14	85115.3
13	815352.1	13	755333.0	13	1219592.9	13	388114.7
12	960740.4	12	1474648.2	12	846903.3	12	782547.1
11	640963.7	11	1496235.6	11	729208.3	11	527696.6
10	915205.0	10	1387045.6	10	417473.8	10	468148.8
9	1255904.3	9	2186874.5	9	394494.5	9	673787.4
8	2031865.6	8	1468521.7	8	721527.8	8	1736749.1
7	2407293.6	7	773662.9	7	1812010.7	7	2150747.6
6	2449080.1	6	588480.2	6	3125935.8	6	2634786.8
5	3523100.8	5	1178140.7	5	5527972.9	5	3669593.2
4	858609.7	4	4713671.3	4	8779110.9	4	5215759.6
3	1345775.5	3	2478228.4	3	2558204.1	3	2341053.0
2	3456339.0	2	1685136.2	2	2116769.0	2	1490691.6
1	6582667.8	1	2374246.3	1	2114354.1	1	5062901.4
Primer	6383951.4	Primer	4430029.0	Primer	1792488.3	Primer	4450058.9
Totals		Totals		Totals		Totals	
1-5	15766492.7	1-5	12429422.8	1-5	21096410.9	1-5	17779998.8
6-10	9059348.5	6-10	6404584.7	6-10	6471442.5	6-10	7664219.7
11-15	2912891.3	11-15	4904812.6	11-15	3656703.4	11-15	1826277.2
16-21	670233.3	16-21	3506291.9	16-21	305829.7	16-21	104160.6
1-21	28408965.8	1-21	27245112.0	1-21	31530386.5	1-21	27374656.4
Total	34792917.2	Total	31675140.9	Total	33322874.8	Total	31824715.3

Table 3.S.4 Extension reactions with alternative template sequences.

Values represent raw data generated from the pixel density of 5′-Cy5-labeled DNA oligo primer bands imaged with a Storm™ 865 imager (GE Healthcare) and quantified using Image Quant™ TL software (GE Healthcare). Headings note the total dNTP concentration of the reactions, whether the dNTP concentrations were equimolar (EM) or unequal molar (PR) and the identity of the template sequence used. The top portion of the data represents pixel density of each individual band; the bottom portion comprises sums of certain sets of bands as detailed in the results section.

100 EM TTAG		100 EM CGAT		100 EM GCTA		66 PR TTAG		66 PR CGAT		66 PR GCTA	
Band No	Volume	Band No	Volume	Band No	Volume	Band No	Volume	Band No	Volume	Band No	Volume
21	275188.0	21	1171446.3	21	52192.2	21	6251.3	21	31474.7	21	11744.4
20	458352.7	20	854471.9	20	211471.9	20	5270.0	20	44514.9	20	13414.1
19	412154.6	19	737953.8	19	347862.9	19	12903.0	19	65882.0	19	13654.3
18	1579110.4	18	511958.2	18	770232.8	18	16008.7	18	59570.8	18	14817.4
17	724165.0	17	460176.1	17	349055.2	17	21338.6	17	82739.6	17	22211.6
16	789735.5	16	1229562.6	16	254612.8	16	27496.7	16	292554.1	16	19904.8
15	605476.7	15	2076521.2	15	343990.4	15	32191.8	15	574327.3	15	43513.7
14	602020.0	14	980087.4	14	286250.4	14	70394.0	14	305850.7	14	42826.3
13	1703362.3	13	1146335.7	13	328388.2	13	358091.8	13	179451.7	13	49408.7
12	2224577.6	12	492465.0	12	759229.1	12	506180.2	12	284324.2	12	140195.8
11	1432383.8	11	724891.0	11	487761.6	11	483259.3	11	703880.0	11	137080.5
10	1043554.0	10	2317240.0	10	849175.9	10	423137.8	10	2488794.0	10	83880.9
9	705215.1	9	1806229.0	9	494526.8	9	516064.5	9	3196461.2	9	107481.5
8	828806.3	8	1854477.3	8	871854.0	8	891057.1	8	2737767.1	8	337474.7
7	1071345.7	7	1620265.2	7	1123568.5	7	1611757.6	7	3085663.5	7	382476.4
6	1049335.4	6	1806950.1	6	5133819.6	6	2256224.8	6	1549394.3	6	1436134.3
5	1470803.1	5	862055.0	5	5630382.4	5	4480210.8	5	2901302.1	5	4516284.3
4	1877883.1	4	453277.1	4	1227454.7	4	3758477.9	4	1503274.3	4	2928693.6
3	1326184.7	3	504715.5	3	1549577.5	3	2492275.4	3	1481813.8	3	6880843.5
2	1194113.2	2	846147.9	2	2141855.4	2	1893142.0	2	1977542.2	2	6684423.1
1	1683236.5	1	1176979.8	1	689311.9	1	5773617.2	1	1107503.6	1	871460.2
Primer	2256862.5	Primer	1470111.7	Primer	1287338.1	Primer	3378158.9	Primer	1584429.0	Primer	1281822.3
Totals											
1-5	7552220.6	1-5	3843175.5	1-5	11238582.0	1-5	18397723.2	1-5	8971435.9	1-5	21881704.7
6-10	4698256.4	6-10	9405161.5	6-10	8472944.8	6-10	5698241.8	6-10	13058080.0	6-10	2347447.9
11-15	6567820.3	11-15	5420300.4	11-15	2205619.7	11-15	1450117.1	11-15	2047833.9	11-15	413025.0
16-21	4238706.3	16-21	4965569.0	16-21	1985427.8	16-21	89268.4	16-21	576736.1	16-21	95746.5
1-21	23057003.6	1-21	23634206.3	1-21	23902574.4	1-21	25635350.4	1-21	24654085.9	1-21	24737924.0
Total	25313866.1	Total	25104318.0	Total	25189912.4	Total	29013509.3	Total	26238514.9	Total	26019746.3

GENERAL DISCUSSION

The study of translesion synthesis (TLS) and DNA polymerase η (pol η) in particular has revealed a rather remarkable strategy used by the cell to tolerate the presence of DNA damage and ensure the conservation of life. Yet, while a great amount is now understood about the process of TLS and the function of human pol η, many fundamental and important details remain obscured. That DNA damage, for example, increases the propensity for miscoding during replication is widely accepted. That miscoding and subsequent mutation introduction are linked to unfavorable human health outcomes is also widely accepted. However, the *explicit* details about how replication occurs past DNA damage are less clear. It is unknown which TLS polymerase is responsible for bypass of most lesions. It is unknown what specifically signals the recruitment of the TLS polymerases to the damage site and what determines which polymerase, in that event, will act. It is unknown how TLS polymerases with such apparent poor fidelity *in vitro* act to suppress mutagenesis *in vivo.* While the scope of this work cannot possibly begin to address the abundant questions that remain, it has attempted to ascertain an understanding of the fine biochemical details of nucleotide mispairing by pol η.

Findings

The totality of this work would suggest that pol η evolved specifically for the purpose of lesion bypass and that its structure is optimized for replication past DNA damage at the cost of mutation introduction. This is supported by the finding that modifications to the highly conserved β-strand in the little finger domain that is critical for substrate binding had

little effect on the fidelity with which both *cis-syn* thymine-thymine cyclobutane pyrimidine dimers (TTD) and 7,8-dihydro-8-oxoguanine (8-oxoG) lesions were bypassed. The nature of these lesions necessitate that pol η possess an open active site; a tightly fit binding pocket as is present in the replicative polymerases would be incompatible. As a result, the open active site likely evolved. Because an open active site, though, would not, by its nature, provide support to a DNA substrate and position the nucleotide pair correctly for catalysis, it is likely that the polymerase evolved an alternative method, which includes the downstream DNA-protein contacts described in chapter two.

Additionally, while we were not able to appreciably alter polymerase fidelity when copying CPDs and 8-oxoG by β-strand amino acid substitution, we were able to affect fidelity by modifying dNTP concentrations as discussed in chapter three. This also supports the notion that the primary function of the polymerase is successful lesion bypass; that, in contrast to replicative polymerases, guardianship of fidelity was not central in its evolution and that the cell is able to tolerate significant and varied nucleotide mispairings and mutation introduction.

Implications and Further Study

Pol η function and fidelity of β-strand mutants. Extension of work from both chapter two and chapter three would be insightful. After analysis of the fidelity data revealed that the T318A mutant consistently made a variety of errors with less frequency than the wild type and other mutated forms of the polymerase, we were prompted to return to the structure and take a closer look at the threonine residue at that position. As discussed, a small region of

protein distal to the active site near T318 appears to be especially important to stabilize the newly synthesized duplex DNA. Interactions additional to those included in our study cooperate with T318 including L317, D355 and R361. A biochemical analysis of the complete set of residues that stabilize the downstream DNA would help to fully elucidate the function of this important region of the polymerase to lesion bypass.

In addition to biochemical studies, cultured XPV cells transfected with the β-strand mutants and other proposed mutated forms of pol η might provide additional insight regarding the significance of this portion of the polymerase to TLS activity. The extent to which the mutated forms of pol η do or do not rescue the XPV phenotype may help to ascertain whether or not our hypothesis that extension is impaired due to disruption of downstream interactions that normally stabilize the active site is correct.

In addition, the use of a recently developed assay that utilizes oligonucleotide probes (oligonucleotide probe retrieval assay, OPRA) synthesized with CPDs and 8-oxoG lesions transfected into human cells (Shen et al., 2014) might be a promising method to elucidate the extent to which pol η synthesizes nucleotides immediately before and/or after a lesion within DNA. As the β-strand mutants displayed altered fidelity when copying undamaged DNA *in vitro*, a similar display of altered fidelity during replication of the DNA probe in cultured cells may provide evidence for the existence of the polymerase's proposed molecular switch two nucleotides beyond the 5′T of the CPD. Further, a similar display of modified fidelity on probes with 8-oxoG lesions may provide additional evidence of the bypass of that lesion *in vivo* by pol η.

Pol η function and fidelity in the presence of unequal dNTP pools. The observed apparent impairment of dCTP incorporation opposite template guanine bases is puzzling and we were not succesful at determining a cause. A review of existing kinetic data revealed no obvious explaination for the consistent stalling observed and as this is the first study of pol η function in the presence of biased dNTP pools, the impairment has not before been documented. A more detailed biochemical study and modeling of the dCTP incorporation would likely be required to explain this observation. While it is difficult at this time to speculate about what consequence this could have *in vivo*, pol η has been implicated in several pathways other than TLS that involve replication on undamaged DNA (Rogozin et al., 2001; Zeng et al., 2001; Kawamoto et al., 2005; Kamath-Loeb et al., 2007; Bétous et al., 2009; Rey et al., 2009). Any base-specific kinetics would certainly be significant to those processes.

In addition to extension impairment at template guanine bases, chapter 3 also described changes to single base substitution error rates at both undamaged bases and TTD lesions in the presence of unequal dNTP pools. This observation could be relevant to cancer progression and a proposed strategy to treat cancer. Because of potential bypass of chemotherapy-induced DNA damage by TLS polymerases, there has been interest in quantifying pol η expression in tumor cells and, as expected, dysregulation in pol η mRNA levels compared to normal cells has been demonstrated in non-small cell lung cancer (Ceppi et al., 2009). More recently, elevation of both pol η mRNA transcripts and protein levels were found in ovarian cancer stem cells isolated from patient primary tumors (Srivastava et al., 2015). In addition to polymerase dysregulation, overexpression of ribonucleotide

reductase (RNR), the enzyme responsible for the rate-limiting step in *de novo* dNTP synthesis, is associated with many cancer types including gastric, ovarian, bladder and colorectal cancer (Morikawa et al., 2010a; 2010b; Lu et al., 2012; Wang et al., 2012; Liu et al., 2013; Aye et al., 2015). In light of our findings that pol η fidelity may be affected by dNTP concentrations, it is plausible that concurrent overexpression of pol η and RNR would result in increased mutation rates as well modified mutation spectra.

It has been proposed that an amplified mutation rate, descibed as a 'mutator phenotype' within cancer cells is important to progression of the disease. Further, it is has also been proposed that targeting the mutation rate may be more a more effective treatment than the current approach that attempts to disrupt oncogene pathways (Loeb, 2011; Fox et al., 2013). Interestingly, while the obvious approach would be to inhibit the ability of mutators within cancer cells, another strategy has been advanced. Adapted from a proposed approach to HIV treatment (Loeb et al., 1999), lethal mutagenesis would attempt to enhance mutagenic pathways to a level unsustainable to the cell and above which cell viability would no longer be possible (reviewed in Fox and Loeb, 2010). It is conceiveable that mutagenesis by pol η may both contribute to a mutator phenotype as well as be a potential target to modulate mutagenesis in cancer cells. Further study, however, would be necessary to more thoroughly understand the effect of changing individual and total dNTP concentrations on pol η function and fidelity. Specifically, *in vitro* cell based assays that attempt to understand how dNTP concentrations change in human cells and how those changes affect TLS would be helpful. Treatment of mutant RNR transfected cultured cells that have modified dNTP concentrations with UVB and/or UVC may be a preliminary tactic to begin to address one of these

questions. Alternatively, UVB/UVC treatment along with exposure to agents shown to affect RNR activity (Fontecave et al., 1998; McCue et al., 2000) or use of the aforementioned OPRA assay in a similar manner may also be acceptable methods.

Limitations

Due to the improved solubility of the truncated protein over the full-length enzyme, we have selected to use the N-terminal portion of the polymerase that includes the catalytic core and comprises amino acid residues 1-511 throughout this work. As previously discussed, human DNA pol η is composed of a N-terminal catalytic region responsible for DNA synthesis and an C-terminal regulatory region that has been shown to include several protein interacting regions (Haracska et al., 2001; Kannouche et al., 2001, 2003; Ohashi et al., 2004; Yang and Woodgate, 2007; Hishiki et al., 2009; Biertümpfel et al., 2010; Yang, 2014). Previous work has demonstrated that the truncated pol η catalytic core is sufficient to correct TT dimer deficiency in XPV cells (Masutani et al., 1999a, 1999b) and retains the same TLS activity as the full-length polymerase (Kusumoto et al., 2004; Biertümpfel et al., 2010, Suarez et al., 2013). In addition, fidelity measurements generated have generally agreed between full-length and truncated forms of the polymerase when copying both undamaged and TTD damaged DNA (McCulloch et al., 2004c; Suarez et al., 2013) as well as 8-oxoG damaged DNA (McCulloch et al., 2009; Suarez et.al. 2013). This would not preclude the possibility that pol η fidelity is modulated though interaction with replication accessory proteins such as proliferating cell nuclear antigen (PNCA), replication protein A (RPA), replication factor C (RFC) and others, however, and this has been proposed to be a possible

mechanism to resolve the apparent disparity between pol η fidelity *in vitro* and mutation rates *in vivo*. Existing data suggests though that accessory proteins do not have any appreciable effect on polymerase fidelity. Results from *in vitro* fidelity studies using both yeast and human pol η, and yeast pol δ in the presence of competitive dNTP selection with RPA, RFC and/or PNCA have not demonstrated any change in fidelity when compared to comparable results in the absence of those proteins on undamaged and damaged substrates (Fortune et al., 2006; McCulloch et al., 2007; McCulloch et al., 2009; Suarez et al., 2014). Thus, while the available studies are clearly not exhaustive, at this time there is not any support to suggest that our results using the catalytic core of pol η would differ from those of the full-length protein.

A significant limitation to this work is the lack of any cell-based or *in vivo* data. Unfortunately, this has been a general challenge for the study of TLS. While it is possible to introduce CPDs and 8-oxoG lesions to DNA in cultured cells, it is not possible to direct that damage to a specific location. In addition, while the general type of damage induced by certain treatments has been described and can also be presumed from sequence in some cases, it is difficult, if not impossible, to introduce a single lesion type which would be ideal to reduce confounding factors, simplify analysis and generate more reliable and repeatable results. In addition, the DNA damage response is complicated and, with out current understanding and technology, it is impossible to identify the exact polymerase responsible for any given bypass event. At this time, responsibility *in vivo* is best identified by polymerase depletion. Any conclusions about fidelity are inferred from the difference in mutation spectra observed between the polymerase competent and polymerase deficient cells.

This has not proved, for obvious reasons, to be a very successful approach, however, and does not allow for the direct observation of lesion bypass by a specific polymerase. Thus, at this time, *in vitro* assays are the most direct and simple method for characterizing TLS.

In addition, we recognize that this work does not address the bypass of CPDs composed of cytosine bases, which while generated less frequently by UV exposure, are significantly more mutagenic than TTDs. As discussed, the synthesis of CC or CT CPDs has not yet been achieved and thus this is also a general challenge to the study of pol η. Until a synthetic solution is designed, the details of CC and CT CPD bypass will remain uncertain.

Last, advances in high-throughput sequencing will provide significant advantages to pol η fidelity measurements. The viral vector based reversion mutation assay used herein was a notable advancement and made it possible to determine error rates during replication past damaged bases in the presence of competition between all four dNTPs, which was previously unavailable. However, both the reversion mutation assay and the gap filling forward mutation assay are limited to the *lacZα* gene seqence and thus, as mutation frequency has been shown to be affected by sequence context, error rates calculated are somewhat specific to the assay. Further, both assays are relatively expensive and labor intensive for the number of sequences ultimately generated. It would likely be of benefit to adopt new methods recently developed that take advantage of high throughput sequencing as they would allow for a greater number of sequences to be analyzed and facilitate the execution of repeats to provide the basis for more rigorous statistical analysis of, and detection of subtle changes within results.

Closing

Our guiding goal throughout this study was to provide previously unavailable details to forward the understanding of DNA damage bypass, pol η fidelity and mechanisms of mutagenesis. Altogether our hope is that this work has yielded insight regarding the those items and is a useful foudation upon which to design future study.

LITERATURE CITED

Ahluwalia, D.; Bienstock, R. J.; Schaaper, R. M. Novel Mutator Mutants of *E. Coli nrdAB* Ribonucleotide Reductase: Insight Into Allosteric Regulation and Control of Mutation Rates. *DNA Repair* **2012**, *11*, 480–487.

Akagi, J.-I.; Masutani, C.; Kataoka, Y.; Kan, T.; Ohashi, E.; Mori, T.; Ohmori, H.; Hanaoka, F. Interaction with DNA Polymerase η Is Required for Nuclear Accumulation of REV1 and Suppression of Spontaneous Mutations in Human Cells. *DNA Repair* **2009**, *8*, 585–599.

Al-Tassan, N.; Chmiel, N. H.; Maynard, J.; Fleming, N.; Livingston, A. L.; Williams, G. T.; Hodges, A. K.; Davies, D. R.; David, S. S.; Sampson, J. R.; et al. Inherited Variants of *Myh* Associated with Somatic G:C→T:A Mutations in Colorectal Tumors. *Nat Genet* **2002**, *30*, 227–232.

Arana, M. E.; Seki, M.; Wood, R. D.; Rogozin, I. B.; Kunkel, T. A. Low-Fidelity DNA Synthesis by Human DNA Polymerase θ. *Nucleic Acids Res* **2008**, *36*, 3847–3856.

Arias-Gonzalez, J. R. Entropy Involved in Fidelity of DNA Replication. *PLoS ONE* **2012**, *7*, e42272.

Armstrong, J. D.; Kunz, B. A. Site and Strand Specificity of UVB Mutagenesis in the *Sup4*-O Gene of Yeast. *Proc Natl Acad Sci USA* **1990**, *87*, 9005–9009.

Aye, Y.; Li, M.; Long, M. J. C.; Weiss, R. S. Ribonucleotide Reductase and Cancer: Biological Mechanisms and Targeted Therapies. *Oncogene* **2015**, *34*, 2011–2021.

Baker, S. M.; Bronner, C. E.; Zhang, L.; Plug, A. W.; Robatzek, M.; Warren, G.; Elliott, E. A.; Yu, J.; Ashley, T.; Arnheim, N.; et al. Male Mice Defective in the DNA Mismatch Repair Gene *Pms2* Exhibit Abnormal Chromosome Synapsis in Meiosis. *Cell* **1995**, *82*, 309–319.

Bansal, M. DNA Structure: Revisiting the Watson-Crick Double Helix. *Current Science* **2003**, *85*, 1556–1563.

Barnes, D. E.; Lindahl, T. Repair and Genetic Consequences of Endogenous DNA Base Damage in Mammalian Cells. *Annu. Rev. Genet.* **2004**, *38*, 445–476.

Barone, F.; McCulloch, S. D.; Macpherson, P.; Maga, G.; Yamada, M.; Nohmi, T.; Minoprio, A.; Mazzei, F.; Kunkel, T. A.; Karran, P.; et al. Replication of 2-Hydroxyadenine-Containing DNA and Recognition by Human MutSα. *DNA Repair* **2007**, *6*, 355–366.

Beardslee, R. A.; Suarez, S. C.; Toffton, S. M.; McCulloch, S. D. Mutation of the Little Finger Domain in Human DNA Polymerase η Alters Fidelity When Copying Undamaged DNA. *Environ. Mol. Mutagen.* **2013**, *54*, 638–651.

Bebenek, K.; Kunkel, T. A. Analyzing Fidelity of DNA Polymerases. *Meth Enzymol* **1995**, *262*, 217–232.

Beese, L. S.; Derbyshire, V.; Steitz, T. A. Structure of DNA Polymerase I Klenow Fragment Bound to Duplex DNA. *Science* **1993**, *260*, 352–355.

Bétous, R.; Rey, L.; Wang, G.; Pillaire, M.-J.; Puget, N.; Selves, J.; Biard, D. S. F.; Shin-ya, K.; Vasquez, K. M.; Cazaux, C.; et al. Role of TLS DNA Polymerases η and κ in Processing Naturally Occurring Structured DNA in Human Cells. *Mol. Carcinog.* **2009**, *48*, 369–378.

Bienko, M.; Green, C. M.; Crosetto, N.; Rudolf, F.; Zapart, G.; Coull, B.; Kannouche, P.; Wider, G.; Peter, M.; Lehmann, A. R.; et al. Ubiquitin-Binding Domains in Y-Family Polymerases Regulate Translesion Synthesis. *Science* **2005**, *310*, 1821–1824.

Biertümpfel, C.; Zhao, Y.; Kondo, Y.; Ramón-Maiques, S.; Gregory, M.; Lee, J. Y.; Masutani, C.; Lehmann, A. R.; Hanaoka, F.; Yang, W. Structure and Mechanism of Human DNA Polymerase η. *Nature* **2010**, *465*, 1044–1048.

Boiteux, S.; Gajewski, E.; Laval, J.; Dizdaroglu, M. Substrate Specificity of the *Escherichia Coli* Fpg Protein (Formamidopyrimidine-DNA Glycosylase): Excision of Purine Lesions in DNA Produced by Ionizing Radiation or Photosensitization. *Biochemistry* **1992**, *31*, 106–110.

Boudsocq, F.; Ling, H.; Yang, W.; Woodgate, R. Structure-Based Interpretation of Missense Mutations in Y-Family DNA Polymerases and Their Implications for Polymerase Function and Lesion Bypass. *DNA Repair* **2002**, *1*, 343–358.

Brash, D. E. UV Mutagenic Photoproducts in *Escherichia Coli* And Human Cells: a Molecular Genetics Perspective on Human Skin Cancer. *Photochemistry and Photobiology* **1988**, *48*, 59–66.

Broughton, B. C.; Cordonnier, A.; Kleijer, W. J.; Jaspers, N. G. J.; Fawcett, H.; Raams, A.; Garritsen, V. H.; Stary, A.; Avril, M.-F.; Boudsocq, F.; et al. Molecular Analysis of Mutations in DNA Polymerase η in Xeroderma Pigmentosum-Variant Patients. *Proc Natl Acad Sci USA* **2002**, *99*, 815–820.

Carty, M. P.; Hauser, J.; Levine, A. S.; Dixon, K. Replication and Mutagenesis of UV-Damaged DNA Templates in Human and Monkey Cell Extracts. *Molecular and Cellular Biology* **1993**, *13*, 533–542.

Ceppi, P.; Novello, S.; Cambieri, A.; Longo, M.; Monica, V.; Iacono, Lo, M.; Giaj-Levra, M.; Saviozzi, S.; Volante, M.; Papotti, M.; et al. Polymerase η mRNA Expression Predicts Survival of Non-Small Cell Lung Cancer Patients Treated with Platinum-Based Chemotherapy. *Clin. Cancer Res.* **2009**, *15*, 1039–1045.

Cheng, K. C.; Cahill, D. S.; Kasai, H.; Nishimura, S.; Loeb, L. A. 8-Hydroxyguanine, an Abundant Form of Oxidative DNA Damage, Causes G → T and A → C Substitutions. *J Biol Chem* **1992**, *267*, 166–172.

Cheng, X.; Kelso, C.; Hornak, V.; de los Santos, C.; Grollman, A. P.; Simmerling, C. Dynamic Behavior of DNA Base Pairs Containing 8-Oxoguanine. *J. Am. Chem. Soc.* **2005**, *127*, 13906–13918.

Cho, B. P.; Kadlubar, F. F.; Culp, S. J.; Evans, F. E. ^{15}N Nuclear Magnetic Resonance Studies on the Tautomerism of 8-Hydroxy-2'-Deoxyguanosine, 8-Hydroxyguanosine, and Other C8-Substituted Guanine Nucleosides. *Chem. Res. Toxicol.* **1990**, *3*, 445–452.

Choi, J.-H.; Pfeifer, G. P. The Role of DNA Polymerase η in UV Mutational Spectra. *DNA Repair* **2005**, *4*, 211–220.

Clark, J. M.; Hanawalt, P. C. Replicative Intermediates in UV-Irradiated Simian Virus 40. *Mutat Res* **1984**, *132*, 1–14.

Cooke, M. S.; Evans, M. D.; Dizdaroglu, M.; Lunec, J. Oxidative DNA Damage: Mechanisms, Mutation, and Disease. *FASEB J.* **2003**, *17*, 1195–1214.

Cordeiro-Stone, M.; Zaritskaya, L. S.; Price, L. K.; Kaufmann, W. K. Replication Fork Bypass of a Pyrimidine Dimer Blocking Leading Strand DNA Synthesis. *J Biol Chem* **1997**, *272*, 13945–13954.

Crenshaw, C. M.; Wade, J. E.; Arthanari, H.; Frueh, D.; Lane, B. F.; Núñez, M. E. Hidden in Plain Sight: Subtle Effects of the 8-Oxoguanine Lesion on the Structure, Dynamics, and Thermodynamics of a 15-Base Pair Oligodeoxynucleotide Duplex. *Biochemistry* **2011**, *50*, 8463–8477.

Cruet-Hennequart, S.; Gallagher, K.; Sokòl, A.; Villalan, S.; Prendergast, A. M.; Carty, M. P. *Genome Stability and Human Diseases, Subcellular Biochemistry*; Nasheuer, H.-P., Ed.; Springer Science+Business Media, 2010.

de Gruijl, F. R. Skin Cancer and Solar UV Radiation. *Eur. J. Cancer* **1999**, *35*, 2003–2009.

de Weerd-Kastelein, E. A.; Keijzer, W.; Bootsma, D. Genetic Heterogeneity of Xeroderma Pigmentosum Demostrated by Somatic Cell Hybridization. *Nature New Biol* **1972**, *238*, 80–83.

de Weerd-Kastelein, E. A.; Keijzer, W.; Bootsma, D. A Third Complementation Group in Xeroderma Pigmentosum. *Mutat Res* **1974**, *22*, 87–91.

de Weerd-Kastelein, E. A.; Kleijer, W. J.; Sluyter, M. L.; Keijzer, W. Repair Replication in Heterokaryons Deprived From Different Repair-Deficient Xeroderma Pigmentosum Strains. *Mutat Res* **1973**, *19*, 237–243.

de Wind, N.; Dekker, M.; Berns, A.; Radman, M.; te Riele, H. Inactivation of the Mouse *Msh2* Gene Results in Mismatch Repair Deficiency, Methylation Tolerance, Hyperrecombination, and Predisposition to Cancer. *Cell* **1995**, *82*, 321–330.

Doetsch, P. W.; Zasatawny, T. H.; Martin, A. M.; Dizdaroglu, M. Monomeric Base Damage Products From Adenine, Guanine, and Thymine Induced by Exposure of DNA to Ultraviolet Radiation. *Biochemistry* **1995**, *34*, 737–742.

Doublié, S.; Tabor, S.; Long, A. M.; Richardson, C. C.; Ellenberger, T. Crystal Structure of a Bacteriophage T7 DNA Replication Complex at 2.2 Å Resolution. *Nature* **1998**, *391*, 251–258.

Dršata, T.; Kara, M.; Zacharias, M.; Lankaš, F. Effect of 8-Oxoguanine on DNA Structure and Deformability. *J Phys Chem B* **2013**, *117*, 11617–11622.

Dumaz, N.; Drougard, C.; Sarasin, A.; Daya-Grosjean, L. Specific UV-Induced Mutation Spectrum in the P53 Gene of Skin Tumors From DNA-Repair-Deficient Xeroderma Pigmentosum Patients. *Proc Natl Acad Sci USA* **1993**, *90*, 10529–10533.

Duncan, B. K.; Weiss, B. Specific Mutator Effects of *Ung* (Uracil-DNA Glycosylase) Mutations in *Escherichia Coli*. *J. Bacteriol.* **1982**, *151*, 750–755.

Edelmann, W.; Cohen, P. E.; Kane, M.; Lau, K.; Morrow, B.; Bennett, S.; Umar, A.; Kunkel, T.; Cattoretti, G.; Chaganti, R.; et al. Meiotic Pachytene Arrest in MLH1-Deficient Mice. *Cell* **1996**, *85*, 1125–1134.

Edelmann, W.; Yang, K.; Umar, A.; Heyer, J.; Lau, K.; Fan, K.; Liedtke, W.; Cohen, P. E.; Kane, M. F.; Lipford, J. R.; et al. Mutation in the Mismatch Repair Gene *Msh6* Causes Cancer Susceptibility. *Cell* **1997**, *91*, 467–477.

Eğe, S. N. *Organic Chemistry : Structure and Reactivity*, 3rd ed.; Lexington, Mass. : D.C. Heath, 1994.

Fenton, H. LXXIII.—Oxidation of Tartaric Acid in Presence of Iron. *Journal Of The Chemical Society, Transactions* **1894**, *65*, 899–905.

Fontecave, M.; Lepoivre, M.; Elleingand, E.; Gerez, C.; Guittet, O. Resveratrol, a Remarkable Inhibitor of Ribonucleotide Reductase. *FEBS Lett* **1998**, *421*, 277–279.

Fortune, J. M.; Stith, C. M.; Kissling, G. E.; Burgers, P. M. J.; Kunkel, T. A. RPA and PCNA Suppress Formation of Large Deletion Errors by Yeast DNA Polymerase δ. *Nucleic Acids Res* **2006**, *34*, 4335–4341.

Fox, E. J.; Loeb, L. A. Lethal Mutagenesis: Targeting the Mutator Phenotype in Cancer. *Seminars in Cancer Biology* **2010**, *20*, 353–359.

Fox, E. J.; Prindle, M. J.; Loeb, L. A. Do Mutator Mutations Fuel Tumorigenesis? *Cancer Metastasis Rev* **2013**, *32*, 353–361.

Frank, E. G.; Sayer, J. M.; Kroth, H.; Ohashi, E.; Ohmori, H.; Jerina, D. M.; Woodgate, R. Translesion Replication of Benzo[*a*]Pyrene and Benzo[*c*]Phenanthrene Diol Epoxide Adducts of Deoxyadenosine and Deoxyguanosine by Human DNA Polymerase ι. *Nucleic Acids Res* **2002**, *30*, 5284–5292.

Friedberg, E. C.; McDaniel, L. D.; Schultz, R. A. The Role of Endogenous and Exogenous DNA Damage and Mutagenesis. *Curr. Opin. Genet. Dev.* **2004**, *14*, 5–10.

Friedberg, E. C.; Walker, G. C.; Siede, W.; Wood, R. D.; Schultz, R. A.; Ellenberger, T. *DNA Repair and Mutagenesis*, 2nd ed.; Washington, D.C. : ASM Press, 2006.

Gan, G. N.; Wittschieben, J. P.; Wittschieben, B. Ø.; Wood, R. D. DNA Polymerase Zeta (Pol ζ) in Higher Eukaryotes. *Cell Res* **2008**, *18*, 174–183.

García-Gómez, S.; Reyes, A.; Martínez-Jiménez, M. I.; Chocrón, E. S.; Mourón, S.; Terrados, G.; Powell, C.; Salido, E.; Méndez, J.; Holt, I. J.; et al. PrimPol, an Archaic Primase/Polymerase Operating in Human Cells. *Molecular Cell* **2013**, *52*, 541–553.

Garibyan, L.; Fisher, D. E. How Sunlight Causes Melanoma. *Curr Oncol Rep* **2010**, *12*, 319–326.

Gedik, C. M.; Collins, A.; ESCODD (European Standards Committee on Oxidative DNA Damage). Establishing the Background Level of Base Oxidation in Human Lymphocyte DNA: Results of an Interlaboratory Validation Study. *FASEB J.* **2005**, *19*, 82–84.

Gratchev, A.; Strein, P.; Utikal, J.; Sergij, G. Molecular Genetics of Xeroderma Pigmentosum Variant. *Exp. Dermatol.* **2003**, *12*, 529–536.

Guo, C.; Kosarek-Stancel, J. N.; Tang, T.-S.; Friedberg, E. C. Y-Family DNA Polymerases in Mammalian Cells. *Cell. Mol. Life Sci.* **2009**, *66*, 2363–2381.

Haber, F.; Weiss, J. The Catalytic Decomposition of Hydrogen Peroxide by Iron Salts. *Proceedings Of The Royal Society A: Mathematical, Physical And Engineering Sciences* **1934**, *147*, 332–351.

Halliwell, B.; Gutteridge, J. M. Biologically Relevant Metal Ion-Dependent Hydroxyl Radical Generation an Update. *FEBS Lett* **1992**, *307*, 108–112.

Haracska, L.; Johnson, R. E.; Unk, I.; Phillips, B.; Hurwitz, J.; Prakash, L.; Prakash, S. Physical and Functional Interactions of Human DNA Polymerase η with PCNA. *Molecular and Cellular Biology* **2001**, *21*, 7199–7206.

Haracska, L.; Prakash, L.; Prakash, S. Role of Human DNA Polymerase κ as an Extender in Translesion Synthesis. *Proc Natl Acad Sci USA* **2002**, *99*, 16000–16005.

Haracska, L.; Prakash, S.; Prakash, L. Replication Past O^6-Methylguanine by Yeast and Human DNA Polymerase η. *Molecular and Cellular Biology* **2000a**, *20*, 8001–8007.

Haracska, L.; Yu, S. L.; Johnson, R. E.; Prakash, L.; Prakash, S. Efficient and Accurate Replication in the Presence of 7,8-Dihydro-8-Oxoguanine by DNA Polymerase η. *Nat Genet* **2000b**, *25*, 458–461.

Hatahet, Z.; Zhou, M.; Reha-Krantz, L. J.; Morrical, S. W.; Wallace, S. S. In Search of a Mutational Hotspot. *Proc Natl Acad Sci USA* **1998**, *95*, 8556–8561.

Heller, R. C.; Marians, K. J. Replication Fork Reactivation Downstream of a Blocked Nascent Leading Strand. *Nature* **2006**, *439*, 557–562.

Hishiki, A.; Hashimoto, H.; Hanafusa, T.; Kamei, K.; Ohashi, E.; Shimizu, T.; Ohmori, H.; Sato, M. Structural Basis for Novel Interactions Between Human Translesion Synthesis Polymerases and Proliferating Cell Nuclear Antigen. *J Biol Chem* **2009**, *284*, 10552–10560.

Hodgson, E.; Smart, R. C. *Molecular and Biochemical Toxicology*, 4 ed.; Smart, R. C., Hodgson, E., Eds.; John Wiley & Sons, Inc.: Hoboken, NJ, 2013.

Hsia, H. C.; Lebkowski, J. S.; Leong, P. M.; Calos, M. P.; Miller, J. H. Comparison of Ultraviolet Irradiation-Induced Mutagenesis of the *lacI* Gene in *Escherichia Coli* and in Human 293 Cells. *Journal of Molecular Biology* **1989**, *205*, 103–113.

Hubscher, U.; Maga, G.; Spadari, S. Eukaryotic DNA Polymerases. *Annu. Rev. Biochem.* **2002**, *71*, 133–163.

Iyer, R. R.; Pluciennik, A.; Burdett, V.; Modrich, P. L. DNA Mismatch Repair: Functions and Mechanisms. *Chem. Rev.* **2006**, *106*, 302–323.

Jansen, J. G.; Tsaalbi-Shtylik, A.; de Wind, N. Roles of Mutagenic Translesion Synthesis in Mammalian Genome Stability, Health and Disease. *DNA Repair* **2015**.

Jena, N. R.; Mishra, P. C. Mechanisms of Formation of 8-Oxoguanine Due to Reactions of One and Two OH* Radicals and the H_2O_2 Molecule with Guanine: a Quantum Computational Study. *J Phys Chem B* **2005**, *109*, 14205–14218.

Johnson, R. E.; Kondratick, C. M.; Prakash, S.; Prakash, L. *hRAD30* Mutations in the Variant Form of Xeroderma Pigmentosum. *Science* **1999**, *285*, 263–265.

Johnson, R. E.; Washington, M. T.; Haracska, L.; Prakash, S.; Prakash, L. Eukaryotic Polymerases ι and ζ Act Sequentially to Bypass DNA Lesions. *Nature* **2000a**, *406*, 1015–1019.

Johnson, R. E.; Washington, M. T.; Prakash, S.; Prakash, L. Fidelity of Human DNA Polymerase η. *J Biol Chem* **2000b**, *275*, 7447–7450.

Jones, S.; Emmerson, P.; Maynard, J.; Best, J. M.; Jordan, S.; Williams, G. T.; Sampson, J. R.; Cheadle, J. P. Biallelic Germline Mutations in MYH Predispose to Multiple Colorectal Adenoma and Somatic G:C→T:A Mutations. *Human Molecular Genetics* **2002**, *11*, 2961–2967.

Kannouche, P.; Broughton, B. C.; Volker, M.; Hanaoka, F.; Mullenders, L. H.; Lehmann, A. R. Domain Structure, Localization, and Function of DNA Polymerase η, Defective in Xeroderma Pigmentosum Variant Cells. *Genes Dev* **2001**, *15*, 158–172.

Kannouche, P.; Fernández de Henestrosa, A. R.; Coull, B.; Vidal, A. E.; Gray, C.; Zicha, D.; Woodgate, R.; Lehmann, A. R. Localization of DNA Polymerases η and ι to the Replication Machinery Is Tightly Co-Ordinated in Human Cells. *EMBO J* **2003**, *22*, 1223–1233.

Kamath-Loeb, A. S.; Lan, L.; Nakajima, S.; Yasui, A.; Loeb, L. A. Werner Syndrome Protein Interacts Functionally with Translesion DNA Polymerases. *Proc Natl Acad Sci USA* **2007**, *104*, 10394–10399.

Kamiya, H.; Murata-Kamiya, N.; Koizume, S.; Inoue, H.; Nishimura, S.; Ohtsuka, E. 8-Hydroxyguanine (7,8-Dihydro-8-Oxoguanine) in Hot Spots of the C-Ha-*Ras* Gene: Effects of Sequence Contexts on Mutation Spectra. *Carcinogenesis* **1995**, *16*, 883–889.

Kasai, H.; Yamaizumi, Z.; Yamamoto, F.; Bessho, T.; Nishimura, S.; Berger, M.; Cadet, J. Photosensitized Formation of 8-Hydroxyguanine (7,8-Dihydro-8-Oxoguanine) in DNA by Riboflavin. *Nucleic Acids Symposium Series* **1992**, 181–182.

Kaufmann, W. K. Pathways of Human Cell Post-Replication Repair. *Carcinogenesis* **1989**, *10*, 1–11.

Kawamoto, T.; Araki, K.; Sonoda, E.; Yamashita, Y. M.; Harada, K.; Kikuchi, K.; Masutani, C.; Hanaoka, F.; Nozaki, K.; Hashimoto, N.; et al. Dual Roles for DNA Polymerase η in Homologous DNA Recombination and Translesion DNA Synthesis. *Molecular Cell* **2005**, *20*, 793–799.

Kokoska, R. J.; McCulloch, S. D.; Kunkel, T. A. The Efficiency and Specificity of Apurinic/Apyrimidinic Site Bypass by Human DNA Polymerase η and *Sulfolobus Solfataricus* Dpo4. *J Biol Chem* **2003**, *278*, 50537–50545.

Kool, E. T. Active Site Tightness and Substrate Fit in DNA Replication. *Annu. Rev. Biochem.* **2002**, *71*, 191–219.

Korona, D. A.; Lecompte, K. G.; Pursell, Z. F. The High Fidelity and Unique Error Signature of Human DNA Polymerase ε. *Nucleic Acids Res* **2011**, *39*, 1763–1773.

Kraemer, K. H. Sunlight and Skin Cancer: Another Link Revealed. *Proc Natl Acad Sci USA* **1997**, *94*, 11–14.

Krutmann, J.; Schroeder, P. Role of Mitochondria in Photoaging of Human Skin: the Defective Powerhouse Model. *J. Investig. Dermatol. Symp. Proc.* **2009**, *14*, 44–49.

Kumar, D.; Abdulovic, A. L.; Viberg, J.; Nilsson, A. K.; Kunkel, T. A.; Chabes, A. Mechanisms of Mutagenesis *in Vivo* Due to Imbalanced dNTP Pools. *Nucleic Acids Res* **2011**, *39*, 1360–1371.

Kunkel, T. A. Biological Asymmetries and the Fidelity of Eukaryotic DNA Replication. *Bioessays* **1992**, *14*, 303–308.

Kunkel, T. A. DNA Replication Fidelity. *J Biol Chem* **2004**, *279*, 16895–16898.

Kusumoto, R.; Masutani, C.; Iwai, S.; Hanaoka, F. Translesion Synthesis by Human DNA Polymerase η Across Thymine Glycol Lesions. *Biochemistry* **2002**, *41*, 6090–6099.

Kusumoto, R.; Masutani, C.; Shimmyo, S.; Iwai, S.; Hanaoka, F. DNA Binding Properties of Human DNA Polymerase η: Implications for Fidelity and Polymerase Switching of Translesion Synthesis. *Genes Cells* **2004**, *9*, 1139–1150.

Lee, D.-H.; Pfeifer, G. P. Translesion Synthesis of 7,8-Dihydro-8-Oxo-2'-Deoxyguanosine by DNA Polymerase Eta in Vivo. *Mutat Res* **2008**, *641*, 19–26.

Lee, J. H.; Hwang, G. S.; Choi, B. S. Solution Structure of a DNA Decamer Duplex Containing the Stable 3′ T · G Base Pair of the Pyrimidine(6-4)Pyrimidone Photoproduct [(6-4) Adduct]: Implications for the Highly Specific 3′ T → C Transition of the (6-4) Adduct. *Proc Natl Acad Sci USA* **1999**, *96*, 6632–6636.

Leeds, J. M.; Slabaugh, M. B.; Mathews, C. K. DNA Precursor Pools and Ribonucleotide Reductase Activity: Distribution Between the Nucleus and Cytoplasm of Mammalian Cells. *Molecular and Cellular Biology* **1985**, *5*, 3443–3450.

Lehmann, A. R. Postreplication Repair of DNA in Ultraviolet-Irradiated Mammalian Cells. *Journal of Molecular Biology* **1972**, *66*, 319–337.

Lehmann, A. R.; Fuchs, R. P. Gaps and Forks in DNA Replication: Rediscovering Old Models. *DNA Repair* **2006**, *5*, 1495–1498.

Lehmann, A. R.; Kirk-Bell, S.; Arlett, C. F.; Paterson, M. C.; Lohman, P. H.; de Weerd-Kastelein, E. A.; Bootsma, D. Xeroderma Pigmentosum Cells with Normal Levels of Excision Repair Have a Defect in DNA Synthesis After UV-Irradiation. *Proc Natl Acad Sci USA* **1975**, *72*, 219–223.

Lemaire, D. G.; Ruzsicska, B. P. Kinetic Analysis of the Deamination Reactions of Cyclobutane Dimers of Thymidylyl-3′,5′-2′-Deoxycytidine and 2′-Deoxycytidylyl-3′,5′-Thymidine. *Biochemistry* **1993**, *32*, 2525–2533.

Levine, R. L.; Miller, H.; Grollman, A.; Ohashi, E.; Ohmori, H.; Masutani, C.; Hanaoka, F.; Moriya, M. Translesion DNA Synthesis Catalyzed by Human Pol η and Pol κ Across 1,N^6-Ethenodeoxyadenosine. *J Biol Chem* **2001**, *276*, 18717–18721.

Lin, Q.; Clark, A. B.; McCulloch, S. D.; Yuan, T.; Bronson, R. T.; Kunkel, T. A.; Kucherlapati, R. Increased Susceptibility to UV-Induced Skin Carcinogenesis in Polymerase H-Deficient Mice. *Cancer Res* **2006**, *66*, 87–94.

Lindahl, T. DNA Glycosylases, Endonucleases for Apurinic/Apyrimidinic Sites, and Base Excision-Repair. In; Progress in Nucleic Acid Research and Molecular Biology; Elsevier, 1979; Vol. 22, pp 135–192.

Lipscomb, L. A.; Peek, M. E.; Morningstar, M. L.; Verghis, S. M.; Miller, E. M.; Rich, A.; Essigmann, J. M.; Williams, L. D. X-Ray Structure of a DNA Decamer Containing 7,8-Dihydro-8-Oxoguanine. *Proc Natl Acad Sci USA* **1995**, *92*, 719–723.

Liu, X.; Zhang, H.; Lai, L.; Wang, X.; Loera, S.; Xue, L.; He, H.; Zhang, K.; Hu, S.; Huang, Y.; et al. Ribonucleotide Reductase Small Subunit M2 Serves as a Prognostic Biomarker and Predicts Poor Survival of Colorectal Cancers. *Clin. Sci.* **2013**, *124*, 567–578.

Livneh, Z.; Ziv, O.; Shachar, S. Multiple Two-Polymerase Mechanisms in Mammalian Translesion DNA Synthesis. *Cell cycle (Georgetown, Tex)* **2010**, *9*, 729–735.

Locatelli, G. A.; Pospiech, H.; Tanguy Le Gac, N.; van Loon, B.; Hübscher, U.; Parkkinen, S.; Syväoja, J. E.; Villani, G. Effect of 8-Oxoguanine and Abasic Site DNA Lesions on *In Vitro* Elongation by Human DNA Polymerase ε in the Presence of Replication Protein a and Proliferating-Cell Nuclear Antigen. *Biochem J* **2010**, *429*, 573–582.

Loeb, L. A. Human Cancers Express Mutator Phenotypes: Origin, Consequences and Targeting. *Nat Rev Cancer* **2011**, *11*, 450–457.

Loeb, L. A.; Essigmann, J. M.; Kazazi, F.; Zhang, J.; Rose, K. D.; Mullins, J. I. Lethal Mutagenesis of HIV with Mutagenic Nucleoside Analogs. *Proc Natl Acad Sci USA* **1999**, *96*, 1492–1497.

Lone, S.; Townson, S. A.; Uljon, S. N.; Johnson, R. E.; Brahma, A.; Nair, D. T.; Prakash, S.; Prakash, L.; Aggarwal, A. K. Human DNA Polymerase κ Encircles DNA: Implications for Mismatch Extension and Lesion Bypass. *Molecular Cell* **2007**, *25*, 601–614.

Lopes, M.; Foiani, M.; Sogo, J. M. Multiple Mechanisms Control Chromosome Integrity After Replication Fork Uncoupling and Restart at Irreparable UV Lesions. *Molecular Cell* **2006**, *21*, 15–27.

Lu, A.-G.; Feng, H.; Wang, P.-X.-Z.; Han, D.-P.; Chen, X.-H.; Zheng, M.-H. Emerging Roles of the Ribonucleotide Reductase M2 in Colorectal Cancer and Ultraviolet-Induced DNA Damage Repair. *World J. Gastroenterol.* **2012**, *18*, 4704–4713.

Lynch, H. T.; la Chapelle, de, A. Hereditary Colorectal Cancer. *N Engl J Med* **2003**, *348*, 919–932.

Maga, G.; Villani, G.; Crespan, E.; Wimmer, U.; Ferrari, E.; Bertocci, B.; Hübscher, U. 8-Oxo-Guanine Bypass by Human DNA Polymerases in the Presence of Auxiliary Proteins. *Nature* **2007**, *447*, 606–608.

Maher, V. M.; Ouellette, L. M.; Curren, R. D.; McCormick, J. J. Frequency of Ultraviolet Light-Induced Mutations Is Higher in Xeroderma Pigmentosum Variant Cells Than in Normal Human Cells. *Nature* **1976**, *261*, 593–595.

Markovitsi, D.; Sage, E.; Lewis, F. D.; Davies, J. Interaction of UV Radiation with DNA. *Photochem. Photobiol. Sci.* **2013**, *12*, 1256–1258.

Martomo, S. A.; Mathews, C. K. Effects of Biological DNA Precursor Pool Asymmetry Upon Accuracy of DNA Replication in Vitro. *Mutat Res* **2002**, *499*, 197–211.

Masutani, C.; Araki, M.; Yamada, A.; Kusumoto, R.; Nogimori, T.; Maekawa, T.; Iwai, S.; Hanaoka, F. Xeroderma Pigmentosum Variant (XP-V) Correcting Protein From HeLa Cells Has a Thymine Dimer Bypass DNA Polymerase Activity. *EMBO J* **1999a**, *18*, 3491–3501.

Masutani, C.; Kusumoto, R.; Iwai, S.; Hanaoka, F. Mechanisms of Accurate Translesion Synthesis by Human DNA Polymerase η. *EMBO J* **2000**, *19*, 3100–3109.

Masutani, C.; Kusumoto, R.; Yamada, A.; Dohmae, N.; Yokoi, M.; Yuasa, M.; Araki, M.; Iwai, S.; Takio, K.; Hanaoka, F. The *XPV* (Xeroderma Pigmentosum Variant) Gene Encodes Human DNA Polymerase η. *Nature* **1999b**, *399*, 700–704.

Mathews, C. K.; Ji, J. DNA Precursor Asymmetries, Replication Fidelity, and Variable Genome Evolution. *Bioessays* **1992**, *14*, 295–301.

Matsuda, T.; Bebenek, K.; Masutani, C.; Hanaoka, F.; Kunkel, T. A. Low Fidelity DNA Synthesis by Human DNA Polymerase-η. *Nature* **2000**, *404*, 1011–1013.

Matsuda, T.; Bebenek, K.; Masutani, C.; Rogozin, I. B.; Hanaoka, F.; Kunkel, T. A. Error Rate and Specificity of Human and Murine DNA Polymerase η. *Journal of Molecular Biology* **2001**, *312*, 335–346.

McAteer, K.; Jing, Y.; Kao, J.; Taylor, J. S.; Kennedy, M. A. Solution-State Structure of a DNA Dodecamer Duplex Containing a *Cis*-*Syn* Thymine Cyclobutane Dimer, the Major UV Photoproduct of DNA. *Journal of Molecular Biology* **1998**, *282*, 1013–1032.

McAuley-Hecht, K. E.; Leonard, G. A.; Gibson, N. J.; Thomson, J. B.; Watson, W. P.; Hunter, W. N.; Brown, T. Crystal Structure of a DNA Duplex Containing 8-Hydroxydeoxyguanine-Adenine Base Pairs. *Biochemistry* **1994**, *33*, 10266–10270.

McCord, J. M.; Day, E. D. Superoxide-Dependent Production of Hydroxyl Radical Catalyzed by Iron-EDTA Complex. *FEBS Lett* **1978**, *86*, 139–142.

McCue, J. M.; Link, K. L.; Eaton, S. S.; Freed, B. M. Exposure to Cigarette Tar Inhibits Ribonucleotide Reductase and Blocks Lymphocyte Proliferation. *J. Immunol.* **2000**, *165*, 6771–6775.

McCulloch, S. D.; Kokoska, R. J.; Chilkova, O.; Welch, C. M.; Johansson, E.; Burgers, P. M. J.; Kunkel, T. A. Enzymatic Switching for Efficient and Accurate Translesion DNA Replication. *Nucleic Acids Res* **2004a**, *32*, 4665–4675.

McCulloch, S. D.; Kokoska, R. J.; Garg, P.; Burgers, P. M.; Kunkel, T. A. The Efficiency and Fidelity of 8-Oxo-Guanine Bypass by DNA Polymerases δ and η. *Nucleic Acids Res* **2009**, *37*, 2830–2840.

McCulloch, S. D.; Kokoska, R. J.; Kunkel, T. A. Efficiency, Fidelity and Enzymatic Switching During Translesion DNA Synthesis. *Cell cycle (Georgetown, Tex)* **2004b**, *3*, 580–583.

McCulloch, S. D.; Kokoska, R. J.; Masutani, C.; Iwai, S.; Hanaoka, F.; Kunkel, T. A. Preferential *Cis*-*Syn* Thymine Dimer Bypass by DNA Polymerase η Occurs with Biased Fidelity. *Nature* **2004c**, *428*, 97–100.

McCulloch, S. D.; Kunkel, T. A. The Fidelity of DNA Synthesis by Eukaryotic Replicative and Translesion Synthesis Polymerases. *Cell Res* **2008**, *18*, 148–161.

McCulloch, S.; Kunkel, T. Measuring the Fidelity of Translesion DNA Synthesis. *Meth Enzymol* **2006**, *408*, 341–355.

McCulloch, S. D.; Wood, A.; Garg, P.; Burgers, P. M. J.; Kunkel, T. A. Effects of Accessory Proteins on the Bypass of a *Cis*- *Syn* Thymine-Thymine Dimer by *Saccharomyces Cerevisiae* DNA Polymerase η. *Biochemistry* **2007**, *46*, 8888–8896.

Meneghini, R. Gaps in DNA Synthesized by Ultraviolet Light-Irradiated WI38 Human Cells. *Biochim. Biophys. Acta* **1976**, *425*, 419–427.

Miller, J. H. Mutagenic Specificity of Ultraviolet Light. *Journal of Molecular Biology* **1985**, *182*, 45–65.

Mitchell, D. L.; Jen, J.; Cleaver, J. E. Sequence Specificity of Cyclobutane Pyrimidine Dimers in DNA Treated with Solar (Ultraviolet B) Radiation. *Nucleic Acids Res* **1992**, *20*, 225–229.

Morikawa, T.; Hino, R.; Uozaki, H.; Maeda, D.; Ushiku, T.; Shinozaki, A.; Sakatani, T.; Fukayama, M. Expression of Ribonucleotide Reductase M2 Subunit in Gastric Cancer and Effects of RRM2 Inhibition in Vitro. *Hum Pathol* **2010a**, *41*, 1742–1748.

Morikawa, T.; Maeda, D.; Kume, H.; Homma, Y.; Fukayama, M. Ribonucleotide Reductase M2 Subunit Is a Novel Diagnostic Marker and a Potential Therapeutic Target in Bladder Cancer. *Histopathology* **2010b**, *57*, 885–892.

Nair, D. T.; Johnson, R. E.; Prakash, L.; Prakash, S.; Aggarwal, A. K. Human DNA Polymerase ι Incorporates dCTP Opposite Template G via a G.C + Hoogsteen Base Pair. *Structure* **2005a**, *13*, 1569–1577.

Nair, D. T.; Johnson, R. E.; Prakash, L.; Prakash, S.; Aggarwal, A. K. Rev1 Employs a Novel Mechanism of DNA Synthesis Using a Protein Template. *Science* **2005b**, *309*, 2219–2222.

Nair, D. T.; Johnson, R. E.; Prakash, S.; Prakash, L.; Aggarwal, A. K. Replication by Human DNA Polymerase-ι Occurs by Hoogsteen Base-Pairing. *Nature* **2004**, *430*, 377–380.

Nelson, D. L.; Cox, M. M. *Lehninger Principles of Biochemistry*, 4 ed.; W.H. Freeman: New York, 2005.

Nick McElhinny, S. A.; Stith, C. M.; Burgers, P. M. J.; Kunkel, T. A. Inefficient Proofreading and Biased Error Rates During Inaccurate DNA Synthesis by a Mutant Derivative of *Saccharomyces Cerevisiae* DNA Polymerase δ. *J Biol Chem* **2007**, *282*, 2324–2332.

Nilsen, H.; Haushalter, K. A.; Robins, P.; Barnes, D. E.; Verdine, G. L.; Lindahl, T. Excision of Deaminated Cytosine From the Vertebrate Genome: Role of the SMUG1 Uracil-DNA Glycosylase. *EMBO J* **2001**, *20*, 4278–4286.

Nilsen, H.; Stamp, G.; Andersen, S.; Hrivnak, G.; Krokan, H. E.; Lindahl, T.; Barnes, D. E. Gene-Targeted Mice Lacking the Ung Uracil-DNA Glycosylase Develop B-Cell Lymphomas. *Oncogene* **2003**, *22*, 5381–5386.

O'Day, C. L.; Burgers, P. M.; Taylor, J. S. PCNA-Induced DNA Synthesis Past *Cis*-Syn and *Trans*-Syn-I Thymine Dimers by Calf Thymus DNA Polymerase δ *In Vitro*. *Nucleic Acids Res* **1992**, *20*, 5403–5406.

Oda, Y.; Uesugi, S.; Ikehara, M.; Nishimura, S.; Kawase, Y.; Ishikawa, H.; Inoue, H.; Ohtsuka, E. NMR Studies of a DNA Containing 8-Hydroxydeoxyguanosine. *Nucleic Acids Res* **1991**, *19*, 1407–1412.

Ohashi, E.; Murakumo, Y.; Kanjo, N.; Akagi, J.-I.; Masutani, C.; Hanaoka, F.; Ohmori, H. Interaction of hREV1 with Three Human Y-Family DNA Polymerases. *Genes Cells* **2004**, *9*, 523–531.

Park, H.; Zhang, K.; Ren, Y.; Nadji, S.; Sinha, N.; Taylor, J.-S.; Kang, C. Crystal Structure of a DNA Decamer Containing a *Cis-Syn* Thymine Dimer. *Proc Natl Acad Sci USA* **2002**, *99*, 15965–15970.

Paterson, M. C.; Lohman, P. H.; Westerveld, A.; Sluyter, M. L. DNA Repair Monitored by an Enzymatic Assay in Multinucleate Xeroderma Pigmentosum Cells After Fusion. *Nature* **1974**, *248*, 50–52.

Patton, J. D.; Rowan, L. A.; Mendrala, A. L.; Howell, J. N.; Maher, V. M.; McCormick, J. J. Xeroderma Pigmentosum Fibroblasts Including Cells From XP Variants Are Abnormally Sensitive to the Mutagenic and Cytotoxic Action of Broad Spectrum Simulated Sunlight. *Photochemistry and Photobiology* **1984**, *39*, 37–42.

Peltomäki, P. Role of DNA Mismatch Repair Defects in the Pathogenesis of Human Cancer. *J. Clin. Oncol.* **2003**, *21*, 1174–1179.

Peyrane, F.; Clivio, P. Sensitized Photochemistry of Di(4-Tetrazolouracil) Dinucleoside Monophosphate as a Route to Dicytosine Cyclobutane Photoproduct Precursors. *Photochem. Photobiol. Sci.* **2013**, *12*, 1366.

Pfeifer, G. P. Formation and Processing of UV Photoproducts: Effects of DNA Sequence and Chromatin Environment. *Photochemistry and Photobiology* **1997**, *65*, 270–283.

Pfeifer, G. P.; You, Y.-H.; Besaratinia, A. Mutations Induced by Ultraviolet Light. *Mutat Res* **2005**, *571*, 19–31.

Pleasance, E. D.; Cheetham, R. K.; Stephens, P. J.; McBride, D. J.; Humphray, S. J.; Greenman, C. D.; Varela, I.; Lin, M.-L.; Ordóñez, G. R.; Bignell, G. R.; et al. A Comprehensive Catalogue of Somatic Mutations From a Human Cancer Genome. *Nature* **2010**, *463*, 191–196.

Plum, G. E.; Grollman, A. P.; Johnson, F.; Breslauer, K. J. Influence of the Oxidatively Damaged Adduct 8-Oxodeoxyguanosine on the Conformation, Energetics, and Thermodynamic Stability of a DNA Duplex. *Biochemistry* **1995**, *34*, 16148–16160.

Pozhidaeva, A.; Pustovalova, Y.; D'Souza, S.; Bezsonova, I.; Walker, G. C.; Korzhnev, D. M. NMR Structure and Dynamics of the C-Terminal Domain From Human Rev1 and Its Complex with Rev1 Interacting Region of DNA Polymerase η. *Biochemistry* **2012**, *51*, 5506–5520.

Prakash, S.; Johnson, R. E.; Prakash, L. Eukaryotic Translesion Synthesis DNA Polymerases: Specificity of Structure and Function. *Annu. Rev. Biochem.* **2005**, *74*, 317–353.

Pray, L. A. Discovery of DNA Structure and Function: Watson and Crick. *Nature Education* **2008**, *1*, 100.

Radicella, J. P.; Dherin, C.; Desmaze, C.; Fox, M. S.; Boiteux, S. Cloning and Characterization of *hOGG1*, A Human Homolog of the *Ogg1* Gene of *Saccharomyces Cerevisiae*. *Proc Natl Acad Sci USA* **1997**, *94*, 8010–8015.

Ravanat, J. L.; Douki, T.; Cadet, J. Direct and Indirect Effects of UV Radiation on DNA and Its Components. *J. Photochem. Photobiol. B, Biol.* **2001**, *63*, 88–102.

Rechkoblit, O.; Zhang, Y.; Guo, D.; Wang, Z.; Amin, S.; Krzeminsky, J.; Louneva, N.; Geacintov, N. E. *Trans*-Lesion Synthesis Past Bulky Benzo[*a*]Pyrene Diol Epoxide N^2-dG and N^6-dA Lesions Catalyzed by DNA Bypass Polymerases. *J Biol Chem* **2002**, *277*, 30488–30494.

Rey, L.; Sidorova, J. M.; Puget, N.; Boudsocq, F.; Biard, D. S. F.; Monnat, R. J.; Cazaux, C.; Hoffmann, J.-S. Human DNA Polymerase η Is Required for Common Fragile Site Stability During Unperturbed DNA Replication. *Molecular and Cellular Biology* **2009**, *29*, 3344–3354.

Reynisson, J. H.; Steenken, S. DNA-Base Radicals. Their Base Pairing Abilities as Calculated by DFT. *Phys. Chem. Chem. Phys.* **2002**, *4*, 5346–5352.

Reynisson, J.; Steenken, S. The Calculated Base Pairing Energy of 8-Oxoguanine in the *Syn–Anti* Conformation with Cytosine, Thymine, Adenine and Guanine. *Journal of Molecular Structure: THEOCHEM* **2005**.

Robbins, J. H.; Kraemer, K. H. Xeroderma Pigmentosum: an Inherited Disease with Sun Sensitivity, Multiple Cutaneous Neoplasms, and Abnormal DNA Repair. *Ann. Int. Med.* **1974**, *80*, 221–248.

Rochette, P. J.; Lacoste, S.; Therrien, J.-P.; Bastien, N.; Brash, D. E.; Drouin, R. Influence of Cytosine Methylation on Ultraviolet-Induced Cyclobutane Pyrimidine Dimer Formation in Genomic DNA. *Mutat Res* **2009**, *665*, 7–13.

Rogozin, I. B.; Pavlov, Y. I.; Bebenek, K.; Matsuda, T.; Kunkel, T. A. Somatic Mutation Hotspots Correlate with DNA Polymerase η Error Spectrum. *Nat Immunol* **2001**, *2*, 530–536.

Rupp, W. D.; Howard-Flanders, P. Discontinuities in the DNA Synthesized in an Excision-Defective Strain of *Escherichia Coli* Following Ultraviolet Irradiation. *Journal of Molecular Biology* **1968**, *31*, 291–304.

Sakumi, K.; Furuichi, M.; Tsuzuki, T.; Kakuma, T.; Kawabata, S.; Maki, H.; Sekiguchi, M. Cloning and Expression of cDNA for a Human Enzyme That Hydrolyzes 8-Oxo-dGTP, a Mutagenic Substrate for DNA Synthesis. *J Biol Chem* **1993**, *268*, 23524–23530.

Sale, J. E. Competition, Collaboration and Coordination--Determining How Cells Bypass DNA Damage. *J Cell Sci* **2012**, *125*, 1633–1643.

Sale, J. E. Translesion DNA Synthesis and Mutagenesis in Eukaryotes. *Cold Spring Harb Perspect Biol* **2013**, *5*, a012708.

Sale, J. E.; Lehmann, A. R.; Woodgate, R. Y-Family DNA Polymerases and Their Role in Tolerance of Cellular DNA Damage. *Nat Rev Mol Cell Biol* **2012**, *13*, 141–152.

Sarasin, A. R.; Hanawalt, P. C. Replication of Ultraviolet-Irradiated Simian Virus 40 in Monkey Kidney Cells. *Journal of Molecular Biology* **1980**, *138*, 299–319.

Sattin, B. D.; Pelling, A. E.; Goh, M. C. DNA Base Pair Resolution by Single Molecule Force Spectroscopy. *Nucleic Acids Res* **2004**, *32*, 4876–4883.

Sawaya, M. R.; Prasad, R.; Wilson, S. H.; Kraut, J.; Pelletier, H. Crystal Structures of Human DNA Polymerase β Complexed with Gapped and Nicked DNA: Evidence for an Induced Fit Mechanism. *Biochemistry* **1997**, *36*, 11205–11215.

Schaaper, R. M.; Mathews, C. K. Mutational Consequences of dNTP Pool Imbalances in *E. Coli*. *DNA Repair* **2013**, *12*, 73–79.

Schmitt, M. W.; Matsumoto, Y.; Loeb, L. A. High Fidelity and Lesion Bypass Capability of Human DNA Polymerase δ. *Biochimie* **2009**, *91*, 1163–1172.

Setlow, J. K. Molecular Basis of Biological Effects of Ultraviolet Radiation and Photoreactivation. *Current Topics Radiation Res.* **1966**, *2*, 195–248.

Shachar, S.; Ziv, O.; Avkin, S.; Adar, S.; Wittschieben, J.; Reissner, T.; Chaney, S.; Friedberg, E. C.; Wang, Z.; Carell, T.; et al. Two-Polymerase Mechanisms Dictate Error-Free and Error-Prone Translesion DNA Synthesis in Mammals. *EMBO J* **2009**, *28*, 383–393.

Shen, J. C.; Rideout, W. M.; Jones, P. A. The Rate of Hydrolytic Deamination of 5-Methylcytosine in Double-Stranded DNA. *Nucleic Acids Res* **1994**, *22*, 972–976.

Shen, J.-C.; Fox, E. J.; Ahn, E. H.; Loeb, L. A. A Rapid Assay for Measuring Nucleotide Excision Repair by Oligonucleotide Retrieval. *Sci Rep* **2014**, *4*, 4894.

Shibutani, S.; Takeshita, M.; Grollman, A. P. Insertion of Specific Bases During DNA Synthesis Past the Oxidation-Damaged Base 8-oxodG. *Nature* **1991**, *349*, 431–434.

Sieber, O. M.; Lipton, L.; Crabtree, M.; Heinimann, K.; Fidalgo, P.; Phillips, R. K. S.; Bisgaard, M.-L.; Orntoft, T. F.; Aaltonen, L. A.; Hodgson, S. V.; et al. Multiple Colorectal Adenomas, Classic Adenomatous Polyposis, and Germ-Line Mutations in *Myh. N Engl J Med* **2003**, *348*, 791–799.

Sievers, F.; Wilm, A.; Dineen, D.; Gibson, T. J.; Karplus, K.; Li, W.; Lopez, R.; McWilliam, H.; Remmert, M.; Söding, J.; et al. Fast, Scalable Generation of High-Quality Protein Multiple Sequence Alignments Using Clustal Omega. *Mol. Syst. Biol.* **2011**, *7*, 539–539.

Silverstein, T. D.; Johnson, R. E.; Jain, R.; Prakash, L.; Prakash, S.; Aggarwal, A. K. Structural Basis for the Suppression of Skin Cancers by DNA Polymerase η. *Nature* **2010**, *465*, 1039–1043.

Slupska, M. M.; Baikalov, C.; Luther, W. M.; Chiang, J. H.; Wei, Y. F.; Miller, J. H. Cloning and Sequencing a Human Homolog (*hMYH*) Of the *Escherichia Coli mutY* Gene Whose Function Is Required for the Repair of Oxidative DNA Damage. *J. Bacteriol.* **1996**, *178*, 3885–3892.

Srivastava, A. K.; Han, C.; Zhao, R.; Cui, T.; Dai, Y.; Mao, C.; Zhao, W.; Zhang, X.; Yu, J.; Wang, Q.-E. Enhanced Expression of DNA Polymerase Eta Contributes to Cisplatin Resistance of Ovarian Cancer Stem Cells. *Proceedings of the National Academy of Sciences* **2015**, *112*, 4411–4416.

Stacks, P. C.; White, J. H.; Dixon, K. Accommodation of Pyrimidine Dimers During Replication of UV-Damaged Simian Virus 40 DNA. *Molecular and Cellular Biology* **1983**, *3*, 1403–1411.

Stary, A.; Kannouche, P.; Lehmann, A. R.; Sarasin, A. Role of DNA Polymerase η in the UV Mutation Spectrum in Human Cells. *J Biol Chem* **2003**, *278*, 18767–18775.

Suarez, S. C.; Beardslee, R. A.; Toffton, S. M.; McCulloch, S. D. Biochemical Analysis of Active Site Mutations of Human Polymerase η. *Mutat Res* **2013**, *745-746*, 46–54.

Suarez, S. C.; Toffton, S. M.; McCulloch, S. D. Biochemical Analysis of DNA Polymerase η Fidelity in the Presence of Replication Protein A. *PLoS ONE* **2014**, *9*, e97382.

Sung, R.-J.; Zhang, M.; Qi, Y.; Verdine, G. L. Sequence-Dependent Structural Variation in DNA Undergoing Intrahelical Inspection by the DNA Glycosylase MutM. *Journal of Biological Chemistry* **2012**, *287*, 18044–18054.

Svoboda, D. L.; Briley, L. P.; Vos, J. M. Defective Bypass Replication of a Leading Strand Cyclobutane Thymine Dimer in Xeroderma Pigmentosum Variant Cell Extracts. *Cancer Res* **1998**, *58*, 2445–2448.

Svoboda, D. L.; Vos, J. M. Differential Replication of a Single, UV-Induced Lesion in the Leading or Lagging Strand by a Human Cell Extract: Fork Uncoupling or Gap Formation. *Proc Natl Acad Sci USA* **1995**, *92*, 11975–11979.

Swan, M. K.; Johnson, R. E.; Prakash, L.; Prakash, S.; Aggarwal, A. K. Structure of the Human Rev1-DNA-dNTP Ternary Complex. *Journal of Molecular Biology* **2009**, *390*, 699–709.

Taylor, J. S.; Garrett, D. S.; Brockie, I. R.; Svoboda, D. L.; Telser, J. ^{1}H NMR Assignment and Melting Temperature Study of Cis-Syn and Trans-Syn Thymine Dimer Containing Duplexes of d(CGTATTATGC)·d(GCATAATACG). *Biochemistry* **1990**, *29*, 8858–8866.

Tessman, I.; Kennedy, M. A. The Two-Step Model of UV Mutagenesis Reassessed: Deamination of Cytosine in Cyclobutane Dimers as the Likely Source of the Mutations Associated with Photoreactivation. *Mol. Gen. Genet.* **1991**, *227*, 144–148.

Thomas, D. C.; Kunkel, T. A. Replication of UV-Irradiated DNA in Human Cell Extracts: Evidence for Mutagenic Bypass of Pyrimidine Dimers. *Proc Natl Acad Sci USA* **1993**, *90*, 7744–7748.

Tornaletti, S.; Rozek, D.; Pfeifer, G. P. The Distribution of UV Photoproducts Along the Human P53 Gene and Its Relation to Mutations in Skin Cancer. *Oncogene* **1993**, *8*, 2051–2057.

Traut, T. W. Physiological Concentrations of Purines and Pyrimidines. *Mol Cell Biochem* **1994**, *140*, 1–22.

Trincao, J.; Johnson, R. E.; Escalante, C. R.; Prakash, S.; Prakash, L.; Aggarwal, A. K. Structure of the Catalytic Core of S. Cerevisiae DNA Polymerase η: Implications for Translesion DNA Synthesis. *Molecular Cell* **2001**, *8*, 417–426.

Ummat, A.; Rechkoblit, O.; Jain, R.; Roy Choudhury, J.; Johnson, R. E.; Silverstein, T. D.; Buku, A.; Lone, S.; Prakash, L.; Prakash, S.; et al. Structural Basis for Cisplatin DNA Damage Tolerance by Human Polymerase η During Cancer Chemotherapy. *Nat Struct Mol Biol* **2012a**, *19*, 628–632.

Ummat, A.; Silverstein, T. D.; Jain, R.; Buku, A.; Johnson, R. E.; Prakash, L.; Prakash, S.; Aggarwal, A. K. Human DNA Polymerase η Is Pre-Aligned for dNTP Binding and Catalysis. *Journal of Molecular Biology* **2012b**, *415*, 627–634.

Vaisman, A.; Kuban, W.; McDonald, J. P.; Karata, K.; Yang, W.; Goodman, M. F.; Woodgate, R. Critical Amino Acids in *Escherichia Coli* UmuC Responsible for Sugar Discrimination and Base-Substitution Fidelity. *Nucleic Acids Res* **2012**, *40*, 6144–6157.

Vaisman, A.; Masutani, C.; Hanaoka, F.; Chaney, S. G. Efficient Translesion Replication Past Oxaliplatin and Cisplatin GpG Adducts by Human DNA Polymerase η. *Biochemistry* **2000**, *39*, 4575–4580.

van Loon, B.; Markkanen, E.; Hubscher, U. Oxygen as a Friend and Enemy: How to Combat the Mutational Potential of 8-Oxo-Guanine. *DNA Repair* **2010**, *9*, 604–616.

Vasquez-Del Carpio, R.; Silverstein, T. D.; Lone, S.; Swan, M. K.; Choudhury, J. R.; Johnson, R. E.; Prakash, S.; Prakash, L.; Aggarwal, A. K. Structure of Human DNA Polymerase κ Inserting dATP Opposite an 8-OxoG DNA Lesion. *PLoS ONE* **2009**, *4*, e5766.

Wacker, A.; Dellweg, H.; Trager, L.; Kornhauser, A.; Lodemann, E.; Turck, G.; Selzer, R.; Chandra, P.; Ishimoto, M. Organic Photochemistry of Nucleic Acids. *Photochemistry and Photobiology* **1964**, *3*, 369–394.

Wang, L.-M.; Lu, F.-F.; Zhang, S.-Y.; Yao, R.-Y.; Xing, X.-M.; Wei, Z.-M. Overexpression of Catalytic Subunit M2 in Patients with Ovarian Cancer. *Chin. Med. J.* **2012**, *125*, 2151–2156.

Wang, Y. C.; Maher, V. M.; McCormick, J. J. Xeroderma Pigmentosum Variant Cells Are Less Likely Than Normal Cells to Incorporate dAMP Opposite Photoproducts During Replication of UV-Irradiated Plasmids. *Proc Natl Acad Sci USA* **1991**, *88*, 7810–7814.

Wang, Y. C.; Maher, V. M.; Mitchell, D. L.; McCormick, J. J. Evidence From Mutation Spectra That the UV Hypermutability of Xeroderma Pigmentosum Variant Cells Reflects Abnormal, Error-Prone Replication on a Template Containing Photoproducts. *Molecular and Cellular Biology* **1993**, *13*, 4276–4283.

Washington, M. T.; Johnson, R. E.; Prakash, L.; Prakash, S. Accuracy of Lesion Bypass by Yeast and Human DNA Polymerase η. *Proc Natl Acad Sci USA* **2001a**, *98*, 8355–8360.

Washington, M. T.; Johnson, R. E.; Prakash, S.; Prakash, L. Mismatch Extension Ability of Yeast and Human DNA Polymerase η. *J Biol Chem* **2001b**, *276*, 2263–2266.

Watanabe, T.; Nunoshiba, T.; Kawata, M.; Yamamoto, K. An *In Vivo* Approach to Identifying Sequence Context of 8-Oxoguanine Mutagenesis. *Biochem Biophys Res Commun* **2001**, *284*, 179–184.

Waters, H. L.; Seetharam, S.; Seidman, M. M.; Kraemer, K. H. Ultraviolet Hypermutability of a Shuttle Vector Propagated in Xeroderma Pigmentosum Variant Cells. *J. Invest. Dermatol.* **1993**, *101*, 744–748.

Waters, L. S.; Minesinger, B. K.; Wiltrout, M. E.; D'Souza, S.; Woodruff, R. V.; Walker, G. C. Eukaryotic Translesion Polymerases and Their Roles and Regulation in DNA Damage Tolerance. *Microbiol Mol Biol Rev* **2009**, *73*, 134–154.

Watson, J. D.; Crick, F. H. Molecular Structure of Nucleic Acids; a Structure for Deoxyribose Nucleic Acid. *Nature* **1953**, *171*, 737–738.

Wikonkal, N. M.; Brash, D. E. Ultraviolet Radiation Induced Signature Mutations in Photocarcinogenesis. *J. Investig. Dermatol. Symp. Proc.* **1999**, *4*, 6–10.

Williams, J. I.; Cleaver, J. E. Perturbations in Simian Virus 40 DNA Synthesis by Ultraviolet Light. *Mutat Res* **1978**, *52*, 301–311.

Wimmer, K.; Etzler, J. Constitutional Mismatch Repair-Deficiency Syndrome: Have We So Far Seen Only the Tip of an Iceberg? *Hum. Genet.* **2008**, *124*, 105–122.

Wood, A.; Garg, P.; Burgers, P. M. J. A Ubiquitin-Binding Motif in the Translesion DNA Polymerase Rev1 Mediates Its Essential Functional Interaction with Ubiquitinated Proliferating Cell Nuclear Antigen in Response to DNA Damage. *J Biol Chem* **2007**, *282*, 20256–20263.

Wood, M. L.; Dizdaroglu, M.; Gajewski, E.; Essigmann, J. M. Mechanistic Studies of Ionizing Radiation and Oxidative Mutagenesis: Genetic Effects of a Single 8-Hydroxyguanine (7-Hydro-8-Oxoguanine) Residue Inserted at a Unique Site in a Viral Genome. *Biochemistry* **1990**, *29*, 7024–7032.

Yamaguchi, R.; Hirano, T.; Asami, S.; Chung, M. H.; Sugita, A.; Kasai, H. Increased 8-Hydroxyguanine Levels in DNA and Its Repair Activity in Rat Kidney After Administration of a Renal Carcinogen, Ferric Nitrilotriacetate. *Carcinogenesis* **1996**, *17*, 2419–2422.

Yang, W. An Overview of Y-Family DNA Polymerases and a Case Study of Human DNA Polymerase η. *Biochemistry* **2014**, *53*, 2793–2803.

Yang, W.; Woodgate, R. What a Difference a Decade Makes: Insights Into Translesion DNA Synthesis. *Proc Natl Acad Sci USA* **2007**, *104*, 15591–15598.

Yoon, J.-H.; Bhatia, G.; Prakash, S.; Prakash, L. Error-Free Replicative Bypass of Thymine Glycol by the Combined Action of DNA Polymerases κ and ζ in Human Cells. *Proc Natl Acad Sci USA* **2010**.

Yuasa, M. S.; Masutani, C.; Hirano, A.; Cohn, M. A.; Yamaizumi, M.; Nakatani, Y.; Hanaoka, F. A Human DNA Polymerase η Complex Containing Rad18, Rad6 and Rev1; Proteomic Analysis and Targeting of the Complex to the Chromatin-Bound Fraction of Cells Undergoing Replication Fork Arrest. *Genes Cells* **2006**, *11*, 731–744.

Zeng, X.; Winter, D. B.; Kasmer, C.; Kraemer, K. H.; Lehmann, A. R.; Gearhart, P. J. DNA Polymerase η Is an A-T Mutator in Somatic Hypermutation of Immunoglobulin Variable Genes. *Nat Immunol* **2001**, *2*, 537–541.

Zhang, W.; Tan, S.; Paintsil, E.; Dutschman, G. E.; Gullen, E. A.; Chu, E.; Cheng, Y.-C. Analysis of Deoxyribonucleotide Pools in Human Cancer Cell Lines Using a Liquid Chromatography Coupled with Tandem Mass Spectrometry Technique. *Biochemical Pharmacology* **2011**, *82*, 411–417.

Zhang, Y.; Yuan, F.; Wu, X.; Rechkoblit, O.; Taylor, J. S.; Geacintov, N. E.; Wang, Z. Error-Prone Lesion Bypass by Human DNA Polymerase η. *Nucleic Acids Res* **2000a**, *28*, 4717–4724.

Zhang, Y.; Yuan, F.; Wu, X.; Taylor, J. S.; Wang, Z. Response of Human DNA Polymerase ι to DNA Lesions. *Nucleic Acids Res* **2001**, *29*, 928–935.

Zhang, Y.; Yuan, F.; Wu, X.; Wang, M.; Rechkoblit, O.; Taylor, J. S.; Geacintov, N. E.; Wang, Z. Error-Free and Error-Prone Lesion Bypass by Human DNA Polymerase κ *In Vitro*. *Nucleic Acids Res* **2000b**, *28*, 4138–4146.

Zhao, B.; Wang, J.; Geacintov, N. E.; Wang, Z. Pol H, Pol Z and Rev1 Together Are Required for G to T Transversion Mutations Induced by the (+)- and (-)-*Trans*-*Anti*-BPDE-N^2-dG DNA Adducts in Yeast Cells. *Nucleic Acids Res* **2006**, *34*, 417–425.

Zhao, Y.; Biertümpfel, C.; Gregory, M. T.; Hua, Y.-J.; Hanaoka, F.; Yang, W. Structural Basis of Human DNA Polymerase η-Mediated Chemoresistance to Cisplatin. *Proceedings of the National Academy of Sciences* **2012**, *109*, 7269–7274.

Ziegler, A.; Jonason, A. S.; Leffell, D. J.; Simon, J. A.; Sharma, H. W.; Kimmelman, J.; Remington, L.; Jacks, T.; Brash, D. E. Sunburn and P53 in the Onset of Skin Cancer. *Nature* **1994**, *372*, 773–776.

APPENDICES

APPENDIX A: ANALYSIS OF XPV R361S MISSENSE MUTATION

Abstract

DNA polymerase η (pol η) is responsible for the bypass of both cyclobutane pyrimidine dimers (CPD) and 7,8-dihydro-8-oxoguanine (8-oxoG) during DNA replication. Both are ubiquitous; the former is produced by exposure to UV radiation, while the latter is generated by reactive oxygen species. Lack of functional pol η results in the variant form of the human xeroderma pigmentosum (XPV) syndrome. Because we have previously shown that changes to amino acids important to position the DNA into the polymerase active site did not appreciably affect fidelity during translesion synthesis (TLS), we are interested in TLS efficiency and fidelity of natural variant missense mutations linked to DNA binding and XPV. In particular, the documented XPV mutation G1083T that results in an R361S amino acid change is proposed to disrupt the same protein-template DNA contacts we previously demonstrated important to polymerase function. To study the effect of this mutation we expressed the catalytic core of wild type human pol η in *E. coli* as well as polymerase with single amino acid substitutions R361A and R361S. Overexpressed protein was purified by chromatography and purified protein fractions were used in *in vitro* assays to evaluate primer extension activity and replication fidelities when copying DNA containing *cis-syn* thymine-thymine cyclobutane dimer and 8-oxoG lesions. We find that the R361S amino acid substituted enzyme does retain both polymerase activity, and TLS ability with altered fidelity and thus propose that it is the entire TLS process that is relevant to XPV and mutation suppression. Further, the results confirm our previous finding that enzyme-template DNA interactions distal to the active site are important to polymerase function and fidelity.

Introduction

The lack of functional human DNA polymerase η (pol η) results in the hereditary condition known as xeroderma pigmentosum variant (XPV) (Johnson et al., 1999; Masutani et al., 1999b). Symptoms of the autosomal recessive disease include increased sensitivity to UV light, freckling and UV-induced skin cancers (Gratchev et al., 2003). Several mutations in the *POLH* gene, which encodes pol η, have been documented and described in patients and include both nonsense and missense point mutations, and small insertions and deletions that result in frame shifts (Johnson et al., 1999; Masutani et al., 1999b; Broughton et al., 2002; Yuasa et al., 2006; Biertümpfel et al., 2010). A majority of these mutations result in truncated enzyme. Truncations can result in a sufficiently shorted and thus effectively absent enzyme or, alternatively, in an intact catalytic domain capable of polymerase function that lacks the nuclear location signal necessary for delivery of the polymerase to the nucleus (Broughton et al., 2002). XPV mutations documented that do not precipitate truncated polymerase are restricted to the catalytic core and include an in-frame deletion that has not been characterized (Broughton et al., 2002), and missense mutations that disturb the active site or affect binding of the DNA template or primer (Biertümpfel et al., 2010).

The homozygous mutation of guanine to thymine at nucleotide 1083 (G1083T) in the *POLH* gene resulting in the amino acid substitution of arginine with serine at reside 361 (R361S) has been described in a single patient (Broughton et al., 2002). The patient, at age 57 was described as having less than 10 tumors. The crystal structure solution of human pol η suggested that hydrogen bonding between Arg 361 and Pro 316, which is located at the origin of the little finger β-strand and important for DNA template strand binding, acts to

anchor the β-strand and the R361S amino acid change disrupts this important interaction (Biertümpfel et al., 2010). Biochemical analysis of this mutation has not been carried out, however, so the exact basis for the XPV phenotype is uncertain.

We have previously detailed biochemical enzyme properties of human pol η with amino acid substitutions at several residues within the little finger β-strand including P316 and T318 (Chapter 2). In that work, we showed that polymerase with P316A and T318A changes retained DNA synthesis activity as well as translesion synthesis (TLS) bypass efficiency past both *cis-syn* thymine-thymine cyclobutane pyrimidine dimers (TTD) and 7,8-dihydro-8-oxoguanine (8-oxoG) damaged bases (Chapter 2 Results, Table 2.1). Because the R361S amino acid change would, presumably, modify the way in which the downstream duplex DNA is stabilized in the same way as the P316A and T318A amino acid changes, we hypothesized that the R361S amino acid change may demonstrate similar preservation of activity and lesion bypass efficiency.

As the XPV phenotype is predominantly the consequence of complete absence of TTD bypass, the prospect that R361S may retain even limited lesion bypass is intriguing. As it has also been proposed that translesion synthesis (TLS) polymerases may participate in the replication of short stretches of undamaged bases surrounding the damaged base (McCulloch et al., 2004c), our finding that the fidelity of P316A and T318A forms of pol η was modified only when copying normal DNA may also be relevant to a patient with a G1083T mutation. Thus, to better understand the function and fidelity of the R361S amino acid substituted polymerase, we have carried out assays to assess its biochemical properties, providing a

foundation for further study and characterization to better understand the way in which this mutation results in XPV.

Materials and Methods

Materials. Reaction buffer for all assays consisted of 40 mM Tris (pH 8.0), 250 μg/mL bovine serum albumin, 10 mM dithiothreitol, 10 mM magnesium chloride, 60 mM potassium chloride and 1.25% glycerol. Primer extension and reversion mutation assays were supplemented with all four dNTPs to a final concentration of 0.1 mM each. All cell lines, bacteriophage and reagents for lesion bypass fidelity assays have been previously described (Bebenek and Kunkel, 1995; McCulloch and Kunkel, 2006). DNA sequencing was performed by Genewiz, Inc. (South Plainfield, NJ). Oligonucleotides were purchased from Integrated DNA Technologies, Inc. (Coralville, IA) and The Midland Certified Reagent Company, Inc. (Midland, TX). Nucleotides and restriction enzymes were obtained from New England Biolabs, Inc. (Ipswich, MA).

Expression and Purification of Pol η. The three forms of pol η (wild type, R361A, R361S) were overexpressed and purified as previously detailed (Suarez et al., 2013). Briefly, the vector pET21b-XPV, which codes for the catalytic core amino acids 1-511 of human pol η and includes a C-terminal 6x histidine tag, was utilized. The truncated pol η catalytic core has been shown to retain the same TLS activity as the full-length polymerase (Kusumoto et al., 2002; Biertümpfel et al., 2010). Amino acid substitutions were introduced by use of a QuikChange II XL Site-Directed Mutagenesis Kit (Agilent Technologies, Inc.) and targeted changes were validated by sequencing. Proteins were overexpressed in *E. coli*

BL21(DE3) cells and the protein product was purified by affinity chromatography using $NiSO_4$ charged HiTrap™ Chelating HP (GE Healthcare) with subsequent application of pol η enriched fractions to Mono S™ (GE Healthcare) as described (Suarez et al., 2013).

Primer Extension Assay. Substrates were created by annealing a 5′-Cy5-labeled DNA primer strand to a 1.1x molar excess of complementary template strand in 100 mM sodium chloride and 20 mM Tris (pH 8.0). 17-mer primer sequence 5′-Cy5-GCAGGTCGACTCCAAAG-3′ and 33-mer template sequence 5′-Cy5-TCGGTACCGGGTTAxCCTTTGGAGTCGACCTGC-3′ were used for G/8-oxoG reactions where x represents either guanine or 8-oxoG. 26-mer primer sequence 5′-Cy5-AATTTCTGCAGGTCGACTCCAAAGGC-3′ and 45-mer template sequence 5′-CCAGCTCGGTACCGGG*TT*AGCCTTTGGAGTCGACCTGCAGAAATT-3′ were used for TT dimer reactions where the italicized TT is a TT dimer. Regions paired with primer are underlined. Reaction mixtures containing 1.0 μM DNA substrate were initiated by the addition of 1.7 μM R361A, 1.1 μM R361S or 390 nM WT polymerase, incubated at 37 °C for 5 or 30 minutes and quenched by adding an equivalent volume of 95% formamide, 25 mM EDTA (formamide loading dye). Reaction products were separated by electrophoresis on a denaturing 10% polyacrylamide gel, imaged with a Storm™ 865 imager (GE Healthcare) and quantified using Image Quant™ TL software (GE Healthcare).

Reversion Mutation Assay and Analysis for Fidelity of Lesion Bypass. Analysis of lesion bypass fidelity was carried out as reported previously (McCulloch and Kunkel, 2006). Substrates used for the lesion bypass assay were created by annealing a primer strand to a template strand (24-mer primer 5′-Cy5-AATTTCTGCAGGTCGACTCCAAAG-3′ to 26-mer

CCAGCTCGGTACCGGGTTAxCCTTTGGAGTCGACCTGCAGAAATT-3′ where x represents either guanine or 8-oxoG). Reaction mixtures (30 μL) containing 330 nM DNA and ~50 μCi ^{32}P-α-dCTP were initiated with 170 nM polymerase and incubated for 30 minutes at 37 °C and products (G/8-oxoG) were digested with *Pst*I. An equal volume of formamide loading dye was added to prepare the samples for separation by electrophoresis on a denaturing 10% polyacrylamide gel. Newly synthesized strand was recovered and annealed to M13 gapped circular DNA. Annealed DNA was transformed into *E. coli* strain MC1061 cells and plated in a soft agar overlay atop a layer of CSH50 cells. The lesions are located within an amber stop codon in the *lacZα* gene sequence. Correct synthesis results in preservation of the amber stop codon and thus complementation of the N-terminally truncated *lacZ* gene in CSH50 does not occur, which generates plaques with a light blue phenotype. Errors generated when copying the stop codon result in a functional *lacZα* gene and dark blue plaques are produced. Plaques were counted and assessed for color phenotype to determine mutant frequencies and DNA from individual colonies was amplified using Illustra™ TempliPhi (GE Healthcare) and sequenced to determine the spectrum of changes. Error rates were calculated as described (Kokoska et al., 2003; McCulloch and Kunkel, 2006).

Results and Discussion

To both assess the polymerase properties of the R361S amino acid substituted enzyme and also to be able to compare the effects of modifying Arg 361 to the effects observed in response to modifying Pro 316 and Thr 318, we created both R361S and R361A

amino acid substituted polymerase η (Figure A.1). As in our previous study, we employed the use of a vector that codes for the catalytic core of human pol η which has been shown to retain the same TLS activity as full-length polymerase (Kusumoto et al., 2002; Biertümpfel et al., 2010).

First we assessed the extent to which the polymerases could extend a DNA primer-template substrate. The modified forms of the polymerase were allowed to catalyze DNA synthesis in the presence of dNTPs on undamaged, and 8-oxoG and TTD damaged templates. By quantifying the bands generated by imaging the separated reaction products, we calculated the percent of full-length extension achieved by R361A and R361S as well as the percent of reaction products that represented successful replication past damaged bases.

R361A and R361S amino acid changes affect pol η extension and lesion bypass. We consistently observed that extension was impaired, to varying magnitudes, for the R361A and R361S forms at both 5 and 30 minute time points relative to wild type enzyme (Figure A.2, left). On undamaged template, the percent of reaction products that represented full-length extension (bases 15-17) were 22%, 21% and 60% after 5 minutes for R361A, R361S and WT, respectively (Table A.S.1). After 30 minutes the values calculated were 55%, 58% and 66% for R361A, R361S and WT, respectively. This suggests that while the activity of R361A and R361S is compromised compared to that of wild type with pronounced compromise at shorter time points, the amino acid substituted forms are proficient for replication. This is consistent with previous results that the calculated rate of nucleotide incorporation for P316A was 57% of the value determined for wild type enzyme (Table 2.1).

When allowed to replicate DNA on a template that included an 8-oxoG modified base, extension impairment was observed at the damaged base in reactions in which R361A or R361S polymerase was present (Figure A.2, center). Of the reaction products that reached the damaged base (bands 1-17), 43% incorporated a nucleotide opposite that base and also extended the 8-oxoG base pair (bands 3-17) for the R361A reaction after 5 minutes. For R361S, 52% were extended beyond the damaged base and 83% of the wild type products were extended (Table A.S.2). Results were comparable after 30 minutes; additional extension was observed for all three polymerases, but the relative values were effectively the same as calculated for the 5 minute time point. The corresponding values for undamaged DNA would suggest that the presence of 8-oxoG leads to a preferential impairment to extension. At 5 minutes, of the reaction products that reached the corresponding undamaged base in the R361A reaction, 85% incorporated a nucleotide and also extended the base pair. For R361S, the corresponding value is 82% and 90% for wild type (Table A.S.1).

The presence of TTD also appeared to impair extension (Figure A.2, right). After 5 minutes, 79% of the reaction products that reached the damaged base were also extended beyond the TTD in the R361A reaction, 44% in the R361S reaction and 96% in the WT reaction (Table A.S.3). After 30 minutes, however, 91%, 93% and 97% of the reaction products that reached the damaged base were also extended in the R361A, R361S and WT reactions, respectively.

Thus, damaged bases affect replication by R361A and R361S. The presence of 8-oxoG appeared to affect both R361A and R361S similarly (Figure S.2, center). That is, TLS past the damaged base occurs, but appears to be somewhat impaired. Interestingly, synthesis

past TTD may be superior in reactions with R361A, as at 5 minutes, extension past the damaged base is strongly impaired when R361S is present in the reaction compared to R361A (Figure A.2, right). Previous analysis of pol η structure proposed that the R → S amino acid change would relax the interactions between the protein and DNA (Biertümpfel et al., 2010). Although not stated explicitly, the authors, presumably, were attributing the XPV phenotype to the absence of hydrogen bonding between Arg 361 and Pro 316 (Figure A.1). The findings presented herein suggest that perhaps deficient TTD bypass is not solely due to lack of hydrogen bonding from Arg 361 to Pro 316 as TTD bypass may be affected to a lesser extent for reactions in which R361A was the acting polymerase. It is possible that the replacement of the positively charged, extremely hydrophobic arginine side chain with a less hydrophobic, polar serine side chain destabilizes the protein structure in that region in a way that negatively affects TTD bypass. Nevertheless, TTD TLS remains intact for R361S, as at 30 minutes bypass of the TTD lesion was robust. Therefore, we hypothesize that it is slow/inefficient TTD bypass rather than the lack of TTD bypass that is responsible for the XPV phenotype. Further study including more rigorous TLS efficiency studies, molecular modeling and crystal structure analysis of R361S as well as polymerase with amino acid substitutions at residues that interact with recently synthesized duplex DNA would be interesting and important to more completely characterize and understand the contribution of these interactions to pol η function.

R361A and R361S amino acid changes affect pol η fidelity when copying undamaged and 8-oxoG damaged DNA. TLS fidelity assays were also completed to determine the fidelity of lesion bypass past 8-oxoG. With one exception, results were consistent with those of our

previous study of the little finger β-strand amino acid substituted polymerases (Chapter 2). In that work, we observed that modifying amino acid residues distal to the active site (Figure 2.1A) affected pol η fidelity when copying undamaged DNA but not when copying 8-oxoG or TTD damaged DNA (Figure 2.3). For R361A and R361S forms, we again observed that fidelity was affected when copying undamaged DNA and calculated error rates for total single base substitutions as well as 3′T → C and G → T changes (Figure A.3). The error rates for total single base substitutions were 64×10^{-4} and 90×10^{-4} for R361A and R361S, respectively (Figure A.3A). Both values correspond to 0.2x change from wild type. A similar suppression in error rate was also observed for P316A; the error rate for that form was 130×10^{-4}, which corresponds to a 0.3x change compared to wild type. For a 3′T → C change, the error rate was 53×10^{-4} for R361A and 66×10^{-4} for R361S (both 0.2x change compared to WT) (Figure A.3B). For a G → T single base substitution, the error rate for R361A was 3.5×10^{-4} and 2.7×10^{-4} for R361S (0.3x and 0.2x compared to WT, respectively) (Figure A.3C). Both single base substitution values calculated for R361A and R361S were effectively equal to those of P316A. Following from our previous results, we hypothesized that amino acid substitutions distal to the pol η active site ablated protein-DNA interactions or protein structure important to stabilizing newly synthesized DNA duplex and that, in the absence of those interactions, mispairing at the active site was also destabilized leading to an increase in observed fidelity. The finding that error rates are also suppressed when copying undamaged DNA by R361A and R361S are consistent and further underscore the importance that newly synthesized duplex DNA be constrained by the polymerase.

While in our previous study we did not oberve a change in fidelity when copying damaged DNA by the amino acid substituted polymerases, the modification of Arg 361 did result in a change in polymerase error rate when copying 8-oxoG. The error rate was previously reported as 3900×10^{-4} for WT pol η and 5100×10^{-4} for P316A (1.3x change compared to WT) (Figure A.3D). The error rate for R361A was 1300×10^{-4} and 1000×10^{-4} for R361S. That the error rates of R361A and P316A were appreciably different was an unexpected result. It is consistent, however, with the observation that TLS of 8-oxoG was somewhat impaired in the primer extension assay and suggests that for the bypass of this specific lesion the identity of the residue at this position, and likely the hydrogen bonding in which it participates, is important.

As the G1083T mutation that leads to R361S pol η is a documented XPV mutation, the fidelity of TTD bypass is clearly of principal interest, however the TLS assay with a TTD lesion has not been completed at this time. Completion of those measurements as well as study of Glu 355, which provides two hydrogen bonds to Arg 361, and additional modeling and structural analysis of R361S would be helpful to better understand the foundation for the XPV phenotype reported.

Acknowledgements

This work was supported by the National Institute of Environmental Health Sciences of the National Institutes of Health [R01 ES016942] (SM) and [T32 ES007046] (SM, RB) and the College of Agriculture and Life Sciences at North Carolina State University (ST).

Figures

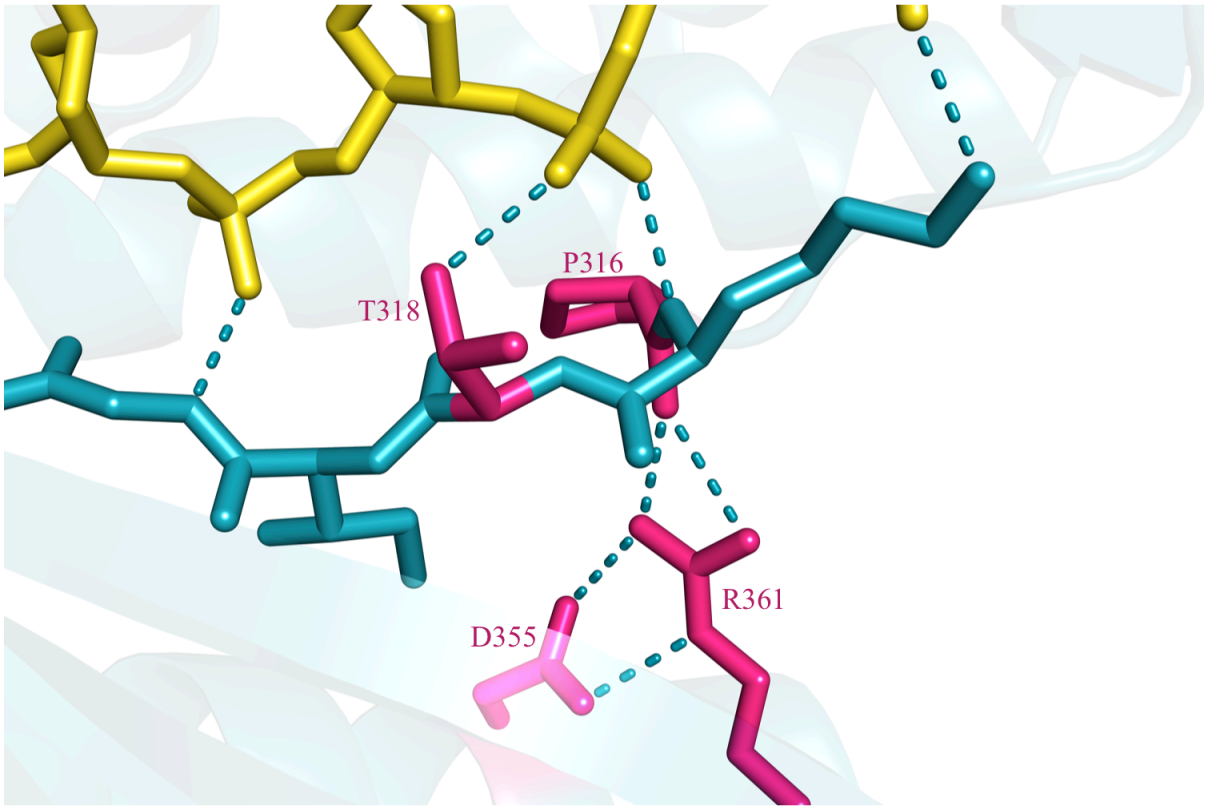

Figure A.1 Pol η and the R361 residue.

Magnified view of pol η amino acid residues that stabilize the DNA template strand. Hydrogen bonds (cyan dashed lines) from amino acid residues P316, K317, T318 and G320 are shown interacting with the template strand of recently copied DNA (the third, fourth and fifth bases away from the templating base:incoming dNTP pair). Hydrogen bonds (also cyan dashed lines) from D355 and R361 form a hydrogen bond network with P316 that provides further stabilizing interactions to newly synthesized DNA duplex. P316, T318, D355 and R361 represented by magenta sticks; remaining little finger β-strand amino acids represented by cyan sticks; remaining pol η enzyme represented by transparent cyan ribbon cartoon; DNA template strand represented by yellow sticks. DNA primer strand not shown for clarity. Image prepared from PDB entry 3MR2 (Biertümpfel et al., 2010) using the PyMOL Molecular Graphics System, Version 1.3 Schrödinger, LLC (http://www.pymol.org/).

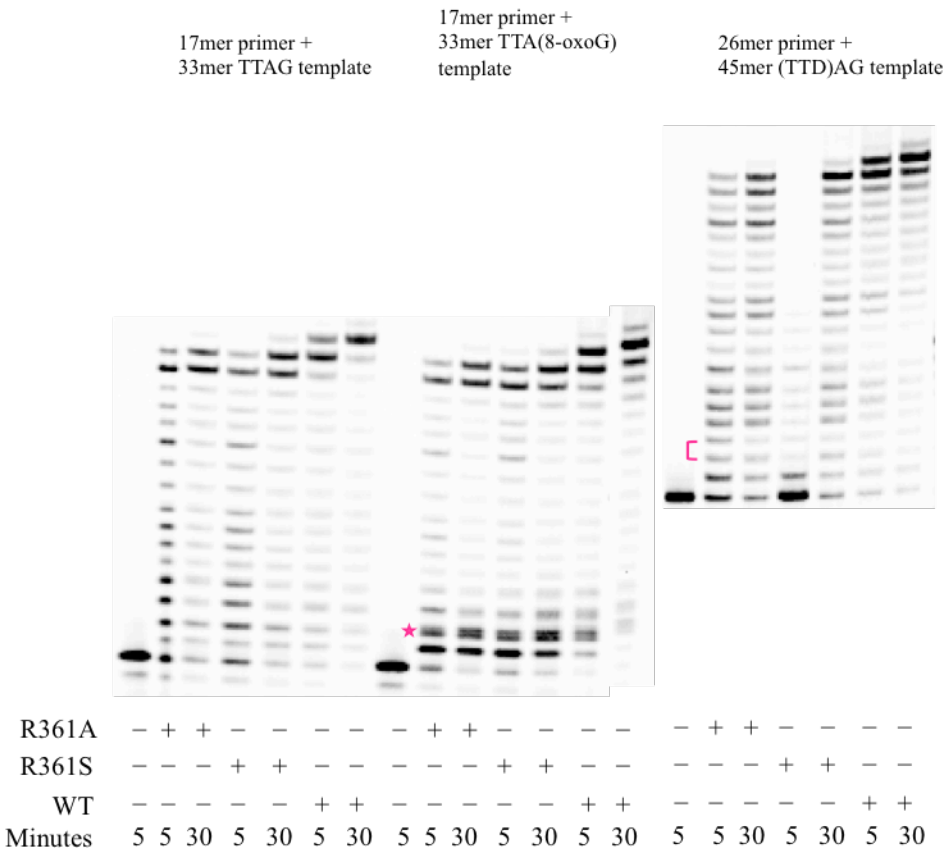

Figure A.2 Primer extension by R361A, R361S and wild type human pol η.

R361A, R361S and wild type polymerase primer extension reaction product separation by denaturing polyacrylamide gel electrophoresis. Undamaged substrate, left; substrate with 8-oxoG damaged base, center; substrate with TTD damaged base, right. Position of 8-oxoG within the template sequence designated by a magenta star and position of covalently linked thymine bases of TTD within the template sequence designated by a magenta square bracket.

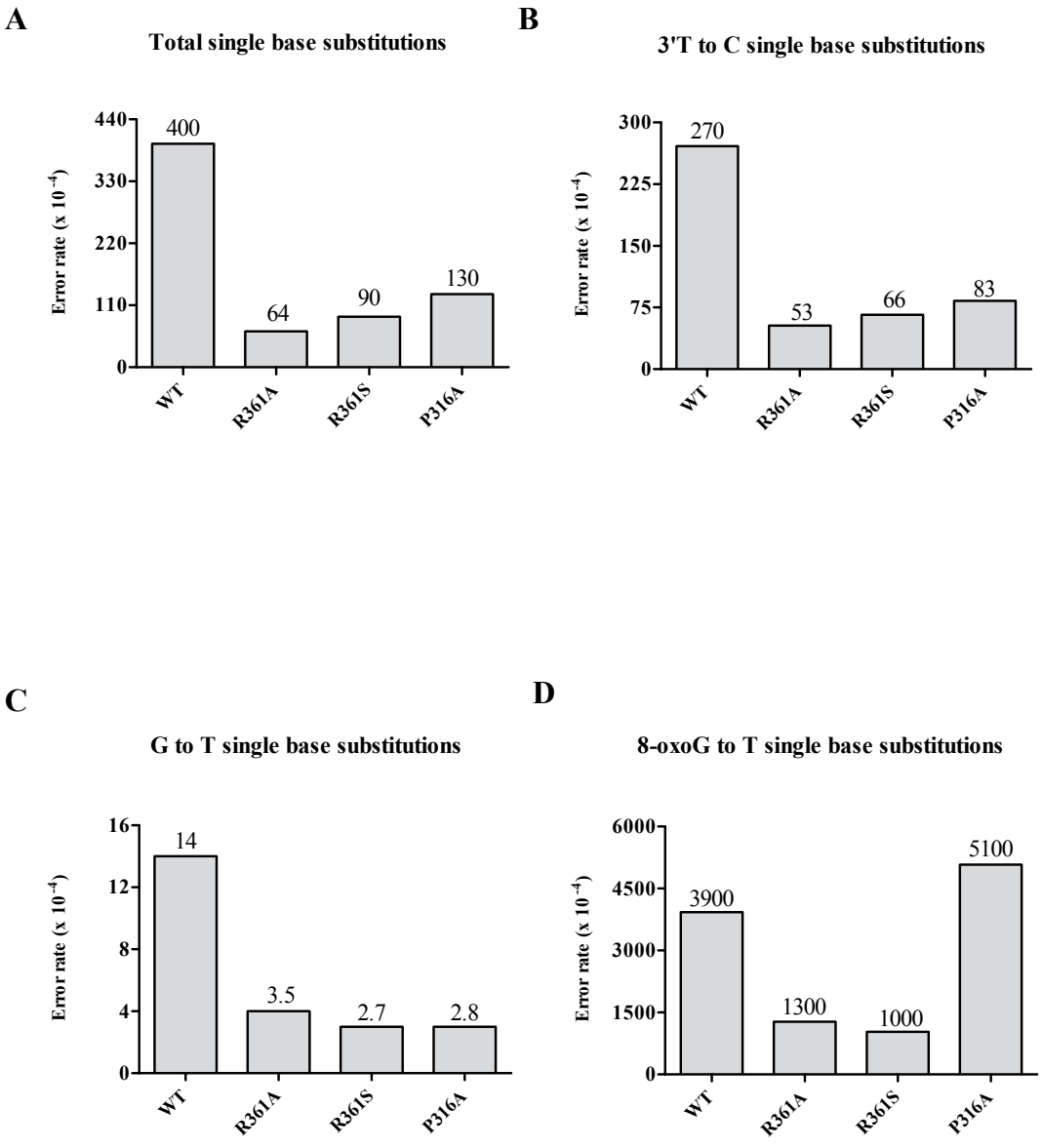

Figure A.3 Substitution at amino acid residue R361 affects fidelity.

A. Total single base substitution error rates for reversion mutation assay. **B.** T → C error rates for reversion mutation assay. **C.** G → T error rates for reversion mutation assay. **D.** 8-oxoG → T error rates for reversion mutation assay. Error rates for R361A and R361S were consistently suppressed for several changes analyzed.

Supplemental Information

Table A.S.1 Extension reactions with undamaged DNA template.

Values represent raw data generated from the pixel density of 5′-Cy5-labeled DNA oligo primer bands imaged with a Storm™ 865 imager (GE Healthcare) and quantified using Image Quant™ TL software (GE Healthcare). Headings note the total dNTP concentration of the reactions. The top portion of the data represents pixel density of individual bands; the bottom portion comprises sums of certain sets of bands as detailed in the results section.

R361A 5 minutes		R361A 30 minutes		R361S 5 minutes		R361S 30 minutes		Wild type 5 minutes		Wild type 30 minutes	
Band No	Volume	Band No	Volume	Band No	Volume	Band No	Volume	Band No	Volume	Band No	Volume
17	64968.2	17	189028.9	17	90330.6	17	505205.2	17	2977798.7	17	6600958.9
16	1024615.3	16	3121011.8	16	1239024.9	16	5627591.3	16	5751279.4	16	1045532.6
15	3951190.1	15	6289088.7	15	3204480.2	15	4285620.5	15	1161245.2	15	252659.1
14	438978.9	14	516256.5	14	364730.8	14	505870.5	14	212332.5	14	100093.5
13	624060.6	13	296077.5	13	507038.4	13	255635.2	13	256721.3	13	121400.3
12	646796.3	12	432735.5	12	531087.4	12	358039.8	12	353268.4	12	171039.6
11	1692735.4	11	469177.3	11	1419449.1	11	340105.6	11	356172.7	11	226862.8
10	661473.9	10	365723.6	10	641049.6	10	376645.1	10	306902.2	10	202110.2
9	757050.9	9	401273.9	9	696597.9	9	359422.6	9	281928.0	9	188089.7
8	1029738.9	8	477548.6	8	1074928.3	8	428357.5	8	432090.5	8	263684.1
7	1528923.8	7	444261.5	7	1584995.1	7	382045.5	7	394635.6	7	266843.1
6	1184222.0	6	482939.9	6	1205285.2	6	434012.8	6	383862.3	6	271184.4
5	849005.1	5	435661.6	5	868598.3	5	444825.5	5	357725.4	5	256198.5
4	2429354.7	4	781775.4	4	2327268.5	4	605780.9	4	615200.5	4	415745.0
3	2594367.1	3	707947.6	3	2405982.9	3	784885.6	3	961678.6	3	705252.4
2	2553687.9	2	1364545.4	2	2848008.5	2	1439094.9	2	906497.0	2	523175.4
1	1013264.5	1	730175.4	1	1087905.2	1	911358.9	1	767363.8	1	353467.2
Primer	3685387.4	Primer	1430788.5	Primer	3317461.4	Primer	1013223.9	Primer	621772.9	Primer	348508.1
Totals		Totals		Totals		Totals		Totals		Totals	
15-17	5040773.5	15-17	9599129.4	15-17	4533835.8	15-17	10418417.0	15-17	9890323.3	15-17	7899150.6
3-17	19477481.0	3-17	15410508.2	3-17	18160847.2	3-17	15694043.6	3-17	14802841.2	3-17	11087654.2
1-17	23044433.4	1-17	17505229.0	1-17	22096760.9	1-17	18044497.4	1-17	16476702.0	1-17	11964296.8
Total	26729820.8	Total	18936017.4	Total	25414222.3	Total	19057721.2	Total	17098474.9	Total	12312804.9

Table A.S.2 Extension reactions with DNA template containing 8-oxoG modified base.

Values represent raw data generated from the pixel density of 5′-Cy5-labeled DNA oligo primer bands imaged with a Storm™ 865 imager (GE Healthcare) and quantified using Image Quant™ TL software (GE Healthcare). Headings note the total dNTP concentration of the reactions. The top portion of the data represents pixel density of individual bands; the bottom portion comprises sums of certain sets of bands as detailed in the results section.

R361A 5 minutes		R361A 30 minutes		R361S 5 minutes		R361S 30 minutes		Wild type 5 minutes		Wild type 30 minutes	
Band No	Volume	Band No	Volume	Band No	Volume	Band No	Volume	Band No	Volume	Band No	Volume
17	114088.6	17	268269.8	17	292192.1	17	829076.1	17	8940347	17	2121393.8
16	1185099.3	16	4171376.4	16	3031418.4	16	7453485.9	16	8282419.3	16	16403838.9
15	3046670.7	15	4481047.0	15	4883089.3	15	3885664.2	15	1844521.8	15	4650890.7
14	285849.5	14	424924.1	14	542969.8	14	653786.0	14	633687.4	14	1782420.6
13	306358.7	13	161910.1	13	546180.8	13	239154.3	13	329445.5	13	772649.6
12	340370.6	12	271349.0	12	571339.9	12	285035.5	12	230793.2	12	333985.6
11	799014.0	11	220506.3	11	1068546.0	11	238821.3	11	264631.1	11	200433.1
10	289398.3	10	203821.6	10	369918.6	10	225745.3	10	176371.1	10	254054.2
9	329395.9	9	185083.0	9	314255.7	9	186109.4	9	198951.2	9	142392.2
8	395867.3	8	225551.3	8	392311.2	8	272802.9	8	269117.6	8	169253.9
7	595066.5	7	219372.3	7	456317.8	7	193011.3	7	237963.1	7	191238.1
6	384040.7	6	262013.9	6	312931.7	6	232319.8	6	157583.3	6	164111.0
5	332028.7	5	209906.8	5	268129.2	5	370580.1	5	226580.5	5	85728.6
4	702025.5	4	430711.2	4	577155.4	4	818301.4	4	714021.9	4	142063.4
3	1893928.1	3	1320109.0	3	1452140.0	3	2370473.7	3	1669107.5	3	290970.3
2	4401312.8	2	6078815.3	2	5179930.2	2	7276733.4	2	3952733.5	2	711066.1
1	10312745.5	1	7067658.9	1	8876307.2	1	4727324.5	1	1144533.4	1	998415.3
Primer	2348949.4	Primer	779326.1	Primer	1567262.2	Primer	773692.7	Primer	249148.7	Primer	134167.7
Totals		Totals		Totals		Totals		Totals		Totals	
3-17	10999202.4	3-17	13055951.7	3-17	15078895.8	3-17	18254367.2	3-17	24175541.1	3-17	27705423.8
1-17	25713260.7	1-17	26202426.0	1-17	29135133.2	1-17	30258425.0	1-17	29272807.9	1-17	29414905.3
Total	28062210.1	Total	26981752.1	Total	30702395.5	Total	31032117.7	Total	29521956.6	Total	29549072.9

Table A.S.3 Extension reactions with DNA template containing TTD modified base.

Values represent raw data generated from the pixel density of 5′-Cy5-labeled DNA oligo primer bands imaged with a Storm™ 865 imager (GE Healthcare) and quantified using Image Quant™ TL software (GE Healthcare). Headings note the total dNTP concentration of the reactions. The top portion of the data represents pixel density of individual bands; the bottom portion comprises sums of certain sets of bands as detailed in the results section.

R361A 5 minutes		R361A 30 minutes		R361S 5 minutes		R361S 30 minutes		Wild type 5 minutes		Wild type 30 minutes	
Band No	Volume	Band No	Volume	Band No	Volume	Band No	Volume	Band No	Volume	Band No	Volume
21	115866.3	21	163740.1	21	59834.5	21	197770.6	21	611622.5	21	1523669.1
20	86111.9	20	257365.7	20	10653.3	20	834978.5	20	6787476.4	20	12020441.1
19	1349136.4	19	4322540.9	19	16106.1	19	8060193.6	19	8869090.2	19	5210247.8
18	1722206.2	18	3759050.3	18	8032.9	18	2803641.0	18	2480176.3	18	2020319.2
17	775279.3	17	1434941.8	17	7056.7	17	1153991.0	17	1073615.4	17	983844.8
16	2259000.5	16	3212960.9	16	35888.4	16	1923175.3	16	936175.7	16	718001.2
15	706873.9	15	1171650.9	15	14216.1	15	1180464.3	15	702779.4	15	685122.2
14	334172.9	14	500026.4	14	15929.4	14	554441.7	14	505152.1	14	483558.1
13	640922.5	13	665350.0	13	53217.9	13	590311.3	13	488332.6	13	465022.3
12	243428.2	12	385951.5	12	22799.5	12	500365.8	12	380725.8	12	323912.2
11	1097462.4	11	1545579.9	11	62848.0	11	1338066.7	11	975316.4	11	474167.5
10	1619923.6	10	1655295.9	10	131827.6	10	1300391.3	10	685876.9	10	186004.0
9	972916.9	9	618357.6	9	242522.3	9	575611.4	9	212232.3	9	132083.4
8	729697.7	8	635097.9	8	189067.4	8	667340.0	8	167443.0	8	77179.2
7	2170319.8	7	1162127.2	7	592954.4	7	975255.4	7	314808.6	7	185450.5
6	1961121.2	6	1756537.2	6	457587.4	6	1476804.9	6	639346.5	6	243231.7
5	2270209.6	5	1703570.3	5	395507.2	5	1247625.2	5	752087.4	5	213006.6
4	2196108.5	4	1791041.1	4	385898.9	4	1328190.9	4	421899.5	4	147344.7
3	1210884.0	3	433560.8	3	392793.1	3	366675.0	3	271916.8	3	163439.2
2	1301377.2	2	832342.5	2	484258.0	2	838047.9	2	366054.9	2	175347.2
1	3144668.7	1	1240650.9	1	2493284.0	1	884412.0	1	547563.5	1	351356.4
Primer	5109179.9	Primer	2138615.3	Primer	21849315.3	Primer	1832634.7	Primer	768885.6	Primer	444183.7
Totals		Totals		Totals		Totals		Totals		Totals	
4-21	21250757.7	4-21	26741185.8	4-21	2701947.7	4-21	26708618.9	4-21	27004157.1	4-21	26092605.3
1-21	26907687.5	1-21	29247740.0	1-21	6072282.8	1-21	28797753.8	1-21	28189692.3	1-21	26782748.2
Total	32016867.4	Total	31386355.3	Total	27921598.1	Total	30630388.5	Total	28958577.9	Total	27226931.9